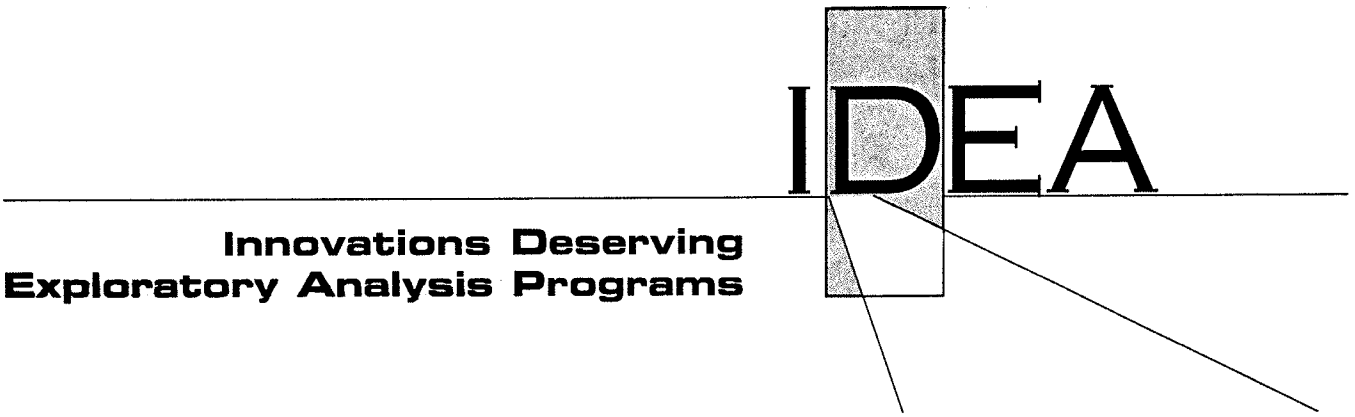

Innovations Deserving Exploratory Analysis Programs

Highway IDEA Program

Robotic Safety Markers

Final Report for NCHRP IDEA Project 90

Prepared by:
Shane Farritor, University of Nebraska, Lincoln, NE

April 2005

TRANSPORTATION RESEARCH BOARD
OF THE NATIONAL ACADEMIES

INNOVATIONS DESERVING EXPLORATORY ANALYSIS (IDEA) PROGRAMS
MANAGED BY THE TRANSPORTATION RESEARCH BOARD (TRB)

This NCHRP-IDEA investigation was completed as part of the National Cooperative Highway Research Program (NCHRP). The NCHRP-IDEA program is one of the four IDEA programs managed by the Transportation Research Board (TRB) to foster innovations in highway and intermodal surface transportation systems. The other three IDEA program areas are Transit-IDEA, which focuses on products and results for transit practice, in support of the Transit Cooperative Research Program (TCRP), Safety-IDEA, which focuses on motor carrier safety practice, in support of the Federal Motor Carrier Safety Administration and Federal Railroad Administration, and High Speed Rail-IDEA (HSR), which focuses on products and results for high speed rail practice, in support of the Federal Railroad Administration. The four IDEA program areas are integrated to promote the development and testing of nontraditional and innovative concepts, methods, and technologies for surface transportation systems.

For information on the IDEA Program contact IDEA Program, Transportation Research Board, 500 5th Street, N.W., Washington, D.C. 20001 (phone: 202/334-1461, fax: 202/334-3471, http://www.nationalacademies.org/trb/idea)

Robotic Highway Safety Markers

1 TABLE OF CONTENTS

Robotic Highway Safety Markers

2 EXECUTIVE SUMMARY

The safety of highway construction and maintenance workers is an important issue and proper traffic control is critical to work zone safety. Devices such as signs, barricades, traffic cones, and plastic safety barrels are used to control traffic. Work zone housekeeping, tasks such as covering and uncovering signs and moving traffic control devices, is one of the most important elements in reducing accidents. While housekeeping is important, it comes at a very high cost. Worker time is required to set up hundreds of safety devices—often at the beginning and end of each workday. However, safety markers located far from the work crew or left in place around the clock leads to driver complacency. In addition, deployment and retrieval activities are extremely dangerous because of the proximity of passing vehicles. New technologies may be useful in reducing accidents.

This project has developed a mobile Robotic Safety Barrel (and a similar Robotic Safety Sign). Safety barrels guide traffic and serve as a visible barrier between traffic and work crews. These barrels consist of a brightly colored plastic drum (approximately 130cm high and 50cm in diameter) that is attached to a heavy base. The robotic safety barrel replaces the heavy base with a mobile robot that transports the safety barrel. The robots work in teams to provide traffic control.

Independent, autonomous barrel motion has several advantages. First, the barrels can self-deploy and self-retrieve, eliminating the dangerous task of manually placing barrels. Second, their positions can be quickly and remotely re-configured as the work zone changes thus reducing the work zone size. Finally, barrels can continuously follow work crews during slow moving maintenance operations such as asphalt overlay.

The proposed approach clearly has a higher equipment cost than traditional systems; however, there are possible cost reductions in labor and increased worker safety. In addition, the cost of traffic congestion in the United States is conservatively estimated to be approximately $100 billion annually and the proposed approach could lead to less congestion by reducing the time required to deploy markers and reducing the size of the work zone. The approach is not fitted for every work zone but there are many situations where it would be useful and practical (e.g. urban lane closures, incident management).

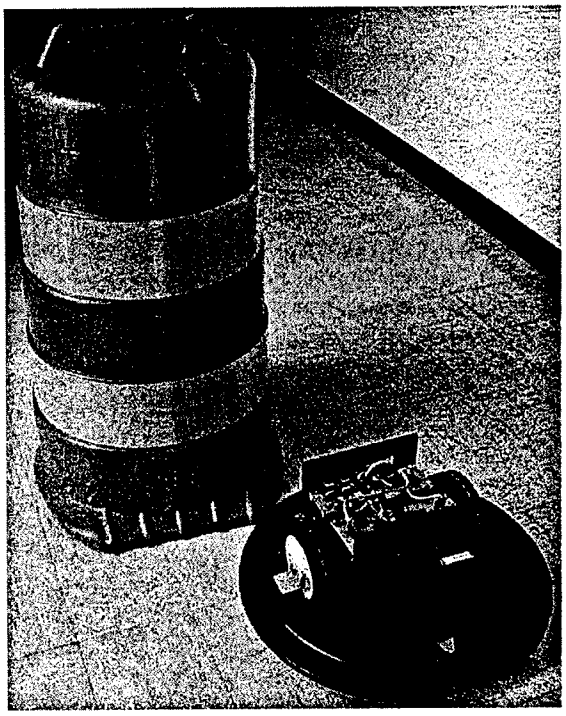

Figure 1:Robotic Safety Barrel

A system that consists of a lead vehicle (or robot) and several low-cost barrel robots was developed. A distributed planning and control approach was created that reduces the per-robot cost by centralizing the intelligence and sensing while keeping communication

bandwidth low by distributing local control. Test results are presented including a statistical analysis of the local controller and field tests of the full system.

This phase one IDEA project has proven the concept of robotic highway safety markers. Eight robotic safety barrels and one robotic sign were constructed. These robots are designed to be low-cost and reliable. A localization sensor system and control system were designed and tested to allow the robot to self-deploy and self-retrieve as well as continuously follow slow moving maintenance operations such as asphalt overlay or lane striping.

All objectives outlined in the original proposal were met and additional achievements were made. Test results were more extensive then originally proposed with over one hundred laboratory tests of the local control system, eight field tests of deployment, and at least four field tests of continuous motion.

Robots Self-Deploy from Road Shoulder

Robot Continuously Follow Motion of Slow Moving Vehicle

Two basic forms of motion were achieved. The first is where the robots are randomly placed on a road side. The user then designates desired positions for the barrels (e.g. taper to close right lane). Then, the robots create a plan and execute a motion to the desired final positions. The second motion was where the user designates a desired formation for the robots. The robots then autonomously maintain that formation behind a slow moving vehicle. Here, the robots match the speed of the vehicle up to 5 mph. This second motion exceeds the proposed objectives of the original phase one proposal and could be useful in slow moving maintenance operations such as asphalt overlay and lane striping.

Great technical progress was made and significant hardware was created during this phase one project. This project has demonstrated the feasibility of the concept. The follow on proposal will lead to more complete field testing and push toward commercial implementation of the concept.

The test results of this project are summarized visually in movies at:

http://robots.unl.edu/projects/current/barrel_robots/index.html

3 IDEA PRODUCT

The goal of this project is to develop commercial robotic highway safety markers.

Independent, autonomous barrel motion has several advantages. First, the barrels can self-deploy and self-retrieve, eliminating the dangerous task of manually placing barrels. Second, their positions can be quickly and remotely re-configured as the work zone changes thus reducing the work zone size. Finally, barrels can continuously follow work crews during slow moving maintenance operations such as asphalt overlay.

The proposed approach clearly has a higher equipment cost than traditional systems; however, there are possible cost reductions in labor and increased worker safety. In addition, the cost of traffic congestion in the United States is conservatively estimated to be approximately $100 billion annually and the proposed approach could lead to less congestion by reducing the time required to deploy markers and reducing the size of the work zone. The approach is not fitted for every work zone but there are many situations where it would be useful and practical (e.g. urban lane closures, incident management).

The future system will consist of a lead vehicle (or robot) and several low-cost barrel robots. The exact system configuration will depend on the task. For example, the barrel robots may be used to follow slow moving maintenance operations such as urban lane closure. In this task, several barrels (9 or 13) could autonomously follow the work vehicle. The work vehicle could serve as the lead robot. The barrel robots would allow for a smaller work zone leading to reduced traffic congestions.

A patent application has been filed and an independent company (Research Triangle Institute (RTI), see Section 9) has been hired to study the marketability of this product.

4 TECHNICAL INVESTIGATION

4.1 SUMMARY OF SYSTEM DESIGN

Eight barrel robots have been created with two requirements for both the hardware and software: 1) high reliability and 2) low per-robot cost. The robots must be reliable because a malfunctioning robot could become a hazard. Cost per robot is critical because multiple (often >100) markers are used and barrels are often destroyed. Specific constraints include stability in 96 km/h (60 mph) winds, low weight (<12 kg so they can be moved by workers), ability to climb slopes (< 7% grade), travel at 8 km/hr, and traverse small (<8cm) obstructions.

There are several physical requirements that a robotic safety barrel must meet. The robot needs to be at least as stable as a traditional safety barrel. The robot and barrel need to remain stationary in 100 mph winds and weigh less than 25 lbs. (so they can be easily moved by workers). The prototypes must have the same footprint as traditional barrels so current transport methods can be used. The device needs to cause minimal damage to vehicles if an impact occurs. It is important that the robots do not become a safety hazard. The robot needs to climb slopes up to 7% grade and travel at 5mph (the speed of some maintenance operations such as striping). The robot needs to traverse obstructions, bumps, and depressions. The robot needs to operate in inclement weather. The robot also needs to maneuver within the work zone. Additionally, there are two systems-level design requirements that need to be addressed if the robot barrels are to be successful: 1) high reliability and 2) low cost.

The system must be very reliable in hardware and software. A robot that malfunctions could enter into traffic and create a significant hazard. The system should be designed so critical components have multiple redundancy. The multi-robot aspect of the approach will be utilized to increase reliability-all robots could monitor their neighbors. Also, an encoded Radio Frequency (RF) carrier wave will be broadcast in the local area so all robots could be stopped in an emergency. There is extensive work in fault tolerant engineering. Robots are now being used in critical operations such as surgery and many systems with human interaction. All reliability issues were not addressed with the prototype robots but are being fully considered in design of the next generation.

Cost per robot is also critical in a decentralized approach to robot safety markers. Multiple safety markers are used in work zones so costly markers are not practical. Also, barrels are often destroyed when struck by passing vehicles. Safety markers with a high replacement cost are not practical. However, robots struck by cars have performed their function by indicating to the driver that the vehicle is not in the correct position.

Mechanically, the robot has two 20 cm diameter wheels that are independently driven and a passive caster, Figure 2. This allows the robot to turn on any radius—including turning in place. Each wheel has an encoder so the robot can determine its position over short distances. The robot itself stands less than 30 cm tall and raises the barrel height by 7 cm.

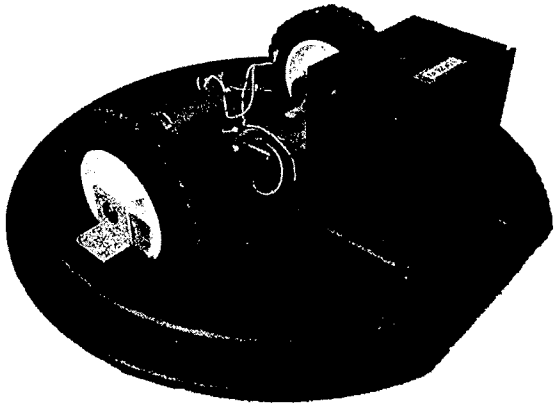

Figure2: Mechanical Design of a Robotic Safety Barrel

Electrically, the robot is powered by a 12-volt lead acid battery—allowing it to operate continuously for approximately 20 hours. The barrel robot has three 8-bit processors: one is used for robot control (RS2000 Rabbit Semiconductor™), one to manage communication with the outside world (PIC), and one to be a watchdog for the RF heartbeat (PIC). Each robot has an RF transceiver for low bandwidth communication.

To increase reliability an encoded RF "heartbeat" is broadcast locally. A loss of this heartbeat causes motor power to be cut through redundant fail-safe electrical relays. Also, each robot's position is monitored by the robot itself as well as by the lead robot. Discrepancies in these redundant sensors (and processors) will cause either a local (robot) or global (heartbeat) shutdown. All communication between the lead and barrels uses a 16-bit CRC checksum to prevent erroneous commands.

4.2 CONTROL OF THE ROBOTIC SAFETY BARRELS

A control system is described here that is specifically designed to reduce the per-robot cost. This is accomplished by centralizing high level computation and the complex/expensive sensors required to globally locate the robots while still maintaining some local control. With this arrangement, individual barrels do not need high computational ability or expensive localization and hazard avoidance sensing. However, since some low computation control is done locally, only a low (0.2 Hz) communication rate between the robots and the central controller is required (i.e. expensive transceivers are eliminated).

Global control is performed with one central vehicle (or mobile robot) base station that has a user interface and localizes each barrel, plans its path, communicates waypoints, and monitors performance. Local control is distributed to each individual barrel robot. This approach is analogous to a general/troops approach to system behavior.

4.2.1 GLOBAL CONTROL

Motion planning for mobile robots has been extensively studied. Several approaches have been developed such as behavior control (Brooks, 1986), artificial potential fields (Khatib, 1986), probabilistic maps (Borenstein and Koren, 1991), genetic planning (e.g. Farritor et al., 1998), and others. The global planning approach used in this work is similar to an approach first developed for cooperative industrial manipulators (Mohri et al., 1993) but incorporates aspects of behavior control. The barrel robot planning problem is somewhat special in that the area to be traversed, a roadway, is relatively (compared to unstructured environments, e.g. planetary exploration) well known, flat, and obstacle free. The primary obstacles for the barrel robots are other robots. The roadway may have identifiable areas that cannot be traversed, such as potholes or a sharp drop off at the pavements edge, but these areas can be designated by the operator and easily avoided by the planner.

Consider the robot planning problem shown in Figure 3. Here two robots are required to move from random locations on the roadside shoulder to positions in a taper, or wedge, used to close a lane. Such lane closures are common, and this task is demonstrated in section 5.

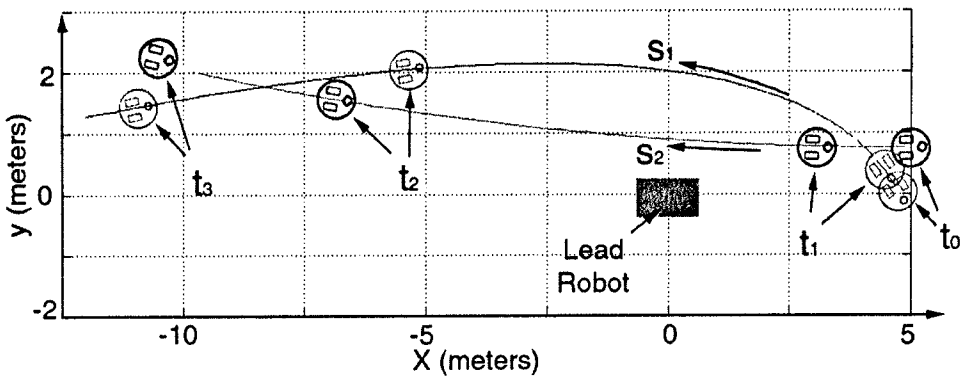

Figure 3: Global Planning

A parabolic polynomial is used to create the desired robot path. The initial position, initial orientation, and final position serve as boundary conditions. This approach ensures the non-holonomic constraints are considered. The final orientation of the path is not constrained so a new destination can be given while maintaining smooth motion (the path always begins with locally forward motion). More on when to re-plan the path can be found in (Murphy, et al., 1997).

To generate this path, a local right-handed coordinate system, M, is attached to robot, i, with the x-axis directed forward and the z-axis parallel to gravity. A transformation matrix is used to transform the desired final position of the robot in the global frame N to the local robot frame M:

$$ {}^{N}P = {}^{N}_{M}T\,{}^{N}P \text{ where } {}^{N}_{M}T = \begin{bmatrix} \cos\Psi_i & \sin\Psi_i & 0 & x_i \\ -\sin\Psi_i & \cos\Psi_i & 0 & y_i \\ 0 & 0 & 1 & 0 \\ 0 & 0 & 0 & 1 \end{bmatrix} $$

where the absolute position of robot i is given by x_i and y_i and its orientation is Ψ_i. The absolute position is given by a laser rangefinder, Figure 4, mounted on the lead (central) robot. The sensor provides distance measurements (R) as it sweeps from 0 to 180 degrees in 0.5 degree increments. Figure 4 shows five robots in a lane closure taper, or wedge, as in the field tests (section 5). The absolute orientation, ψ, is given by a compass sensor on each robot.

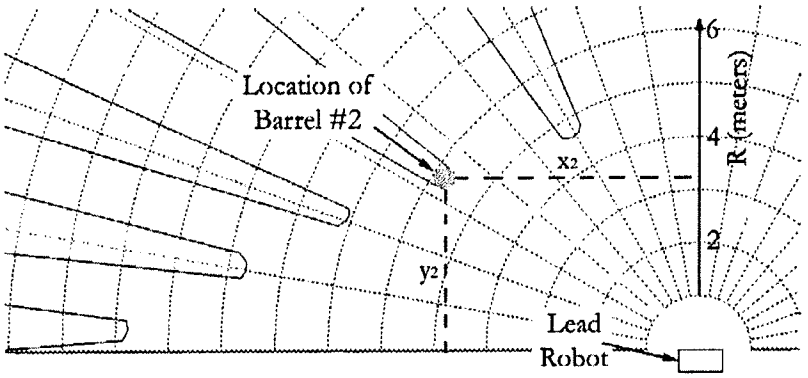

Figure 4: Global Localization of Barrel Robots

With this data, the parabolic path can then be written in the local robot frame as:

$$y(x) = A_i x^2 + B_i x + C_i \qquad \text{with}: \quad \left[\frac{dy}{dx}\right]_{x=0} = 0, \quad {}^{M}\begin{bmatrix} x \\ y \end{bmatrix}_{final} \text{ on the path}$$

Assuming the paths are not coincident, each robot can collide with any other robot a maximum of two times.

The desired position of the robot is then rewritten as a distance along the parabola given by S_1 and S_2, shown in Figure 4 where subscripts 1 and 2 denote two robots for the simplest case). The planning problem for the i^{th} robot can then be expressed in terms of the path variable, S_i, where S_i changes from $S_{i,o}$ to $S_{i,f}$. The robot's motion along the path is planned in these new variables, Figure 5.

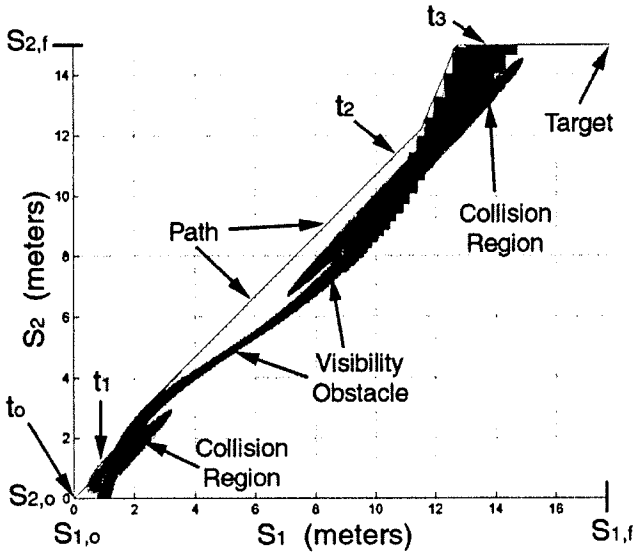

Figure 5: Global Path Planning

Here, the collisions between the robots are shown as elliptical shapes. The collision regions are enlarged to account for a safety margin between robots that assumes the error of the local controller is bounded (section 5). The second darkened region represents areas where both robots do not have line-of-sight contact with the localization sensor. The robot's positions cannot be determined if they are not "visible" to the global sensor. Such regions are considered impassable unless the "invisible" robot is stationary (e.g. t_3 in Figure 4).

The "visibility obstacle" is stepped because of the finite angular resolution of the rangefinder. It is possible for no solution to exist. If this occurs, a robot is commanded to turn in place to create a passable region.

A path can now be plotted to the goal while avoiding impassable regions using several methods (e.g. tangent graphs). Acceleration and velocity constraints limit the curvature of the path. For the barrel robots, the time to complete the motion is bounded by the solution that moves one robot to the goal while the other robot waits (vertical while $S_1=0$) and then the second robot moves (horizontal while $S_2=S_{2f}$). Here, a behavior based approach is employed where priority is given to the robot that must travel the greatest distance. Since all robots are similar, this ensures that the time required to complete the total motion is minimized (Shen, 2003). An expression of S_i can now be found as a function of time with waypoints spaced along this curve. This approach is expanded to 5 robots and used in the field tests in section 5. Discussion of the stability issues with respect to the global controller can be found in (Shen, 2003).

4.2.2 LOCAL CONTROL

Each barrel robot receives a waypoint from the global controller. A local planning and control scheme is used to obtain each waypoint. The use of local control allows low bandwidth communication, and hence, an inexpensive transceiver, since only the waypoints need to be transmitted to the barrel robot.

For the j^{th} waypoint transformed into the moving robot frame, ${}^{M}\underline{x}_{w,j} = \left[{}^{M}x_{w,j}, {}^{M}y_{w,j}\right]$ a local path, ${}^{M}y = F_j = func({}^{M}x)$, is used to move the robot to the waypoint, Figure 6.

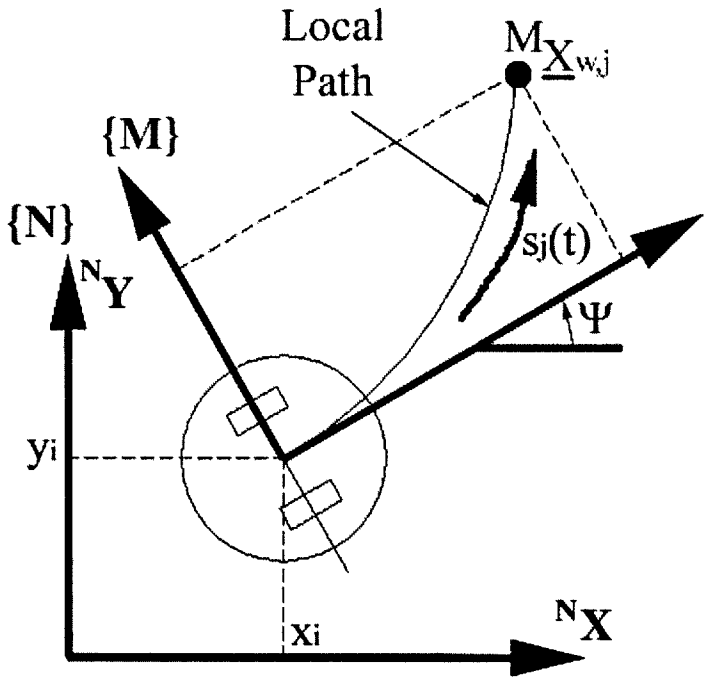

Figure 6: Local Path to a Waypoint

To ensure smooth motion, the non-holonomic constraints require the following boundary conditions on this path:

$$(1)\ F_j(0)=0$$

$$(2)\ \frac{dF_j}{d^{M}x}\Big|_{{}^{M}x=0} = 0$$

$$(3)\ F_j({}^M x_{w,j}) = {}^M y_{w,j}$$

This constrains the initial position, waypoint position, and requires that initial direction of travel is locally forward, but does not constrain the final orientation. A simple parabola is again chosen over more complex paths (e.g. geodesics Belta and Kumar, 2002) because of its sufficiency (w.r.t. boundry conditions) and it is practical to implement on an 8-bit processor (Shen, 2003).

$$ {}^M y = F_j = C_j\left({}^M x^2\right) \quad \text{where } C_j = \frac{{}^M y_{w,j}}{{}^M x_{w,j}^2}$$

It is then convenient to define a variable, s_j, as a distance along this parabolic path, Figure 3. The motion along this path can be found as a function of time, $s_j(t)$ where the robot moves a total distance of L_{fj} to the waypoint in some time T_{fj}. Again, to make a smooth motion, the initial and final positions and velocities are constrained:

$$(1)\ s_j(0) = 0$$
$$(2)\ s_j(T_{fj}) = L_{fj}$$
$$(3)\ \left.\frac{ds_j}{dt}\right|_{t=0} = V_i$$
$$(4)\ \left.\frac{ds_j}{dt}\right|_{t=T_{f,j}} = V_f$$

A cubic polynomial is used to satisfy these constraints and ensure the robot's acceleration is continuous, given by:

$$s_j(t) = a_3 t^3 + a_2 t^2 + a_1 t$$

where: $a_1 = V_i$

$$a_2 = \frac{3}{T_{f,j}^2} L_{f,j} - \frac{2}{T_{f,j}} V_i - \frac{1}{T_{f,j}} V_f$$

$$a_3 = \frac{2}{T_{f,j}^3} L_{f,j} - \frac{1}{T_{f,j}^2}\left(V_f - V_i\right)$$

Now, the function $s_j(t)$ can be transformed into the moving cartesian frame {M}. An analytical expression for this transformation is possible but it is too computationally expensive for the on board 8-bit processor, therefore, a numerical approximation is used (Shen, 2003). Consider the segment of the parabola, s_j, shown in Figure 7.

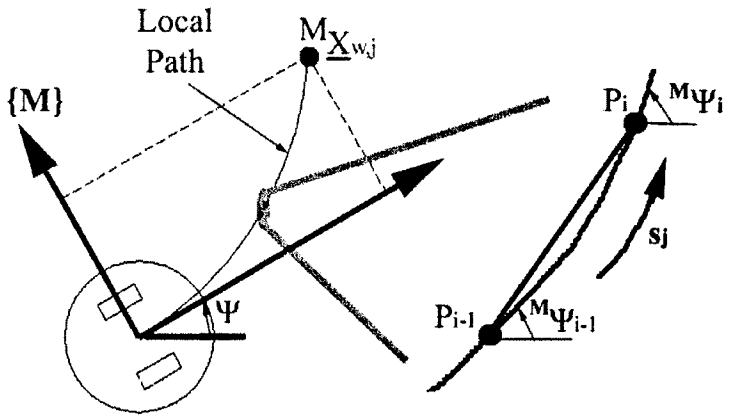

Figure 7: Approximation of position as a function of time

Suppose the point i-1 has been obtained at time point t_{i-1}, and its coordinates $({}^Mx_{i-1}, {}^My_{i-1})$ and direction ${}^M\psi_{i-1}$ are all known. What we want to solve is the coordinates and orientation of the next waypoint t_i. The length of the straight line segment $\overline{P_iP_{i-1}}$ can be approximated by the arc length $(s_j(t_i)-s_j(t_{i-1}))$ and using the initial direction of travel ${}^M\psi_{i-1}$ as the angle of this line segment the i^{th} cartesian can be calculated.

$$ {}^Mx_i = {}^Mx_{i-1}+[s_j(t_i)-s_j(t_{i-1})]* cos({}^M\psi_{i-1}) $$

Then, using the path function (4),

$$ {}^My_i = C_j*{}^Mx_i^2 $$
$$ {}^M\psi_i = arctan(2*C_j*{}^Mx_i) $$

The error with the iteration tends to accumulate with the extension of the path, but the precision is acceptable with the current application. For a typical motion–obtaining a waypoint ${}^Mx_{w,j}=[1, 1]$ in 5 seconds with a 20 Hz. control cycle–the accumulated error is less than 0.7% (Shen, 2003).

Finally, the cartesian positions ${}^M\underline{x}_i=[x_i y_i]$ are transformed into "joint" space given by the wheel positions $\underline{\theta}_i=[\theta_{L,i}, \theta_{R,i}]$. To find this relationship, consider the top view in Figure 8. Here the robot has moved an amount $\delta\underline{x}=[\delta x, \delta y]$ and rotated $\delta\Psi$ between times t_{i-1} and t_i. During this time the wheels rotated an amount $\delta\underline{\theta}=[\delta\theta_L, \delta\theta_R]$.

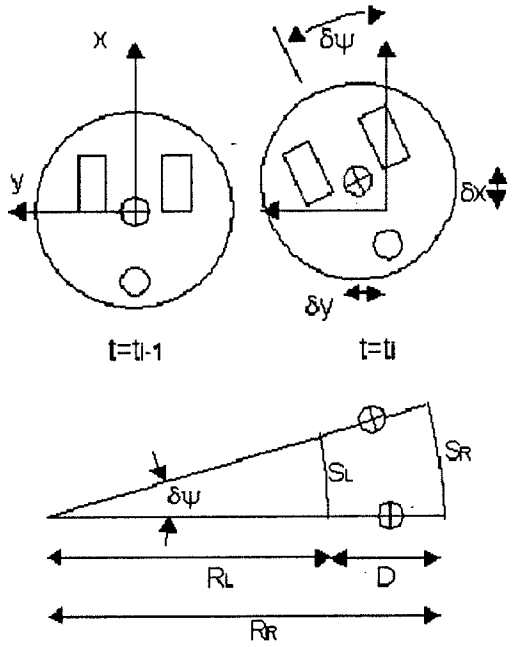

Figure 8: Differential Robot Motion

S_L and S_R are the path lengths traveled by the left and right wheels. No slip and planar motion is assumed so the path lengths are related to the change in wheel rotation by $S_k=(\delta\theta_k \times r)$ where r is the wheel radius and $\delta\theta_k$ is given by the motor encoders for wheel k. D is the distance between the wheels and R_L and R_R are the turning radii for each wheel.

Assuming $[^M x_i, ^M y_i]$ is in the first quadrant (signs change in other quadrants) and small motions, the differential motions in joint space can be calculated based on the differential motion in cartesian space. Using geometry, the relationships are given by:

$$\delta\theta_L = \frac{2}{r}\sqrt{\delta x^2 + \delta y^2} - \frac{2D}{r}\cdot \arctan(\frac{\delta y}{\delta x})$$

$$\delta\theta_R = \frac{2}{r}\sqrt{\delta x^2 + \delta y^2} + \frac{2D}{r}\cdot \arctan(\frac{\delta y}{\delta x})$$

This relationship is only valid for small motions. For large motions, the wheel angles are non-observable based on the cartesian position of the robot. The inverse of these relationships are also used to estimate the robot's position using dead reckoning.

Finally, a PID control scheme is used to guide the robot to the waypoint, Figure 9. The desired wheel angles, calculated from the plan using the above techniques, are the input to the controller and an error is created based on wheel encoder measurements. This error is then acted upon by a traditional PID controller to create torque commands $(\underline{\tau}=[\tau_l, \tau_r])$ for the robot's motors. The joint space results for a typical motion–obtaining a waypoint $^M x_{wj}=[1, 1]$ in 5 seconds with a 20 Hz. control cycle–are shown as a solid line with the dashed line indicating the desired positions. Control of this type has well known limitations (ignores dynamic effects, non-holonomic constraints), but tests have shown acceptable results (statistical analysis in section 5.1) for barrel placement.

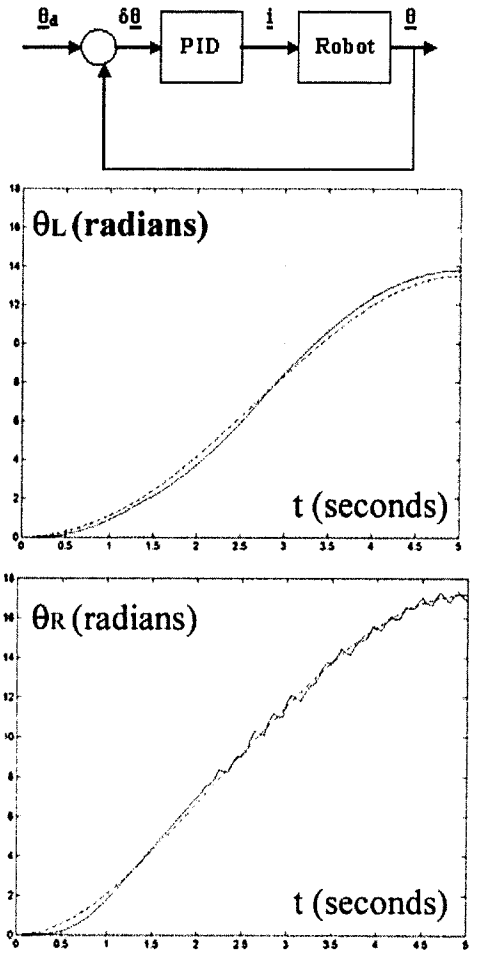

Figure 9: Control Diagram and Joint Space Results

The local control scheme has been shown, under stated assumptions, to be globally asymptotically stable for all proportional control gains (Shen, 2003).

5 RESULTS

Test results were more extensive then originally proposed. The tests conducted can be divided into three categories: 1) laboratory evaluation of local robot control, 2) field tests of self-deployment for urban lane closure, and 3) field tests of continuous following of slow moving maintenance operations. Each set of tests is discussed in this section.

All of the results of these tests can be viewed in a movie format at:

http://robots.unl.edu/projects/current/barrel_robots/index.html

5.1 LOCAL CONTROL TESTS

Both the local and global planning and control schemes were tested. To evaluate the local control scheme the robot was commanded to move to a location 1 meter forward and 1 meter to the left, $\underline{x}_d = \begin{bmatrix} x_d \\ y_d \end{bmatrix} = \begin{bmatrix} 1 \\ 1 \end{bmatrix} m$. This is a typical local motion for the robot and this experiment was repeated 100 times to determine the accuracy of the controller, Figure 10. Calculations were also performed on random subsets of this data to ensure statistical significance. The final position of the robot $\underline{x}_{i,f} = \begin{bmatrix} x_{i,f} \\ y_{i,f} \end{bmatrix}$ was recorded using a vision-based external measurement device with an accuracy of <0.3 mm (Polaris, Northern Digital Inc.). The error $\underline{E} = \begin{bmatrix} E_x \\ E_y \end{bmatrix}$ is defined as the difference between the desired position and the final position. A Bivariate Normal (BN) distribution was fit to the data to establish expected values and standard deviations for the errors in x and y. This expresses the two dimensional probability distribution of the final position of the robot. Lines of equal probability density are shown as ellipses with the highest probability inside the center ellipse, Figure 10.

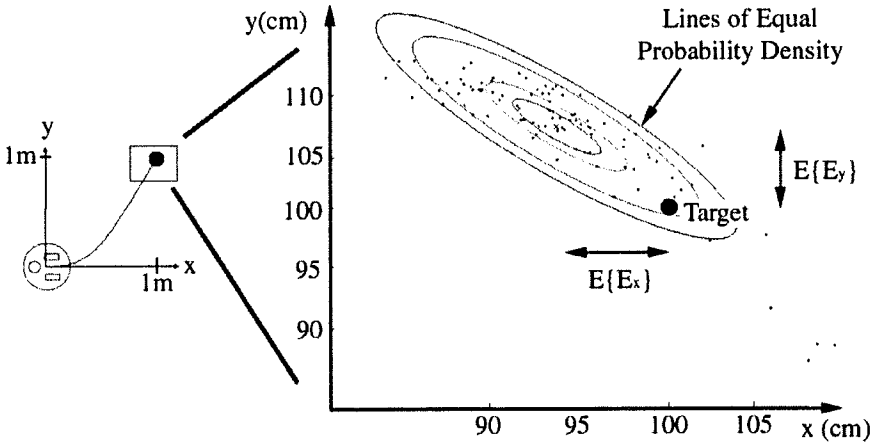

Figure 10: One Hundred Experiments to Evaluate Local Controller

Since the major axis of each ellipse is much greater than the minor axis, it can be said that the x and y errors are correlated with a correlation coefficient for the bivariate normal distribution equal to 0.88. Furthermore, the angle of the major axis (54°) corresponds to the desired final orientation of the robot given

by the planning parabola (63°). This error is a result of the sensors used by the control system to estimate the robots position. The wheel encoders are very accurate at measuring the forward motion of the robot but much less accurate at detecting small changes in the robot's heading, hence the correlation.

The data can also be plotted as the distribution of the magnitude of error $||E||$ given by $\sqrt{E_x^2 + E_y^2}$, Figure 11. This plot shows two distributions: 1) the error based on the position estimate from on-board sensors (i.e. where the robot "thinks" it stopped), and 2) the error from external measurements (i.e. where the robot actually stopped). Both were fit with a gamma distribution. The error based on on-board sensors had an expected value of 4.2 cm (variance =1.48 cm^2) and the error based on external measurement had an expected value of 10.2 cm (variance=9.6 cm^2)

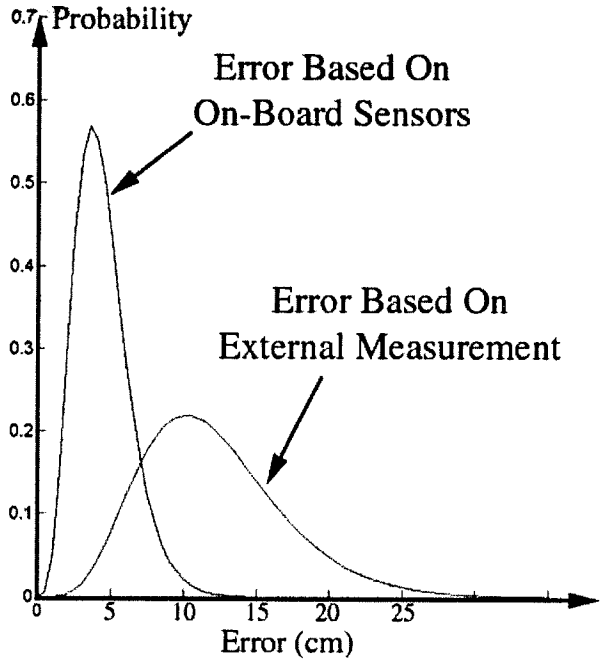

Figure 11: Distribution of the Magnitude of Error

This data shows the robot "thought" it was very close to the target (4.2 cm) but the actual error was larger (10.2 cm). The robot needs to move ≈142 cm therefore this represents 7.3% of the total distance. A perfect controller could command the robot to zero error when measured with on board sensors, however, the larger portion of the error could only be eliminated by improving the localization scheme. This larger error is periodically eliminated using the global sensor.

5.2 SELF-DEPLOYMENT TESTS

Both the global and local control schemes were tested in a realistic field environment. Five robots were randomly placed on the shoulder of the road and commanded to move into a taper, or wedge, to close the right lane of a two lane road, Figure 12. This is a very common task in many maintenance operations where the barrel robots could be useful (Traynowicz, 2002).

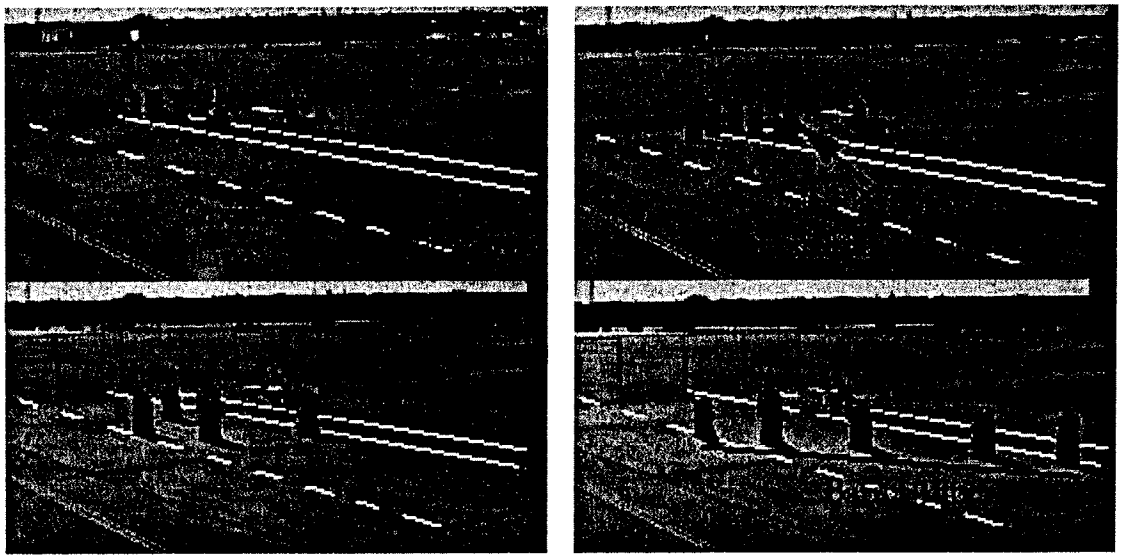

Figure 12: Lane Closure with Five Barrel Robots

Figure 13 shows the desired (dashed line) and actual path (solid line) for each robot during deployment. The symbols on each actual path represent where individual robots reached a waypoint and their position was updated. Lines connecting symbols only approximate robot motion between points. The maximum deviation from the desired path was 23 cm and the maximum final error for all robots was 11 cm. This accuracy is well within the requirements for barrel placement and exceeds the accuracy of current human deployment.

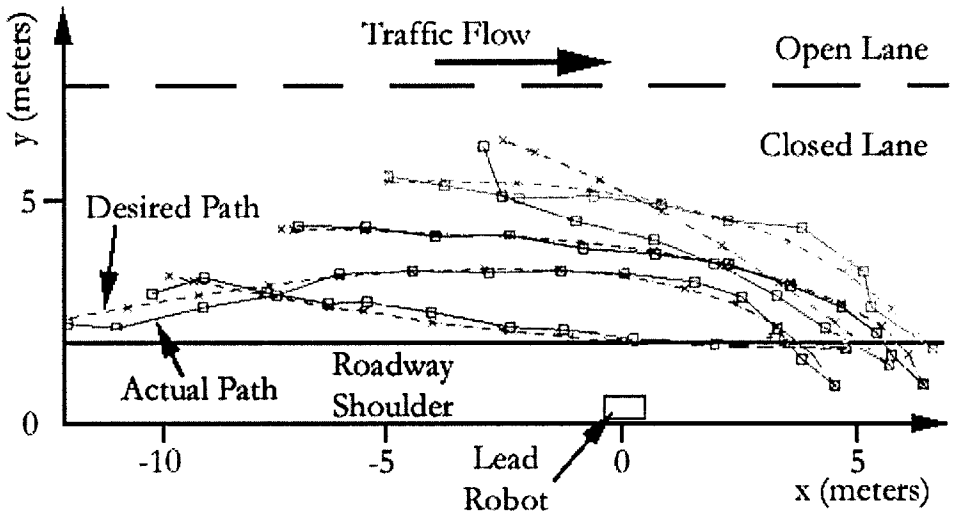

Figure 13: Desired and Actual Paths During Field Test

5.3 CONTINIOUS FOLLOWING TESTS

The ability of a formation of robots to follow slow moving maintenance operations was tested in a realistic field environment. In the first tests, five robots were placed in a lane closure taper and asked to move forward at a set velocity, see Figure 14. The robots were able to move forward with a maximum error of only 25 cm.

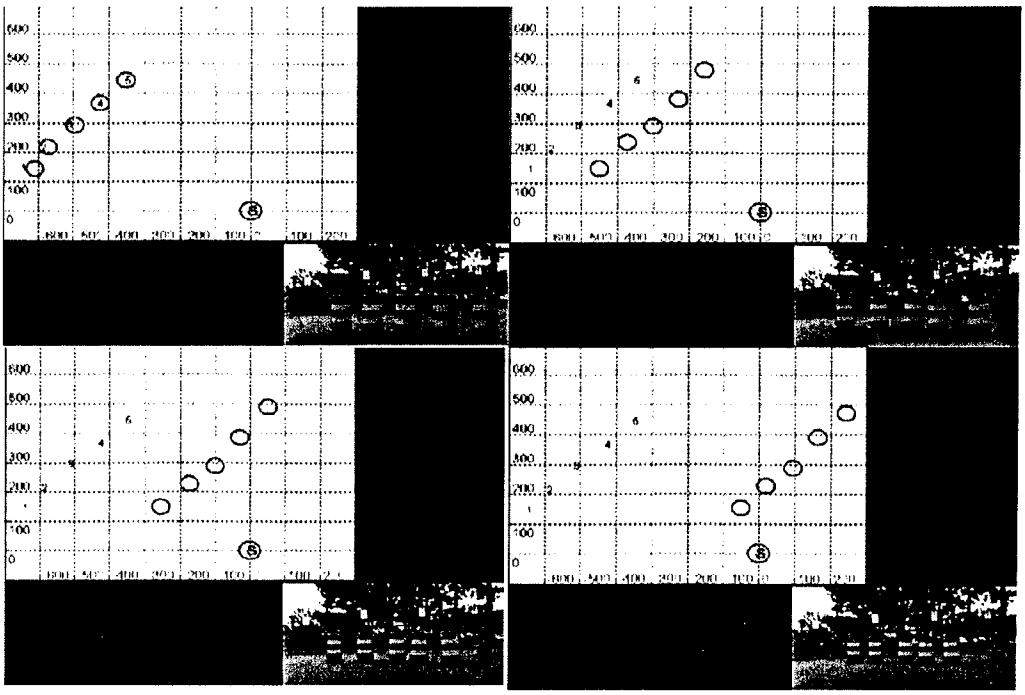

Figure 14: Follow Test Images

Figure 14 shows four images from the motion of the barrel robots in a follow test. The top left (white) inset in each of the four images shows the location of the barrel robots as found by the global sensor system. The location of the barrel robots are tracked in real time (10 hertz) to ensure reliability. The bottom right inset in each of the four images shows the motion of the barrel robots as they move away from the camera (note they get smaller in the image). The full movie of this test can be found at http://robots.unl.edu/projects/current/barrel_robots/index.html

The actual path of the robots is shown in Figure 15.

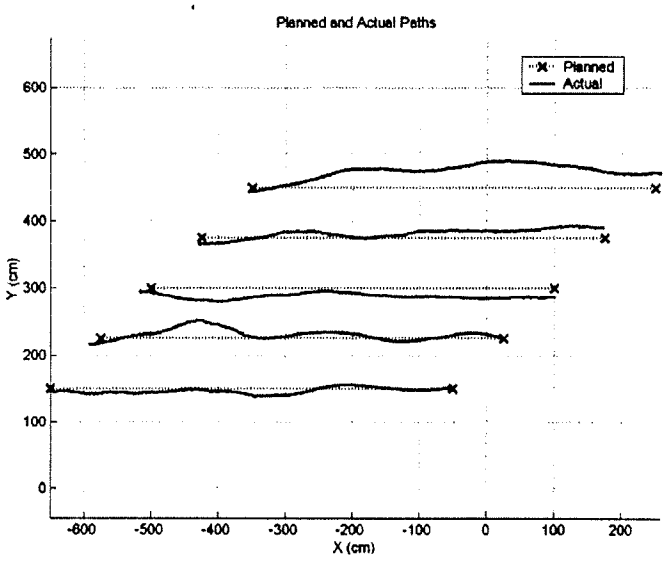

Figure 15: Robot Paths

An additional test can be seen in Figure 16. This test shows three robots that were required to move forward in the taper formation and to MATCH the velocity of the lead vehicle (cart pushed by the student in this image). For example, as the lead vehicle stops, the robots stop. If the lead vehicle moves, the robots move. The robots are moving from the top of the image to the bottom.

This work has been completed since progress report #5 was filed. The full movie of this test can be found at http://robots.unl.edu/projects/current/barrel_robots/index.html

Figure 16: Second Follow Test Images

6 SUMMARY OF PROJECT OBJECTIVES

All of the original project objectives were met. The original project was divided into three sections. This section summarizes the original project objectives and gives a brief description of how they were accomplished. Details are given in the remainder of the report. Additional accomplishments, beyond the original objectives, are outlined in the following section.

Period 1	
Summary of Task	***Summary of Accomplishment***
Task 1. Create a functional Diagram to Design a Reliable Robot	Functional diagrams were created as reported in the first progress report. These diagrams were used to determine which subsystems needed to be redundant and to provide a cost break down for the robot design.
Task 2. Create a detailed physical simulation	A detailed physical simulation was created and used to design the control system. Results are presented in section 4.
Task 3. Design a localization sensor system	A localization system was designed that requires only one global sensor. Details are given in section 4.
Task 4. Created detailed robot design	Detailed robot designs were created and eight robots were built.
Period 2	
Summary of Task	***Summary of Accomplishment***
Task 1. Robot fabrication	Seven functioning barrel robots were built and one robot sign.
Task 2. Control system design	The control system has been created and tested for accuracy and reliability. Results are presented in section 4.
Task 3. Creation of localization sensor system	The localization sensor system has been created and tested for accuracy and reliability. Results are presented in section 4.
Task 4. Report	Progress reports have been regularly submitted and work from this project has been presented in journals and conferences.
Period 3	
Summary of Task	***Summary of Accomplishment***
Task 1. Initial Robot Tests	Initial tests showed a reliable local control system. Over 100 tests were performed and are quantified in (Shen, 2003)
Task 2. Filed Tests	At least eight field tests were performed in realistic highway environments. Results are presented in section 5.
Task 3. Journal Publication	Shen, X., Dumpert, J., Farritor, S., "Robotic Highway Safety Markers," pending publication in the ASME/IEEE Transactions on Mechatronics.

7 ACCOMPLISHMENTS BEYOND ORIGINAL PROPOSAL OBJECTIVES

Several milestones were reached that were beyond the original proposal objectives. These include:

1) Continuous movement capabilities so robotic safety markers can follow slow moving maintenance operations such as asphalt overlay or lane striping.

2) Achievement of robot position and orientation localization from one sensor.

3) Demonstration of deployment and retrieval activities on at least eight field tests.

4) Demonstration of continuous following in at least 4 field tests.

8 SUMMARY OF PUBLICATIONS

Journal Papers:

Shen, X., Dumpert, J., Farritor, S., "Robotic Highway Safety Markers," ASME/IEEE Transactions on Mechatronics, pending publication.

Conference Papers

Farritor, S., Rentchler, M., "Robotic Highway Safety Markers," Proceedings of *ASME International Mechanical Engineering Congress*, New Orleans, Louisiana, Nov. 17-22, 2002.

Blurbs:

"Can They Polka Too?" Ignition, Issue 2, Winter 2003, Transportation Research Board of the National Academies.

Presentations:

1) Highway IDEA Committee Meeting, Irvine, CA, November 14, 2003.

2) AASHTO RAC Region III Conference in Lincoln, NE, September 8, 2003.

3) AASHTO Sub-committee on Construction, Asheville, NC, August 2, 2003.

4) State of Nebraska Highway Commission, January 17, 2003.

5) "Robotic Highway Safety Markers", Department of Mechanical Engineering Seminar Series, University of California – Davis, April 10, 2003.

6) Midwest Smart Work Zone Development Initiative annual meeting, October 16, 2001.

9 PLANS FOR IMPLEMENTATION

Several contacts have been made with users of the barrel robots including the Nebraska Department of Roads, the Texas Transportation Institute, CALTRANS, Federal Highway Administration, Trafcon, the Intelligent Transportation Systems Heartland Chapter, and the Midwest Smart Work zone Development Initiative. All the above groups expressed interest in the concept pending the work to be completed in phase II of this project.

A patent application has been field and is pending with the U.S. Patent Office. The consulting firm Research Triangle Institute (RTI) was hired by the University of Nebraska to study the marketability of this project. An excerpt from their report in included:

> ***Brief Market Summary***
>
> *Estimated market size: Large: > $ 100 million*
>
> *The addressable market is large because of the extent of the road infrastructure in the U.S. With approximately 4 million miles of urban and rural roads, one can assume 0.5% of the miles are involved in construction projects at any one time. If the need for barrels is one per 25 feet, the total number of barrels deployed would be over 4 million. Traffic cones were not considered.*
>
> *Inventors cite a machine (developed by UC-Davis) that deploys and retrieves cones. Also, cones are commonly handled manually from a device attached to a truck. Both are safer than walking the highway work site, but the former may save labor. The need for a robotically controlled device for cones is somewhat weak, in our opinion. Autonomous devices, however, may save sufficient labor to worthwhile. The design challenges are daunting. The chances for causing accidents as a result of malfunction must be designed out to essentially zero.*
>
> *The invention may be patentable. No other similar U.S. patent was found, the closest being U.S. 5,722,788-Traffic delineator with wheels.*

Phase II will include the development of a user interface and ground station, transportation methods, and extensive testing. A phase II proposal will be submitted that will include tasks to be completed for implementation of the proposed project. An SBIR proposal is also being prepared.

10 CONCLUSIONS

Great progress was made during this 18 month project. The completion of this project, as reported in this document, demonstrates the feasibility of using robotic highway safety markers. All objectives outlined in the original proposal were met and additional achievements were made. Test results were more extensive then originally proposed with over one hundred laboratory tests of the local control system, eight field test of deployment, and at least four field tests of continuous motion.

All objectives outlined in the original proposal were met and additional achievements were made. Technical progress included first the design and construction of seven barrel robots as well as the design of a control system for individual barrel robots and one for groups of robots. The test results were more extensive then originally proposed with over one hundred laboratory tests of the local control system, eight field tests of deployment, and at least four field tests of continuous motion.

Two basic forms of motion were achieved. The first is where the robots are randomly placed on a road side. The user then designates desired positions for the barrels (e.g. taper to close right lane). Then, the robots create a plan and execute a motion to the desired final positions. The second motion was where the user designates a desired formation for the robots. The robots then autonomously maintain that formation behind a slow moving vehicle. Here, the robots match the speed of the vehicle up to 5 mph. This second motion exceeds the proposed objectives of the original phase one proposal and could be useful in slow moving maintenance operations such as asphalt overlay and lane striping.

Great technical progress was made and significant hardware was created during this phase one project. This project has demonstrated the feasibility of the concept. The follow on proposal will lead to true field testing and commercial implementation of the concept.

The test results of this project are summarized visually in movies at:

http://robots.unl.edu/projects/current/barrel_robots/index.html

The work done in this project is innovative and can have a large impact in work zone activities. This project represents a small step toward highly automated work zones. It dovetails with other work being performed in smart work zones and intelligent transportation systems. The follow on proposal for phase II funds will lead to implementation of the concept.

SHANE MICHAEL FARRITOR

Contact Information

Phone: (402) 472-5805
Fax: (402) 472-1465
Email: sfarritor@unl.edu
URL: http://robots.unl.edu

N118 Walter Scott Engineering Center
Department of Mechanical Engineering
University of Nebraska-Lincoln
Lincoln, NE 68588-0656

Professional Interests

Bio-Mechatronics
Bio-Robotics
Mechatronic Systems
Mechanical Design
Decision-Based Design Methodologies
Mobile and Industrial Robotics

Education

Massachusetts Institute of Technology Cambridge, MA
Doctor of Philosophy, Mechanical Engineering, June 1998. Thesis directed by Professor Steven Dubowsky entitled "On Modular Design and Planning for Field Robotic Systems."

Master of Science, Mechanical Engineering, May 1994. Thesis directed by David S. Kang, Ph.D. and Professor Warren Seering entitled "The Design and Development of a Three Dimensional Kinematic Simulation, Steering System, and Scientific Instrument Deployment Mechanism for a Planetary Micro-Rover."

University of Nebraska-Lincoln Lincoln, NE
Bachelor of Science, Mechanical Engineering, May, 1992.

Current Positions

University of Nebraska-Lincoln, Department of Mechanical Engineering Lincoln, NE
August 1998 to Present, Assistant Professor

University of Nebraska Medical Center, Department of Orthopaedic Surgery Omaha, NE
2001 to Present, Courtesy Assistant Professor

University of Nebraska Medical Center, Department of Surgery Omaha, NE
2002 to Present, Courtesy Assistant Professor

Experience

Field and Space Robotics Laboratory, MIT Cambridge, MA
March 1995 to June 1998, Graduate Researcher
Performed basic research and hands-on design of field robotic systems for planetary exploration

Jet Propulsion Laboratory, NASA/Cal. Tech. Pasadena, CA

1996, Visiting Researcher
Studied and designed mobile rovers and fixed-base manipulators for planetary exploration

Unmanned Vehicle Lab-Draper Laboratory Cambridge, MA
September 1992 to March 1995, Graduate Researcher
Researched the design and control of unmanned robotic vehicles

Patents

Farritor, S., Arnold, R. C., Normant, C., Elias, S., "On-board, Real-Time Measurement of Railroad Track Modulus" Disclosure filed September, 2003.

Oleynikov, D., **Farritor, S.,** Hadzialict, A., Platt†, S.R., "Micro Robots for Surgical Applications" filed July 8, 2003 – still in review.

Farritor, S., Rentschlert, M., Elder†, J., "Robotic Road Safety Markers" filed August, 19 2001– still in review.

Refereed Journal Publications

Gao†, X., **Farritor, S.,** "Delta Performance Models for Engineering Design," submitted to *ASME Journal of Mechanical Design*, Paper number MD-03-1313, still in review.

Qadi, A., Goddard, S., **Farritor, S.**, "Dynamic Voltage Scaling for Sporadic and Periodic Tasks," in submission to IEEE Transactions on Computers, February, 2004.

Zhang, J., **Farritor, S.,** "Using A Neural Network to Determine Fitness in Genetic Design," submitted to *Inverse Problems in Engineering*, in press.

Platt, S., R., **Farritor, S.**, Haider, H., "Piezoelectric Power Generation within Orthopaedic Implants," submitted to the *ASME/IEEE Transactions on Mechatronics* in press.

Shen, X., Dumpert, J., **Farritor, S.,** "Robotic Highway Safety Markers," *ASME/IEEE Transactions on Mechatronics*, in press.

Platt†, S., R., **Farritor, S.,** Haider, H., "On Piezoelectric Power Generation with PZT Ceramics," *ASME/IEEE Transactions on Mechatronics*, in press.

Mumm, E., **Farritor, S.**, Pirjanian, P., Leger C., Schenker, P., "Planetary Cliff Descent Using Cooperative Robots," *Autonomous Robots* in press.

Farritor, S., and Dubowsky, S., "Genetic Action Planning with Application to Planetary Exploration," *ASME Journal of Dynamic Systems, Measurement and Control*, Vol. 124, No. 4, pp. 698-702, December 2002.

Farritor, S., and Dubowsky, S., "On Modular Design of Field Robotic Systems," *Autonomous Robots*, Vol. 10, No. 1, pp. 57-65, January, 2001.

Refereed Conference Publications (3 reviews of full paper)

Rentschler, M., Hadzialic, A., Dumpert, J., Platt, S.R., **Farritor, S.,** Oleynikov, D., Iagnemma, K., "Theoretical and Experimental Analysis of In Vivo Wheeled Mobility," submitted to *ASME 28th Biennial Mechanisms and Robotics Conference*, September 2004.

Qadi, A., Goddard, S., **Farritor, S.**, "A Dynamic Voltage Scaling Algorithm for Sporadic Tasks," Proceedings of the 24th IEEE Real-Time Systems Symposium, Cancun, Mexico, December 2003, pp. 52-62.

Gao, X., **Farritor, S.,** "Delta Performance Models For Selection In Decision-Based Design," Proceedings of the *ASME Design Engineering Technical Conferences*, Chicago, IL, 2003.

Farritor, S., Rentchler, M., "Robotic Highway Safety Markers," Proceedings of *ASME International Mechanical Engineering Congress*, New Orleans, Louisiana, Nov. 17-22, 2002.

Pirjanian, P., Leger, C., Mumm†, E., Kennedy*, B., Garrett*, M., Aghazarian*, H., Schenker*, P., **Farritor S.,** (* indicates JPL) "Behavior-Based Coordinated Control for Robotic Planetary Cliff Descent" *IEEE International Conference on Robotics and Automation*, May 2002.

Farritor, S., and Zhang, J., "Using A Neural Network To Determine Fitness In Genetic Design," American Society of Mechanical Engineers (ASME) *Design Engineering Technical Conferences*, Pittsburgh, PA, September, 2001.

Farritor, S., Zhang, J., "A Reconfigurable Robotic System To Support Planetary Surface Operations," Self-Reconfigurable Robotics Workshop at the *IEEE International Conference on Robotics and Automation*, Seoul, Korea, 2001.

Bevly, D., **Farritor, S.,** Dubowsky, S., "Action Planning and its Application to an Experimental Climbing Robot," *IEEE International Conference on Robotics and Automation*, 2000.

Farritor, S., Hacot, H., Dubowsky, S., "Physics-based Planning for Planetary Exploration," *IEEE International Conference on Robotics and Automation*, Detroit, MI, May 1998.

Farritor, S., and Dubowsky, S., "A Self-Planning Methodology for Planetary Robotic Explorers," Proceedings of the *8th International Conference on Advanced Robotics* (ICAR), Monterey, CA, July 1997, pp. 499-504.

Farritor, S., and Dubowsky, S., "A Genetic Algorithm Based Navigation and Planning Methodology for Planetary Robotic Exploration," Proceedings of the *American Nuclear Society's (ANS) 7th Topical Meeting on Robotic and Remote Systems*, Augusta, GA, 1997.

Farritor, S., and Dubowsky, S., "On the Design of Rapidly Deployable Field Robotic Systems," Proceedings of the *ASME Design Engineering Technical Conferences*, Irvine, CA, 1996.

Farritor, S., Dubowsky, S., Rutman, N., and Cole, J., "A Systems Level Modular Design Approach to Field Robotic Systems," Proceedings of the *IEEE International Conference on Robotics and Automation*, Minneapolis, MN, 1996.

Medical Conference Publications (Refereed Abstract)

Oleynikov, D., Rentschler†, M., Hadzialic, A., Dumpert, J., Platt, S.R., **Farritor, S.,** "In Vivo Camera Robots Provide Improved Vision for Laparoscopic Surgery," Computer Assisted Radiology and Surgery (CARS), Chicago, IL, June 23 - 26, 2004.

Oleynikov, D., Rentschler, M., Hadzialic, A., Platt, S.R., **Farritor, S.,** "Miniature Robots Can Assist In Laparoscopic Cholesyctectomy" *Society of American Gastrointestinal Endoscopic Surgeons (SAGES) Scientific Conference*, Denver, CO, March 31-April 3, 2004.

Rentschler, M., Hadzialic, A., **Farritor, S.,** Platt, S.R., Oleynikov, D., "In Vivo Robots for Laparoscopic Surgery "*Medicine Meets Virtual Reality*, Newport Beach, CA, Jan. 15-17, 2004.

Haider, H., Platt, S.R., **Farritor, S.M.,** Garvin, K.L., "Self-powered computers within prosthetic joints – is it time?" *Proceedings of American Academy of Orthopaedic Surgeons*, 71st Annual Meeting, March 10 - 14, 2004.

Haider, H., Platt, S.R., **Farritor, S.M.,** Garvin, K.L., "Self-Powered Computers Within Prosthetic Joints – Would Time Degradation Of Piezoelectrics Performance Be An Obstacle?" *Proceedings of the Orthopedics Research Society*, 2003.

Haider, H., Platt, S.R., **Farritor, S.M.,** Garvin, K.L., "Can Piezoelectric Elements Generate Sufficient Electrical Power within Smart Arthroplasty Implants?" *16th Annual Symposium of the International Society for Technology in Arthroplasty (ISTA),* San Francisco, CA, Sept., 2003.

Haider, H., Platt, S.R., **Farritor, S.M.,** Garvin, K.L., "The Feasibility Of Using Piezoelectric Ceramics To Generate Electrical Power In Total Joint Replacement Implants" *Proceedings of the Orthopedics Research Society*, 2002.

Other Conference (Refereed Abstract)

Norman, C., **Farritor, S.,** Arnold, R., Elias, S.E.G., "Preliminary Design Of A System To Measure Track Modulus from A Moving Railcar," Proceedings of *Railway Engineering 2003,* London, England, January 2003.

Mumm, E., Farritor, S., Huntsberger, T., Schenker, P., "Analysis of Behavior Based Control for Planetary Cliff Decent Using Cooperative Robots," Proceedings of the *Unmanned Ground Vehicle Technology Conference, SPIE AeroSense Symposium*, Orlando, FL, April 2003.

Zhang†, J., **Farritor, S.,** "A Modular Robotic Infrastructure to Support Human Mars Exploration" Submitted to *AIAA Space 2000 Conference*, Long Beach, CA, September, 2000.

Kaliardos, W., Cosgrove, M., Chow, T., Steiner, S., **Farritor, S.,** "Companion - Overview of a Telerobotic Ground Vehicle," *Association for Unmanned Vehicle Systems International (AUVSI),* Orlando, FL, 1996.

12 REFERENCES

Anon. "The 11 Best Ways to Improve Work Zone Safety." Better Roads v60, n7 (1990): p20-23.

Advanced Highway Maintenance and Construction Technology (AHMCT) website: http://www.ahmct.ucdavis.edu/ 2002.

Belta, C., Kumar, V., "Motion Generation for Formations of Robots: A Geometric Approach," IEEE International Conference on Robotics & Automation, pp. 1245-1250, May 2001.

Belta, C., Kumar, V., "Trajectory Design for Formations of Robots by Kinetic Energy Shaping," IEEE International Conference on Robotics & Automation, pp. 2593-2598, May 2002.

Borenstein, J., Koren, Y., "The Vector Field Histogram-Fast Obstacle Avoidance for Mobile Robots," IEEE Trans on Robotics and Automation, Vol. 7, No. 3 June 1991.

Brooks, R., "A Robust Layered Control System for a mobile robot," IEEE Transactions on Robotics and Automation, Vol. 2, No. 1, 1986.

Desai, J., Ostrowski, J., Kumar, V., "Controlling formations of multiple mobile robots," IEEE International Conference on Robotics & Automation, pp. 2864-2869, May 1998.

Egerstedt, M., Hu, X., "Formation Constrained Multi-Agent Control," IEEE International Conference on Robotics & Automation, pp. 3961-3966, May 2001.

Farritor S., Hacot H. and Dubowsky S., "Physics-Based Planning for Planetary Exploration" IEEE Intl. Conference on Robotic and Automation, 1998.

Feng, X., and Velinsky, S.A. "Distributed Control of a Multiple Tethered Mobile Robot System for Highway Construction and Maintenance" Microcomputers in Civil Engineering, Vol. 12, pp. 383-392, November, 1997.

Fierro R., Das A.K., Kumar V., Ostrowski J.P., "Hybrid Control of Formations of Robots," IEEE Intl. Conference on Robotic and Automation, 2001.

Gumtau, R. "Richard Gumtau on Traffic Control and Work Zones." Better Roads v63, n9, 1993.

Gentili, F., Martinelli, F., "Robot group formations: a dynamic programming approach for a shortest path computation," IEEE Intl. Conf. on Robotics & Auto., pp. 3152-57, 2000.

Gold, T., Archibald, J., Frost, R., "A Utility Approach to Multi-Agent Coordination," IEEE International Conference on Robotics & Automation, pp. 2052-2057, April 2000.

Hood, F. Hoff, W., King, R., "Evaluation of an Interactive Technique for Creating Site Models from Range Data", ANS Meeting on Robotics and Remote Systems, 1997.

Kang, W., Xi, N., Sparks, A., "Formation Control of Autonomous Agents in 3D workspace," IEEE International Conference on Robotics & Automation, pp. 1755-1760, April 2000.

Khatib, O. "Real-time obstacle avoidance for manipulators and mobile robots," International Journal of Robotics Research, 5 (1), 90-98, 1986.

Lasky, T., Ravani, B. "Sensor-based Path Planning and Motion Control for a Robotic System for Roadway Crack Sealing." IEEE Trans. on Control Systems Tech. v8, n4 (2000): pp. 609-622.

Mohri, A., Yamamoto, M., Marushima, S., "Collision-Free Trajectory Planning for Two Manipulators Using Virtual Coordination Space," IEEE Intl Conf on Robotics & Automation, pp. 674-9, 1993.

Murphy, R., Marzilli, A., Hughes, K., "When to explicitly Re-plan Paths for Mobile Robots," IEEE International Conference on Robotics & Automation, pp. 3519-25, 1997.

Ollis, M., Stentz, A., "Vision-Based Perception for an Autonomous Harvester" Proceedings of IEEE/RSJ Intl. Conf. on Intelligent Robotic Systems, Vol. 3, 1997, pp. 1838 - 1844.

Ravani, B., and Velinsky, S.A. West, T.H. "Requirements for Application of Robotics and Automation in Highway Maintenance and Construction Tasks." ASCE Specialty Conference on Robotics for Challenging Environments (1994): p356-364.

Rihani, Rami A., and Bernold, Leonhard E. "Telerobotic Pavement Marker Application." ASCE Conference on Robotics for Challenging Environments (1996): p171-177.

Shah, S. "New Work Zone Safety Devices." Proceedings of the ASCE 3rd International Conf. on Applications of Advanced Technologies in Transportation Engineering (1993): p308-315.
Shen, X., *Control of Robotic Highway Safety Markers*, Masters Thesis, Department of Mechanical Engineering, University of Nebraska-Lincoln, May 2003.
Stilwell, D., Bishop, B., "A Framework for Decentralized Control of Autonomous Vehicles" IEEE International Conference on Robotics & Automation, pp. 2358-2363, April 2000.
Todt, E., Raush, G., Suarez, R., "Analysis and Classification of Multiple Robot Coordination Methods," IEEE Intl. Conference on Robotics & Automation, pp. 3158-3163, April 2000.
Traynowicz, M., Personal Correspondence, Traffic Research Engineer, Nebraska Department of Roads, February 11, 2002.
Velinsky, S.A., "Heavy Vehicle System for Automated Pavement Crack Sealing," Heavy Vehicle Systems, International Journal of Vehicle Design, Vol. 1, No. 1, pp. 114-128, 1993.
West, Thomas H., and Velinsky, Steven A., and Ravani, Bahram. "Advanced Highway Maintenance and Construction Technology Applications." TR News (1995): p17-23.
White, T. "Evolving Automation in the Asphalt Paving Industry." TR News n176 (1995): p4-6.
Woo, D. "Robotics in Highway Construction" Public Roads v58, n3 (1995): p26-30.
Ye, W., Vaughan, R., Sukhatme, G., Heidemann, J., Estrin, E., Mataric, M., "Evaluating Control Strategies for Wireless-Networked Robots Using an Integrated Robot and Network Simulation," IEEE Intl. Conference on Robotics & Automation, pp. 2941-2947, 2001.
Zhou, Tong, and West, Thomas. "Assessment of the State-of-the-Art of Robotics Applications in Highway Construction and Maintenance." Proc. of the 2nd Intrl. Conf. on Applications of Advanced technologies in Transportation Engineering (1991): p56-60.

DEVELOPMENT OF AN ADAPTIVE DAMPER FOR CABLE VIBRATION CONTROL

IDEA Program Final Report
Contract Number: NCHRP-92

Prepared for
The IDEA Program
Transportation Research Board
National Research Council

Principal Investigator: C. S. Cai
Research Assistant: W. J. Wu

January 2005

Department of Civil and Environmental Engineering
Louisiana State University
Baton Rouge, LA 70803

TABLE OF CONTENTS

EXECUTIVE SUMMARY

For many cable-stayed bridges in the U.S. and worldwide, large amplitude vibration of cables due to wind-rain induced vibrations has been reported recently. This issue has raised great concerns since excessive cable vibrations will be detrimental to the long-term health of bridges. To address this problem, countermeasures such as changing the cable aerodynamic properties, adding crossing ties/spacers or providing mechanical dampers have been initiated to increase the cable damping.

The goal of this study is to develop the concept of an adjustable Tuned Mass Damper – MagnetoRheological (TMD-MR) damper system that can be adjusted to cope with different external loading conditions. The TMD-MR damper system has two combined advantages. On one hand, as a TMD, the TMD-MR damper system can be attached to any place along the cable. On the other hand, by using MR fluids, the damping and/or stiffness of the TMD-MR damper system is adjustable. As a result, a high damping efficiency will be achieved regardless of the frequency and/or mode sensitivity of the traditional TMD dampers and the position restriction of the traditional MR dampers in cable applications.

Experiments on MR dampers, cable-MR damper system, cable-TMD damper system, and cable-TMD-MR damper system were carried out in the laboratory. MR damper design and dynamic characteristics analysis of the cable-TMD-MR damper system were performed. Major tasks are summarized below.

- Literature about wind-rain induced cable vibration, cable dynamics, cable vibration control, MR fluids and MR dampers were reviewed.
- Performance of two different MR dampers manufactured by Lord Corporation was tested with different loading conditions.
- Basic dynamic characteristics were measured for a 7.16 m steel cable.
- Dynamic characteristics of the cable-MR system were measured to verify the vibration reduction effectiveness of MR dampers to the cable.
- Small size MR dampers were designed and manufactured by the research team since appropriate MR dampers that meet the requirement of the TMD-MR damper system were not commercially available.
- Theoretical discussion on the performance of the cable-TMD-MR damper system was conducted.
- Dynamic characteristics of the cable-TMD-MR damper system were measured to confirm its vibration reduction effectiveness to the cable.

In the conclusion, the research team strongly suggests that the proposed TMD-MR damper system be further studied for field applications on actual cables. This damper system is believed to address the low damping problem of cables practically and cost-effectively. Dynamic characteristics of the cable before and after the installation of dampers should be monitored and compared to verify the damping effectiveness in the field study.

IDEA PRODUCT

This NCHRP-IDEA study has developed the concept of an adjustable Tuned Mass Damper – MagnetoRheological (TMD-MR) damper system and demonstrated the effectiveness of this damper to reduce the cable vibration, regardless of the loading conditions. This adjustable TMD-MR damper has combined advantages of both TMD dampers and MR dampers. On one hand, a TMD damper can be put any place along the cable, which overcomes the deficiency of conventional mechanical dampers; on the other hand, a MR damper can provide continuously adjustable damping and also it can change the stiffness in a small range, which can help the whole system be effective under different vibration frequencies. As a result, high damping efficiency can be achieved regardless of both the frequency/mode sensitivity of the TMD dampers and the position restriction of the MR dampers.

CONCEPT AND INNOVATION

Background

As one of the most common but damaging vibration phenomena, wind-rain induced cable vibration has been reported worldwide (Hikami 1986, Matsumoto et al. 1992, Tabatabai and Mehrabi 1999, Main and Jones 2001). Large-amplitude vibrations on the order of 1 to 2m of stay cables have been observed under certain combinations of light rain and moderate wind speeds of about 10 to 15 m/s. Wind-rain induced cable vibrations can cause fatigue problems and damage cable itself and connections at the bridge deck and towers. This has raised great concerns in the bridge community and has been a cause of deep anxiety for the observing public. According to previous researches, a water rivulet on the upper windward surface and the formation of the axial flow in the near wake of the cables are believed to be the main causes of wind-rain induced vibrations (Matsumoto et al., 1995).

To address the severe vibration problem, researchers and engineers have been modestly successful by trial-and-error methods to increase the cable damping, such as by treating cable surface to improve its aerodynamic properties (Flamand 1995, Phelan et al. 2002), adding crossing ties/spacers (Langsoe and Larsen 1987) or providing mechanical dampers (Tabatabai and Mehrabi 2000).

Mechanical dampers have been proven a useful method to reduce cable vibration. However, the reduction effect is not optimal since the traditional mechanical dampers are constrained close to the lower end of cables. TMDs can overcome this restriction and it was experimentally investigated and recommended for cable vibration reduction (Tabatabai and Mehrabi 1999). However, this recommendation was based on the

observed damping effect of TMD dampers on the free vibration of a cable in the first mode. It has been found that the wind-rain cable vibrations are often related to higher mode vibrations. Therefore, A TMD designed for the first mode vibration is most likely not effective for higher mode vibrations since the TMD effectiveness is frequency sensitive.

Objectives

The objective of this study is to develop the concept of an adjustable TMD-MR damper system that can be adjusted to deal with different cable vibrations, regardless of the vibration frequency/mode. The adjustable TMD-MR damper system will be designed using controllable MR fluids.

INVESTIGATION

Investigation Approach

As an important step of this study, a literature review was carried out in the area of MR dampers, wind-rain induced cable vibration, cable dynamic characteristics and other related topics.

To fully understand the dynamic characteristics of cable system with attached TMD-MR dampers and for comparison consideration, it is very important to investigate the individual MR damper, pure cable dynamic property, cable dynamic property with a TMD, and cable dynamic property with a MR damper first. Since no commercial MR dampers can match the experimental requirements, the investigation group designed and manufactured two types of MR dampers. One of them was discarded because of its maintenance problem. Several prototypes of the second design were manufactured with different sizes and one prototype was chosen for the TMD-MR damper system. Finally, under the guidance of some preliminary theoretical results, dynamic characteristics of the cable system with the TMD-MR damper hung on the cable were investigated experimentally.

Investigation of Individual MR Dampers

MR controllable fluids are among those new materials introduced into civil engineering applications in recent years. MR fluids typically consist of micron-sized,

magnetically polarizable particles dispersed in a carrier medium such as water, mineral or silicone oil. An essential characteristic of MR controllable fluids is their ability to reversibly change from a free-flowing, linear viscous fluid to a semi-solid with controllable yield strength in milliseconds when exposed to a magnetic field. MR fluids appear to be attractive for civil engineering applications in controllable fluid dampers because their large output forces, stable performance to temperature variations and impurities, low power supply requirement, and quick response (Carlson 1994, Carlson and Weiss 1994, Carlson et al. 1995).

Though the researches and applications of MR dampers have attracted much attention in civil engineering community, the main previous effort focuses on structures control under seismic excitation. To the investigators' knowledge, there are just a few publications and online resources about the use of MR dampers to reduce the cable vibrations (Johnson 1999a and 1999b, Lou et al. 2000, Christenson 2002). The Dongting Lake Bridge that was finished two years ago in China is the first application of MR dampers for cable vibration control. There is an ongoing similar application for Sutong Bridge over the Yangtze River in China (Lord Corporation, 2004). The Sutong Bridge will be the longest cable stayed bridge in the world with a span length of 1088 m.

Two kinds of MR dampers made by Lord Corporation were tested to obtain their performance curves before they were used to reduce cable vibration. Some relative parameters provided by the company are listed in Table 1. Experiments on the RD-1097-01 MR damper are presented in detail because its output damping force is more suitable for the present cable application than RD-1005-3.

Table 1: Basic Data for MR damper from Lord Corporation

	RD-1005-3	RD-1097-01
Maximum Extension (mm)	53	58
Body Diameter (mm)	41	32
Weight (N)	8	5
Electrical Characteristics:		
Input Current (continuous)	1 amps maximum	0.5 amps maximum
Input Current (intermittent)	2 amps maximum	1.0 amps maximum
Damper Force:		
2 in/sec at 1 amp	>2224 N	>98 N
8 in/sec at 0 amp	<667 N	<9 N

Universal Test Machine (UTM) 5P was used to investigate the two dampers as shown in Photograph 1. This machine has a maximum output force of 5kN. Dampers were tested vertically in the machine frame using a displacement control method with an amplitude of 10mm or 5mm. The force and displacement time series data were read by the computer controlled data acquisition system every 0.01 or 0.02 seconds. Generally, experiments stopped automatically after 20 cycles. The velocity of the MR damper was obtained from the displacement with a forward-difference approximation. An ampere meter and a Wonder Box device controller were connected in series with the MR damper to measure and adjust the current in the MR damper. Different experimental parameters were considered including different working temperatures, loading wave types, loading frequencies and currents provided to the MR dampers.

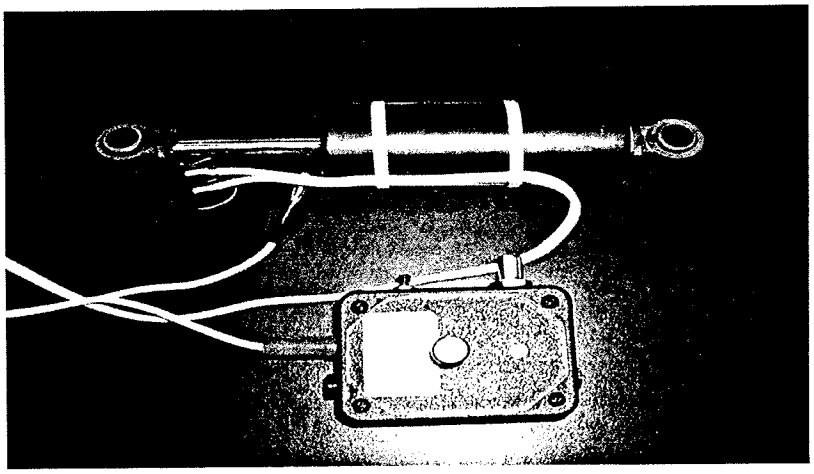

(a) Damper and Wonder Box Device Controller

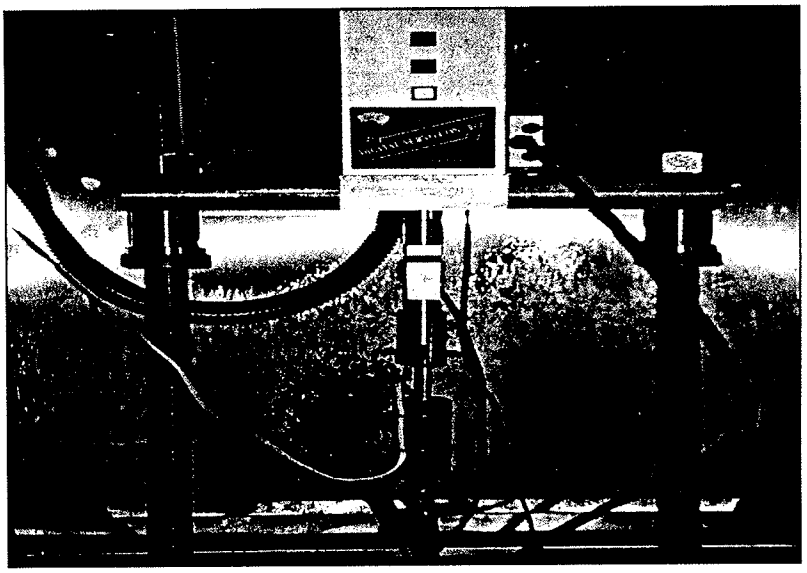

(b) RD-1005-3 in Loading Frame

Photograph 1: Damper and Loading Set-up

MR Damper Performance with Different Currents

Effects of electric currents inside the MR damper on the damper performance are discussed in this part. Eight current levels were considered as 0A, 0.05A, 0.1A, 0.15A, 0.2A, 0.3A, 0.4A and 0.5A. Presented here are some typical performance curves under a sine-loading wave with a constant loading frequency of 1Hz, an amplitude of 10mm, and an experiment temperature of 20°C.

From Fig. 1(a), we can observe that the maximum output damping force is about 10N with a current of 0A, which is called passive mode of the MR damper, and about 80N when the current increases to 0.50A. Therefore, the ratio between the peak output damping force at the maximum current to the one at passive mode, or called the dynamic range of the MR damper, is 8. Fig. 1(b) shows that the curve of displacement versus output damping force is almost a rectangle. From the point of view of energy dissipation, the larger displacement-force curve loop can dissipate more energy since the area of the loop represents the energy dissipated in each cycle. Therefore, with a larger current, the MR damper can dissipate more energy for each cycle. According to Fig. 1(c), the curve of the velocity versus the output damping force can be roughly expressed with some piecewise linear functions. From Fig. 1(d), the relationship curve between the displacement and velocity is almost an ellipse, as we expected. The relationship between the maximum output damping force and the current input is plotted in Fig. 2.

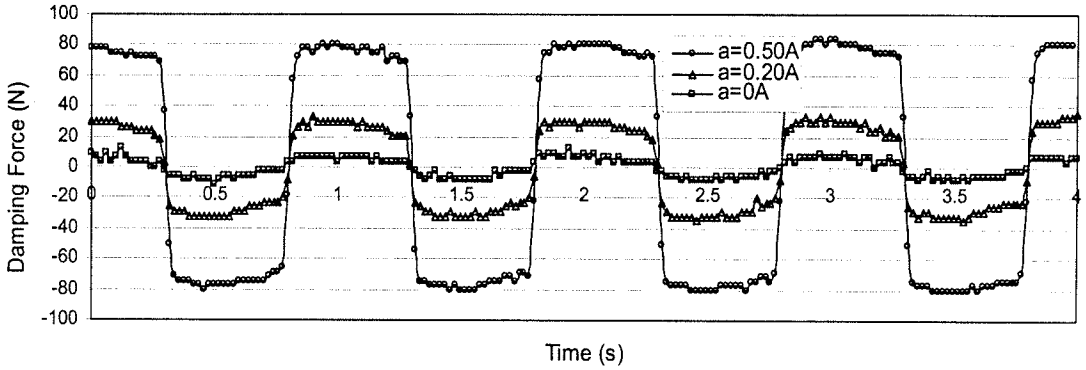

(a) Damping Force Time Series

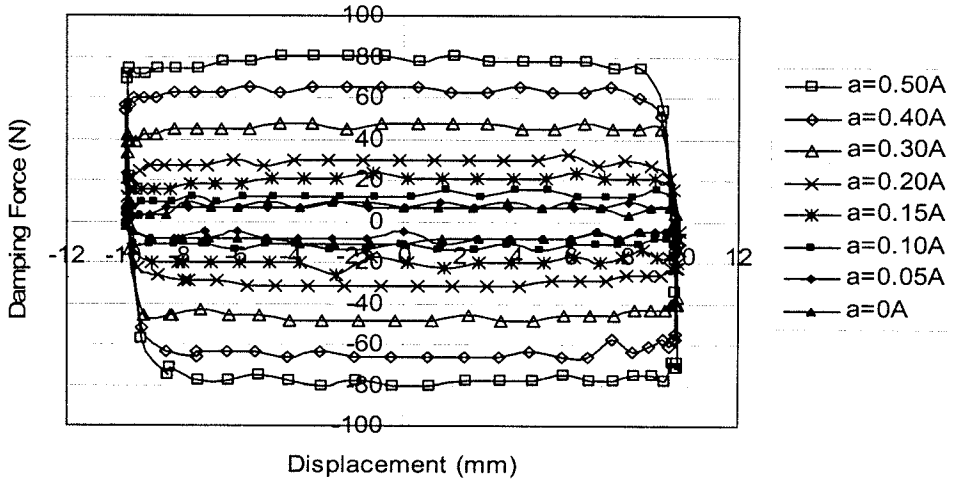

(b) Damping Force versus Displacement

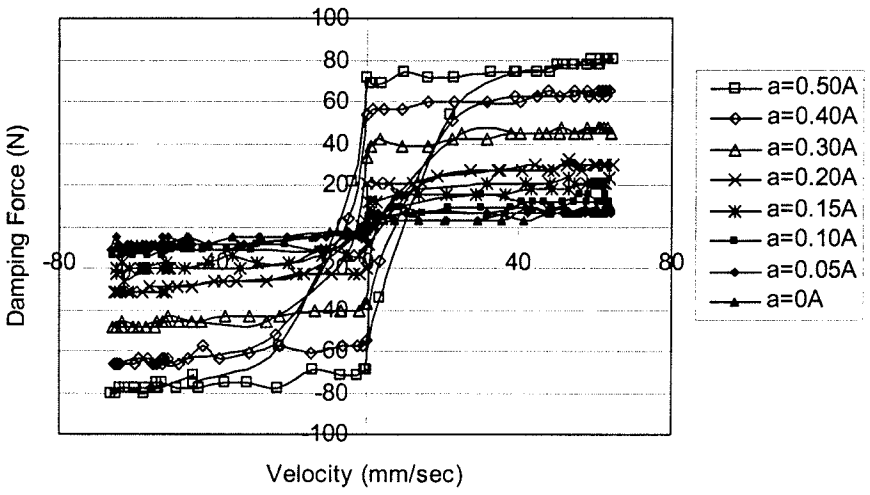

(c) Damping Force versus Velocity

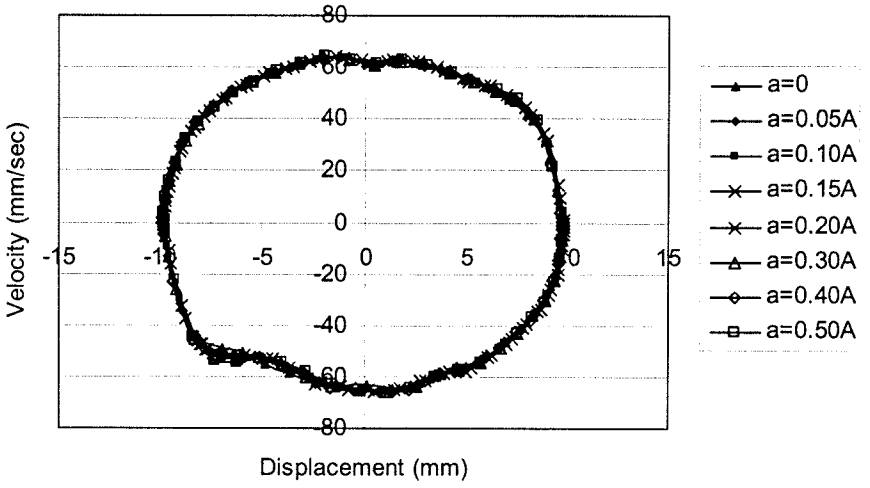

(d) Velocity versus Displacement

Fig. 1: Performance Curve of MR Damper with Different Current

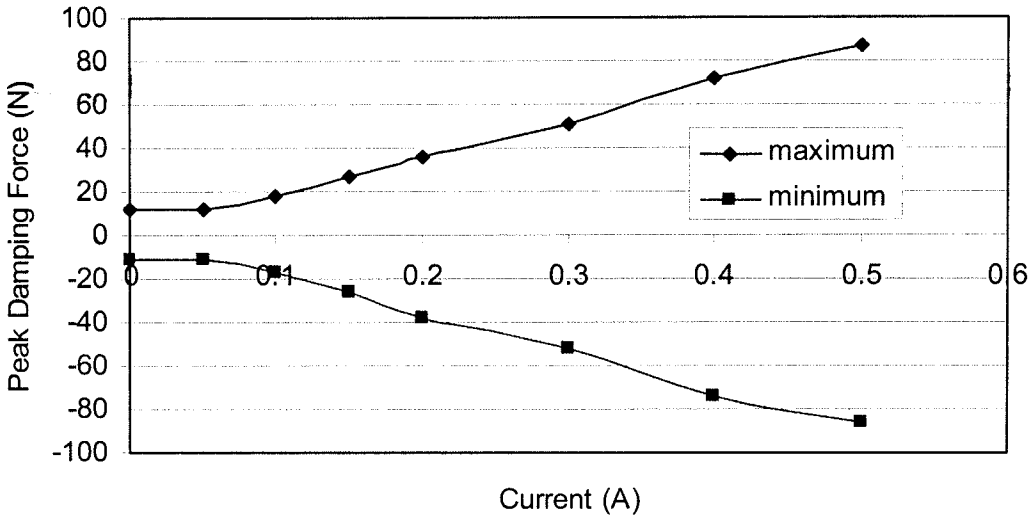

Fig. 2: Peak Output Damping Force versus Current

MR Damper Performance with Different Frequencies

Effects of the loading frequencies on the damper performance are discussed in this part. Five loading frequencies are chosen as 0.5, 1, 2, 2.5 and 5Hz. The currents inside the MR damper chosen to discuss are indicated in the following figures. All the other parameters are the same as in the previous section. In the following figures, "D" means displacement, "F" means output damping force, and "V" means velocity.

From Fig. 3, it can be observed that with the increase of the current, the effect of loading frequency on the output damping force-displacement relationship decreases. However, as shown in Fig. 4, the damping force-velocity relationship is more sensitive to the loading frequency.

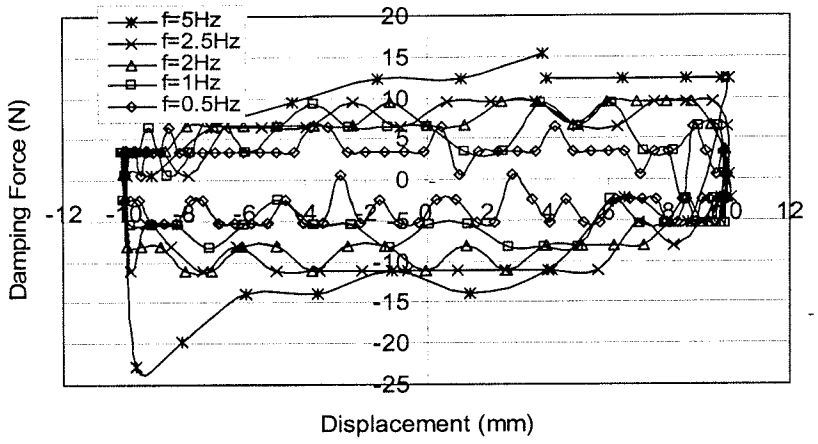

(a) 0A Current

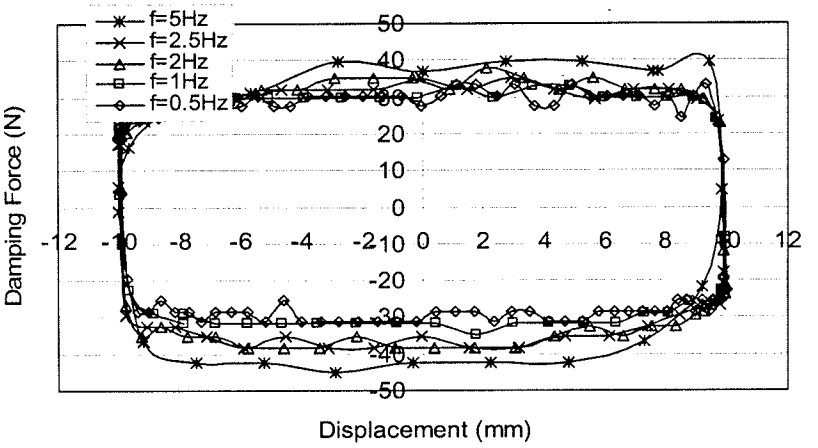

(b) 0.2A Current

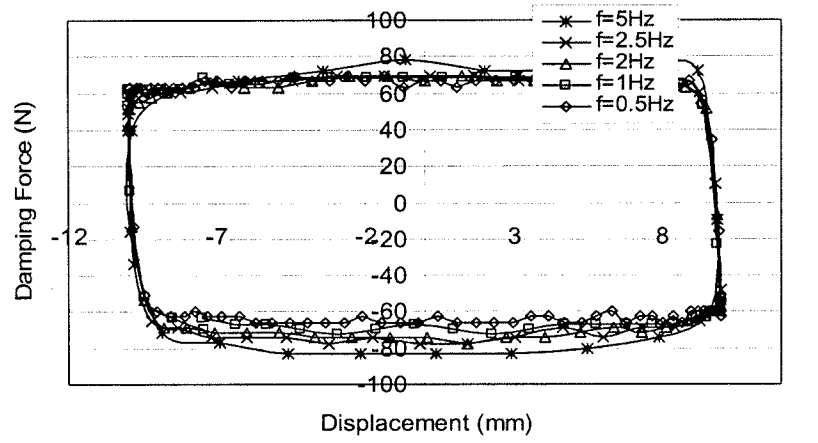

(c) 0.4A Current

Fig. 3: D-F Curve with Different Frequency at Constant Current: (a) 0A, (b) 0.20A, (c) 0.40A

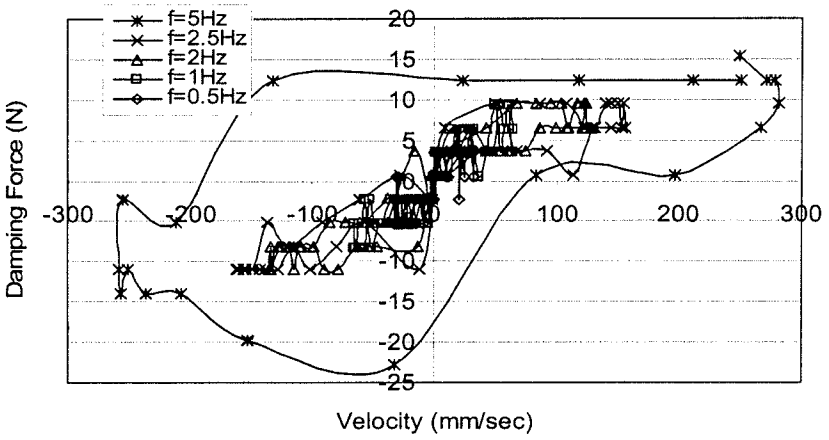

(a) 0A Current

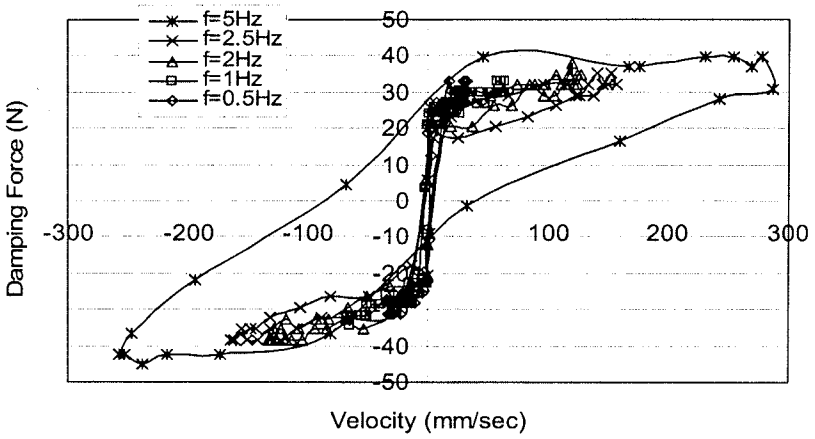

(b) 0.2A Current

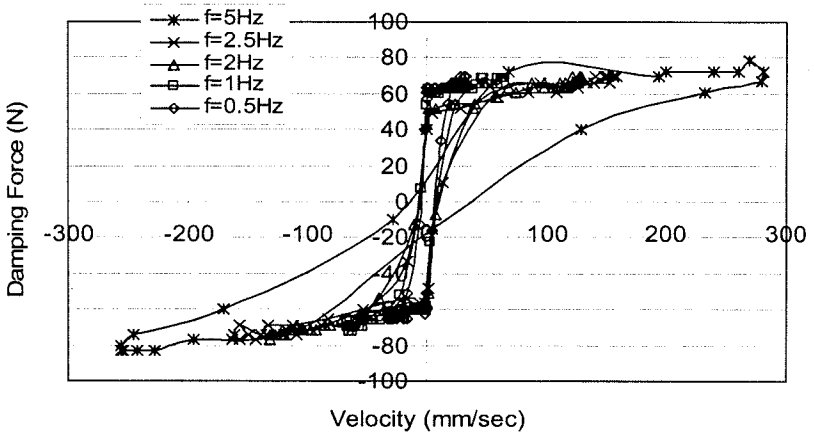

(c) 0.4A Current

Fig. 4: V-F Curve with Different Frequency at Constant Current: (a) 0A, (b) 0.20A, (c) 0.40A

MR Damper Performance with Different Loading Waves

Effects of loading types (simulated using different loading waves) on the damper performance are discussed in this part. Three loading waves are chosen as sine, triangle and pulse waves as shown in Fig. 5(a). All the other experimental parameters are the same as in the previous section, unless specified differently. In the following figures, the current is 0.4A and the loading frequency is 1Hz.

From Fig. 5(b), we can observe that the corresponding output damping force of the triangle-loading wave is less than that of the sine-loading wave. For the pulse-loading wave, the output damping force is also in the form of a pulse wave. From Fig. 5(c), we can observe that, in the case of the pulse-loading wave, the displacement-force curve is a curved quadrangle that is much smaller than the rectangle curves of the other two loading cases. Since the peak velocity of the pulse-loading wave is much larger than (and is thus out of range of) the other two cases, the corresponding curve of the pulse-loading wave is not plotted in Fig. 5(d) and 5(e). From these two figures, it can be observed that the velocity-force curve of the sine-loading wave is flatter than that of the triangle-loading wave. The ellipse displacement-velocity curve loop for the sine-loading wave is larger than that of the triangle-loading wave.

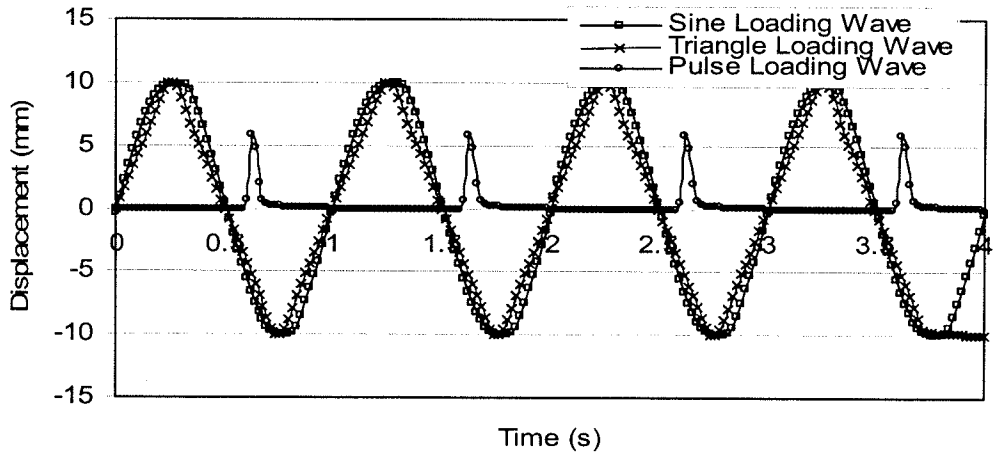

(a) Displacement Time

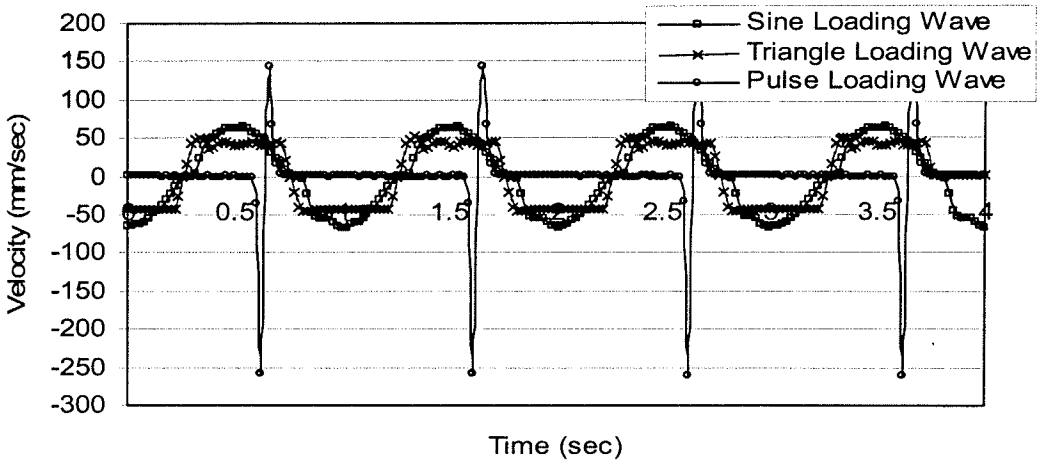

(b) Damping Force Time Series

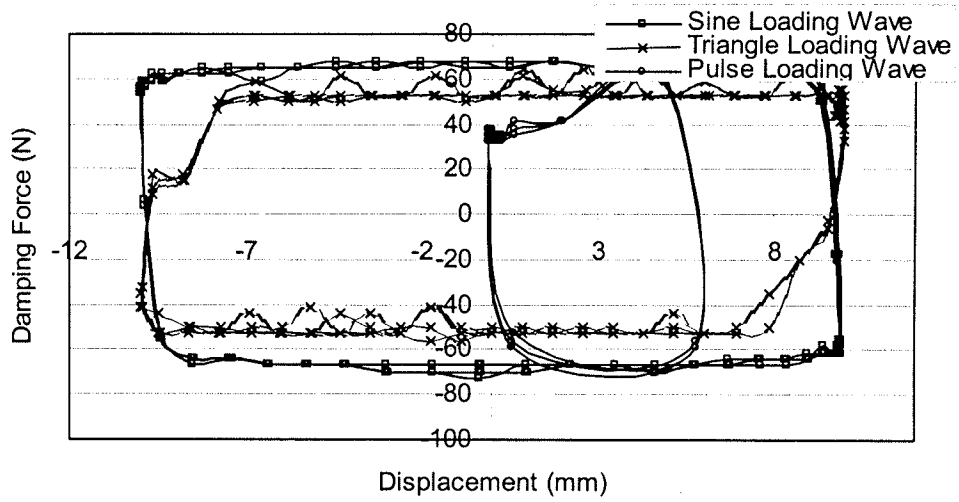

(c) Damping Force versus Displacement

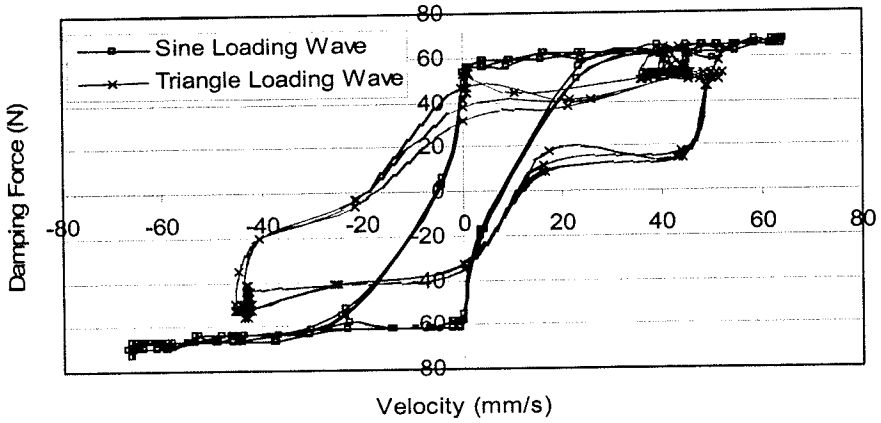

(d) Damping Force versus Velocity

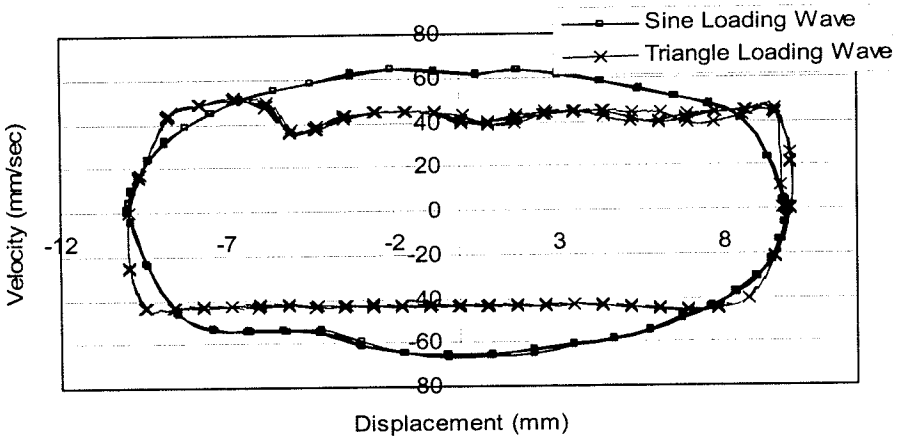

(e) Velocity versus Displacement

Fig. 5: Performance Curve with Different Loading Waves

MR Damper Performance with Different Temperatures

Effects of working temperatures on the damper performance are discussed in this part. The experimental temperatures were set to 0°C, 10°C, 20°C, 30°C, 40°C and 50°C. The currents and frequencies were varied the same way as in the previous tests. Only the sine-loading wave was investigated.

From Fig. 6, we can observe that temperature does have some effect on the performance curve of the MR damper. With the increase of the temperature, the output damping force decreases nonlinearly. The damping force-displacement curves of temperatures at 0°C, 10°C and 20°C are clustered into one group and the other three cases, 30°C, 40°C and 50°C are clustered into another group. Similar observations can be made from the velocity-force curves as shown in Fig. 7, but not as obvious as in Fig. 6. More experimental results are given in Appendix A.

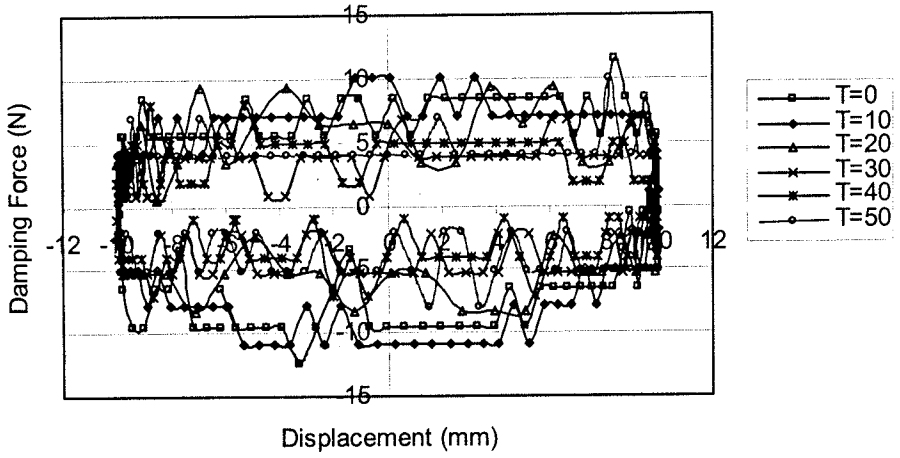

(a) 0A Current

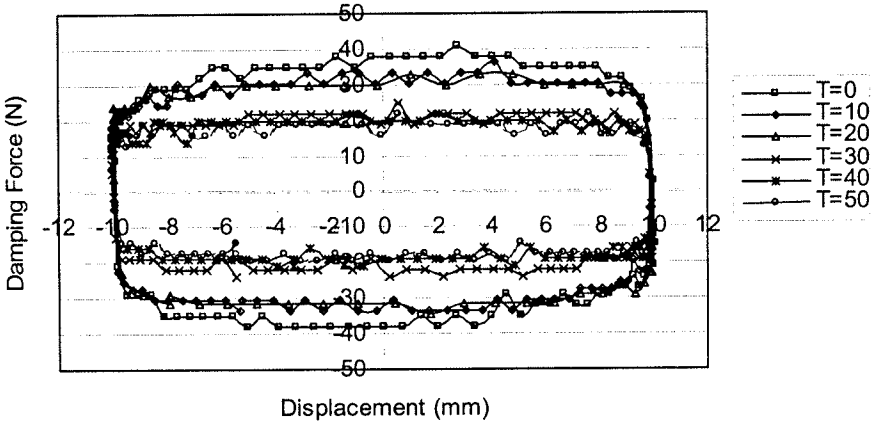

(b) 0.2A Current

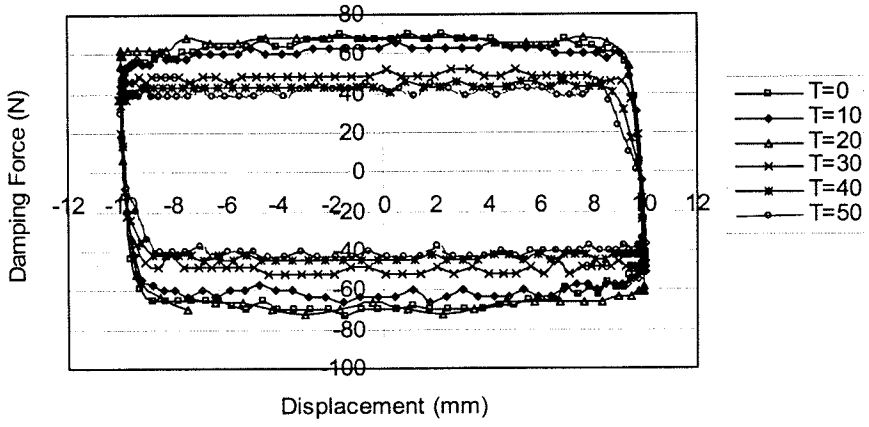

(c) 0.4A Current

Fig. 6: D-F Curve with Different Temperature: (a) 0A; (b) 0.2A; (c) 0.4A

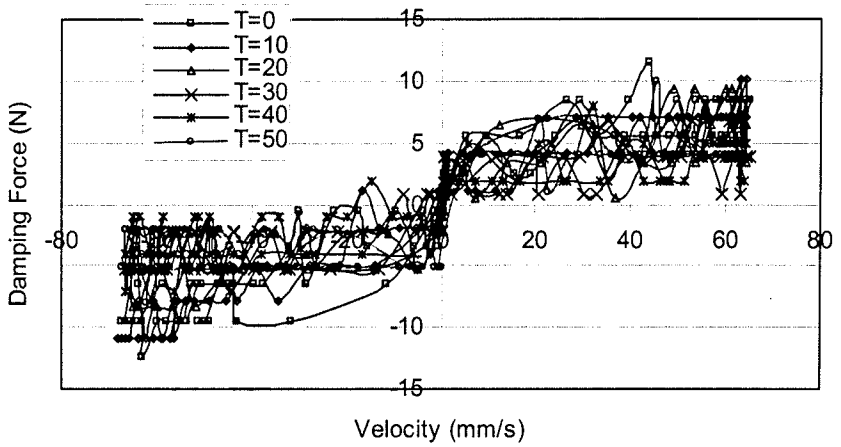

(a) 0A Current

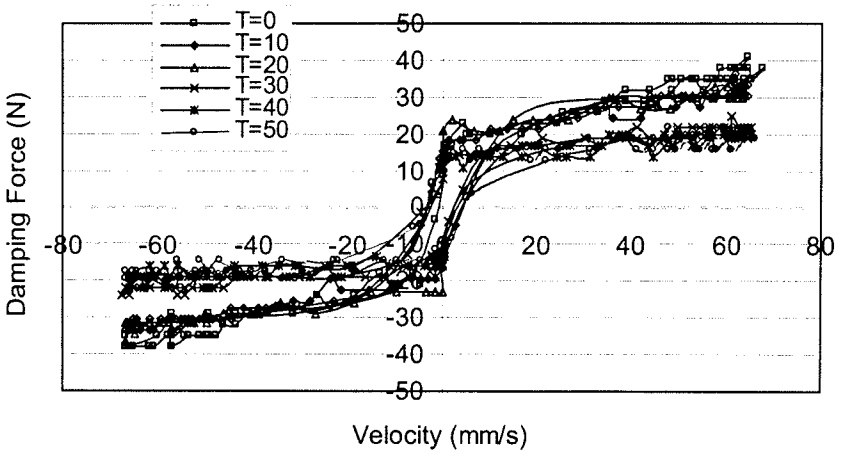

(b) 0.2A Current

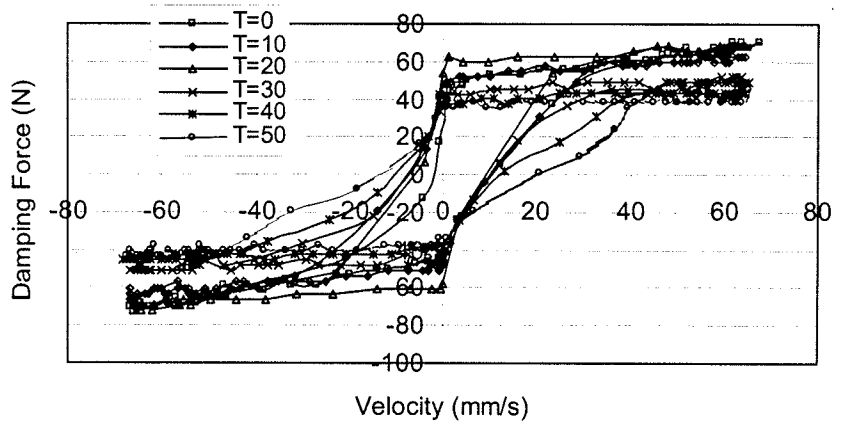

(c) 0.4A Current

Fig. 7: V-F Curve with Different Temperature: (a) 0A; (b) 0.2A; (c) 0.4A

Cable Vibration Control with MR Dampers

Scaling Theory for Model Cable

Generally speaking, scaling factors should be decided accurately according to the scaling principles to maintain the similarities for the majority parameters between the prototype cable and the test model though it is not entirely possible to achieve the similarities for all the parameters. Several different scaling criteria have been proposed for model experiments in the literature. Since there is a wide range of actual cable parameters, and there is no particular prototype in this investigation, we just need to verify that the corresponding prototype stay cable is not too abnormal from the "averaged" value. As stated in Tabatabai and Mehrabi's (1999) report, the average length and outside diameter of cables in their database are 128 and 0.182 meters. The minimum, maximum, and average inclination angles are 19, 82, and 38 degrees, respectively. The minimum and average first mode frequencies are approximately 0.26Hz and 1.15Hz, respectively. The scaling criterion used here is pretty much the same as Tabatabai and Mehrabi's (1999), which means that the scaling factor for velocity between the prototype and the model is 1 and for the length dimension is n, namely 8 in our study. Based on these two scaling factors, scaling factors for other associated parameters can be calculated by physical relationships. Table 2 provides information about the model cable parameters used in the experiments. Parameters about the corresponding prototype cable can be calculated according to Tables 2 and 3.

Table 2: Typical Model Parameters

Frame Distance (l)	7.0 m	Frame Height (h)	1.40 m
Cable Length (L)	7.16 m	Cable Angle (α)	11.27°
Cable Area (A)	98.7 mm^2	Axial Stress (σ)	162.7 Mpa
Cable Number (N)	1	Axial Force (T)*	16064.5 N

*: These parameters may change according to different experiments.

Table 3: Dynamic Scaling Relationships (Tabatabai and Mehrabi, 1999)

Parameter	Scaling factor (model/ prototype)
Dimension	1/n
Area	$1/n^2$
Volume	$1/n^3$
Young's Modulus	1
Material Strength	1
Density	1
Poisson's Ratio	1
Damping Ratio	1
Spring Constant	1/n
Mass	$1/n^3$
Signal Frequency	n
Dynamic Time	1/n
Displacement	1/n
Velocity	1
Acceleration	n
Stress	1
Strain	1
Force	$1/n^2$
Energy	$1/n^3$

Test Setup and Equipments

Fig. 8 shows the setup of the cable model system. The one strand steel stay cable is composed of seven wires with a cross section of 98.7mm^2. Both ends of the cable are anchored to the frames with different heights so that the two ends can be considered as fixed. Since the lower end goes though a hydraulic jack before it is anchored, an adjustable tension force can be put on the cable. Nine tension forces are chosen to measure the vibration control effect of the added MR damper under different tension forces. The geometric relation of some specific points is shown in the figure. As indicated in the figure, point D is the middle point, B and F are the 1/4th points, and C and E are the other two 1/3rd points of the stretched cable. Those points are installation positions for external vibration loadings, the damping device and the measuring sensors.

Photographs 2 through 7 show the equipments used in the experiments. V408 vibrator and PA100E CE amplifier purchased from Ling Dynamic Systems Ltd were used to generate and amplify the forced vibration. Hydraulic jack was used to provide axial tension force. PCB model 352C22 accelerometers and model 480B21 signal conditioner purchased from PCB Piezotronics Inc., and Photon data acquisition from Dactron Incorporated were used to measure, amplify and acquire the acceleration signals, respectively. Photograph 8 shows the damper connected to the cable.

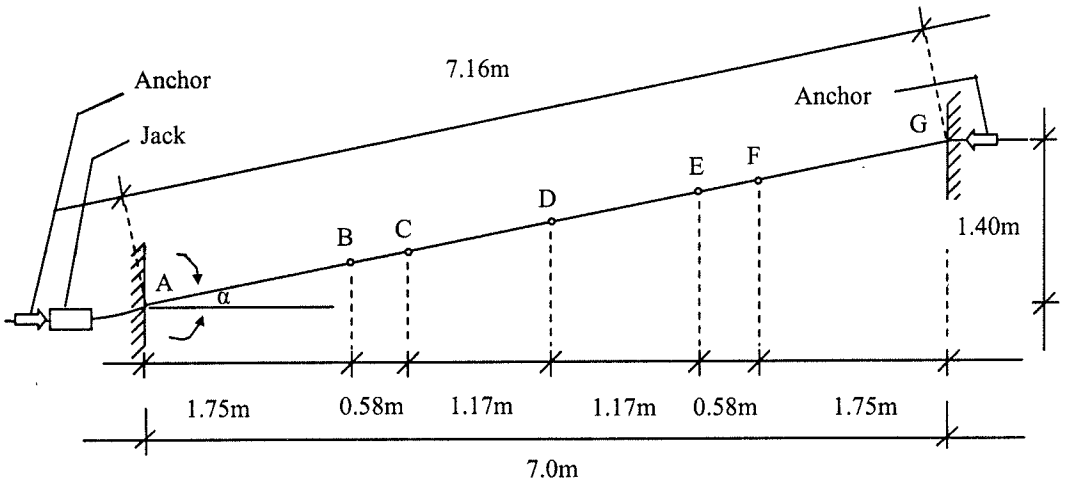

Fig. 8: Experimental Cable Setup

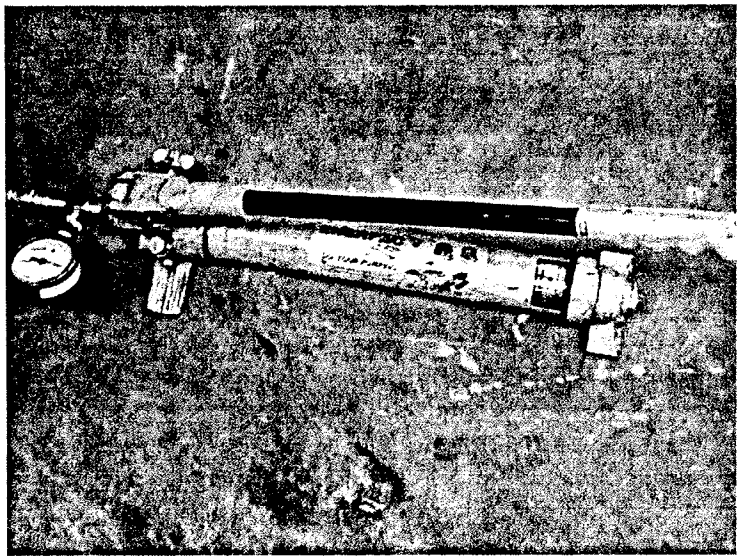

Photograph 2: Hydraulic Jack

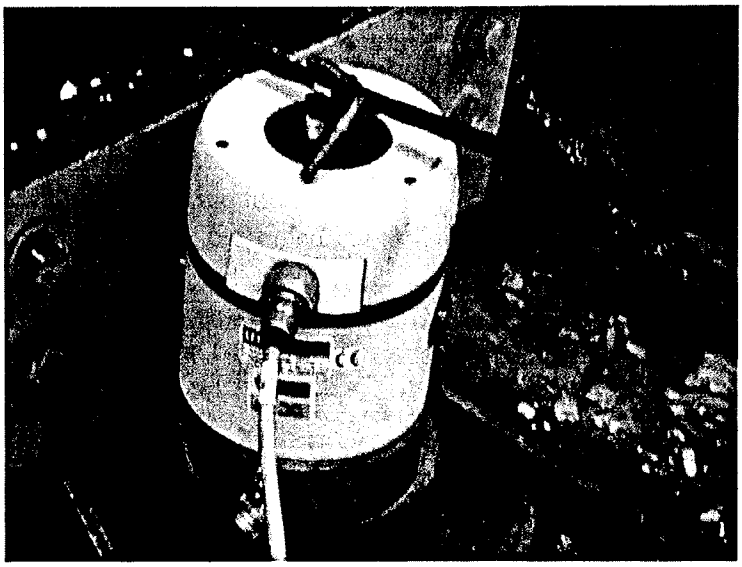

Photograph 3: Vibrator

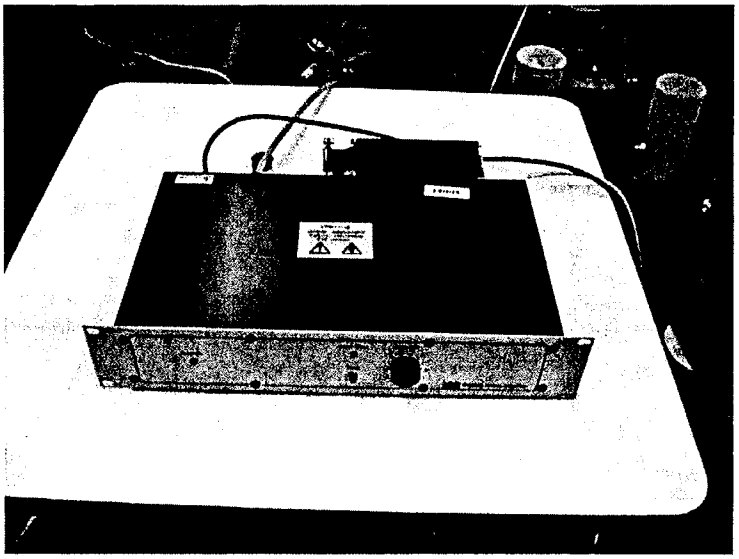

Photograph 4: Amplifier for Vibrator

Photograph 5:
Accelerometer

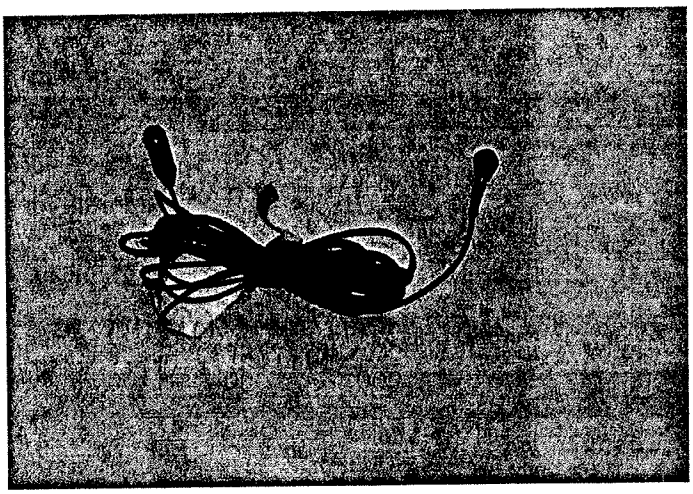

Photograph 6:
Signal Conditioner

Photograph 7:
Data Acquisition

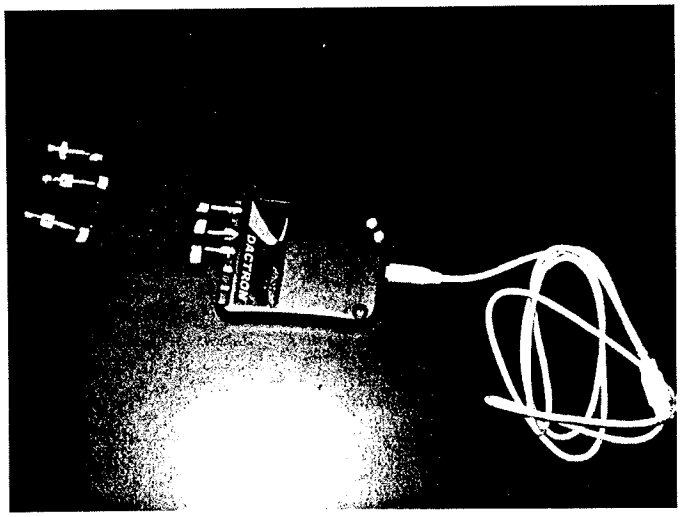

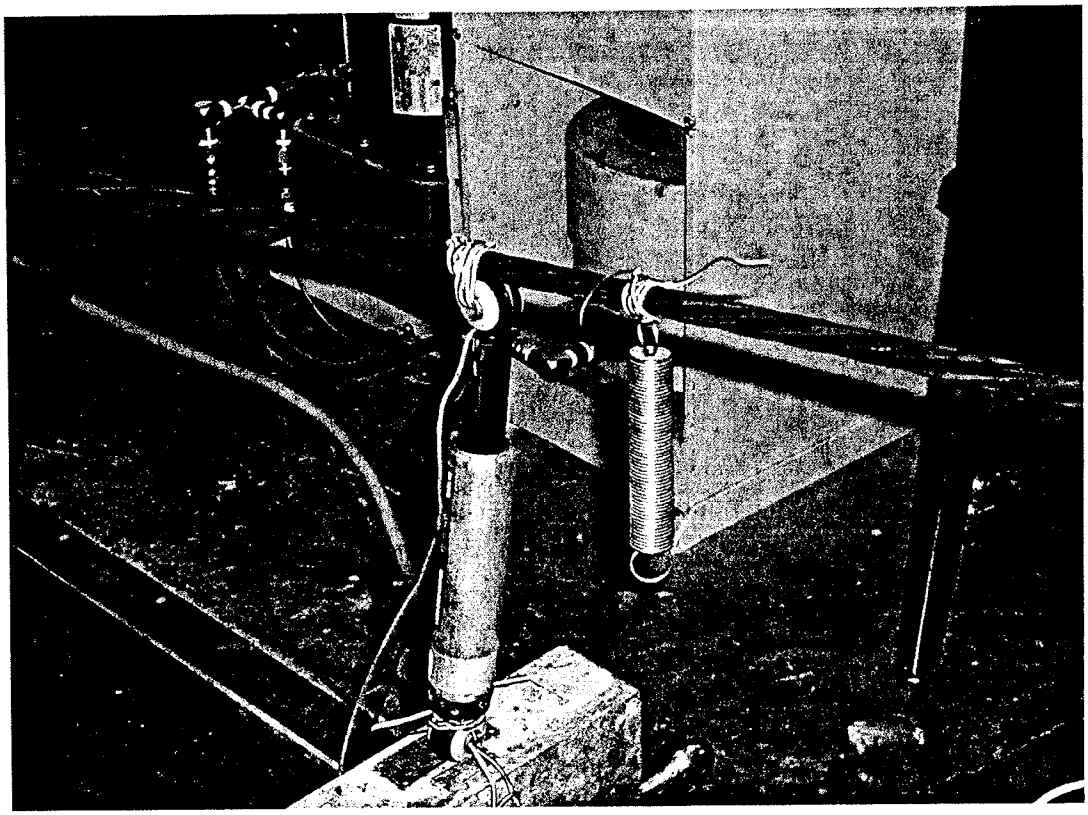

Photograph 8 MR Damper Connected with Cable and Ground

Experiment Results

Frequency Characteristics of Stay Cable

Before installing the damper, a mass weighted 93.4N was hung at the middle point 'D' to give the cable a free vibration by cutting the chord connecting the mass. The acceleration time histories at points 'B' and 'D' were measured by two accelerometers and collected by a Photon® data acquisition system. Fast Fourier Transformation (FFT) of those time history data was carried out to get the frequency spectra. From the frequency spectra, the basic natural frequency of the cable without damper was obtained as 8.93Hz with a cable axial tension force of 16.06KN. Since the scaling factor used is eight, the frequency of the prototype should correspondingly be 1.12Hz, which is within the reasonable range of the actual cable frequency (Tabatabai et al. 1998). Theoretically, the cable natural frequency can be calculated by the following equations (Irvine 1981):

$$\tan(\Omega/2) = \Omega/2 - (4.0/\lambda^2)(\Omega/2)^3 \qquad (1)$$

$$\Omega = 2\pi fL/\sqrt{T/m} \tag{2}$$

$$\lambda^2 = (\frac{mgL\cos(\alpha)}{T})^2 L/\frac{TL_e}{EA} \tag{3}$$

$$L_e = (1+\frac{(\frac{mgL\cos(\alpha)}{T})^2}{8})L \tag{4}$$

in which, E is the Young's modulus, T is the tension force, L is the cable length, α is the inclined angle, L_e is the deformed cable length (Assumed as a parabolic deflected shape), A is the cross section area, m is the mass per unit length, and λ^2 is proportional to the ratio of the axial stiffness to the geometric stiffness. It is a non-dimensional parameter to describe the cable dynamic behavior.

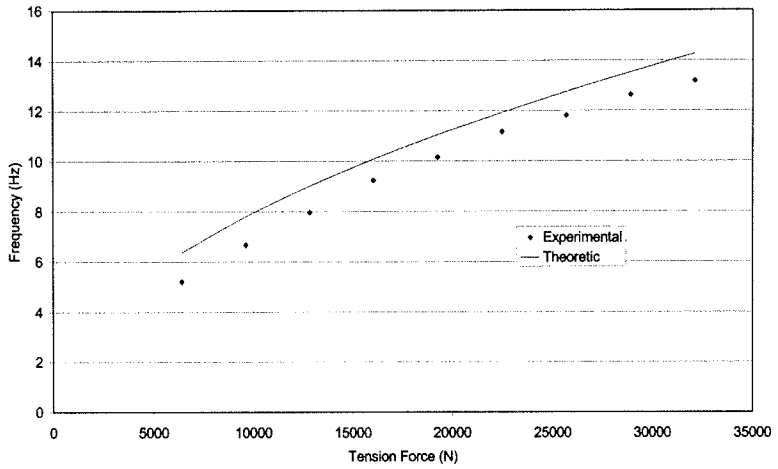

Fig. 9: The Cable Natural Frequencies

From Eqs. (1)~(4), the frequency f can be calculated as 10.08Hz, which is 12.9% higher than the experimental result. If the tension force is changed, the natural frequency of the cable will also be changed. The theoretical and experimental frequencies versus tension forces are plotted in Fig. 9.

Free Vibration

After testing the pure cable, the MR damper was then connected to point 'B' to reduce the cable vibration. The acceleration time history of point 'D' is plotted in Fig. 10, in which all the data are normalized for the convenience of comparison. It can be observed from Fig. 10(a) that even if there is no current provided, the damper provides very large damping so that it reduces the cable vibration efficiently. Fig. 10(b) shows when the current reaches 0.1A, the acceleration response is reduced more quickly than the 0A case. Fig. 10(c) shows the acceleration time history data with currents of 0.1A and 0.2A from 0s to 1.5s in detail. It can be observed that the damper with 0.2A current

reduces the vibration slightly more efficient than that of 0.1A case at the beginning when vibration is large and is almost the same after 0.5 second when the vibration is small. This is because, on one hand, when the measured signals are small, the relative error due to the noise gets bigger. On the other hand, since the MR damper can be considered as a Bingham element, it needs bigger force (or vibration) to overcome the Coulomb friction to pull and push the damper when the current becomes larger. If the driving force provided by the cable vibration is not enough, the MR damper will work as a fixed support (or locked) and the damping effect under different currents beyond some critical current will not differ much.

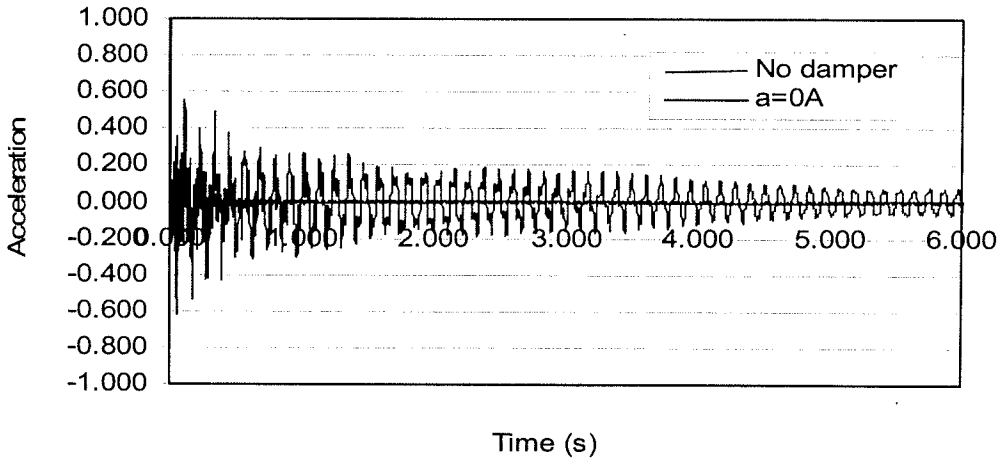

(a) Efficiency of 0A Current

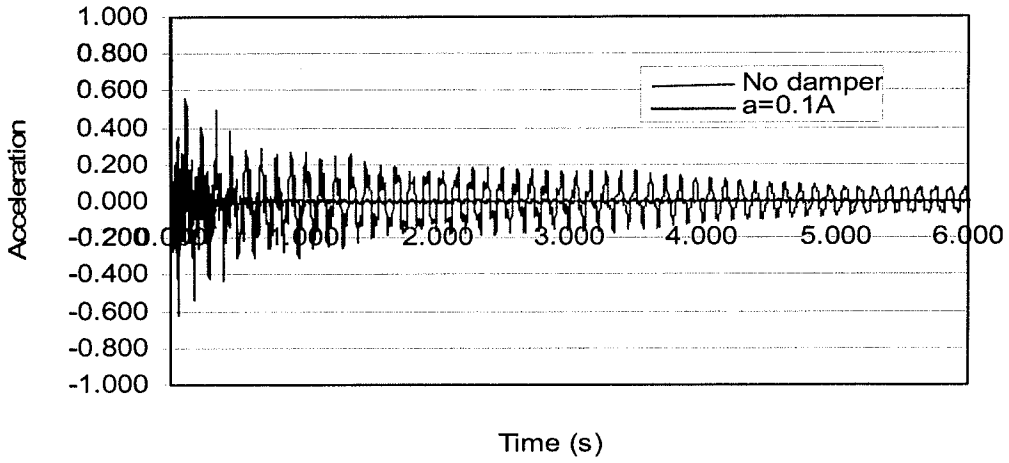

(b) Efficiency of 0.1 Current

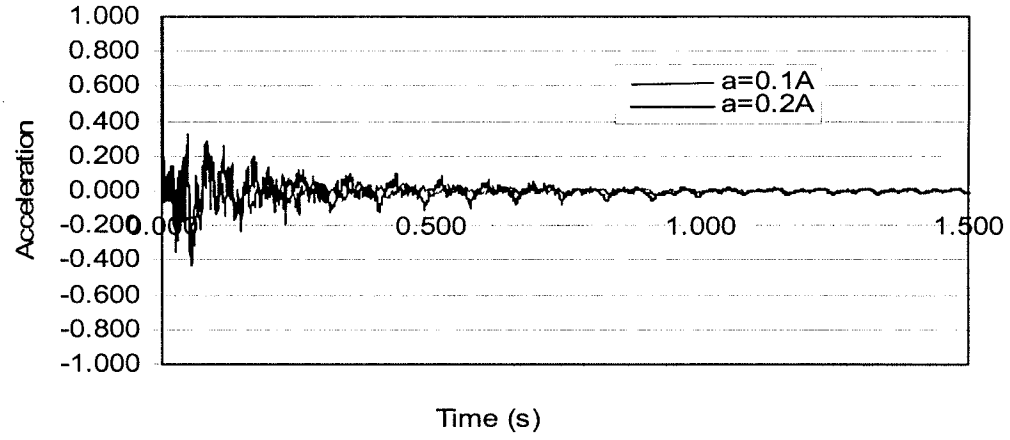

(C) Comparison: 0.1A and 0.2A

Fig. 10: Acceleration Response of Cable with MR Damper

Forced Vibration

For the forced vibration, instead of using the hanging mass, a shaker (vibrator) working as an excitation source was put on 0.18m away from the low end of the cable. It is 2.3% of the whole cable length.

Fig. 11 shows the acceleration response with a 10Hz sine wave excitation. From this figure, it is observed that the stable cable vibration with a damper of 0.1A current is much less than that without damper. The ratio of the peak value between the case of 0.1A current and no damper is about 14.

Fig. 12 shows the peak acceleration response of different cases. In Fig. 12(a), the acceleration is normalized with the peak acceleration of no damper case for each excitation frequency. This figure shows that the effect of reduction is much better at the 9Hz excitation, which corresponds to the resonant frequency of the cable system. When the frequency is away from this resonant frequency, the reduction effect decreases. Fig. 12(b) shows more clearly the high reduction efficiency around the resonant frequency for each current, and the resonance frequency increases slightly with the increase of current. This means that the stiffness of the damper increases with the damper current so that the natural frequency of the cable-damper system becomes larger. This phenomenon is similar to the case when a conventional viscous damper was added to the cable end (Main and Jones 2002a, 2002b). More experimental results are given in Appendix B.

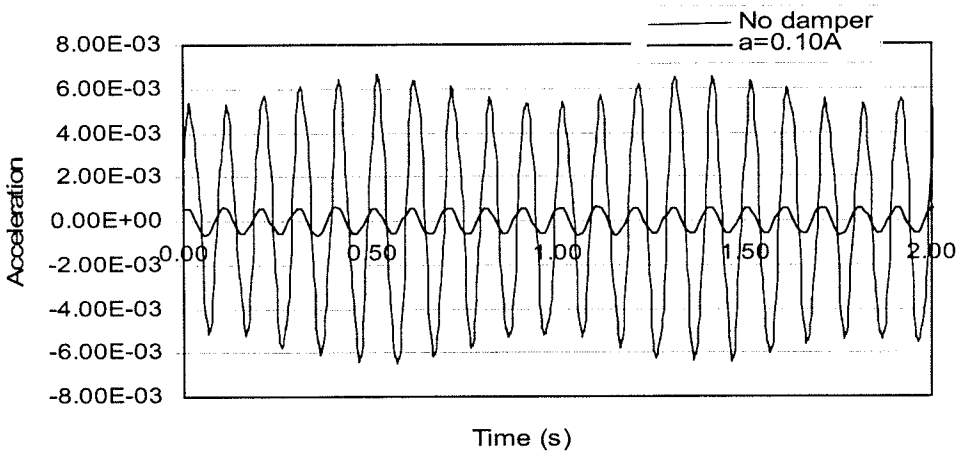

Fig. 11: Cable Acceleration Response under Forced Vibration

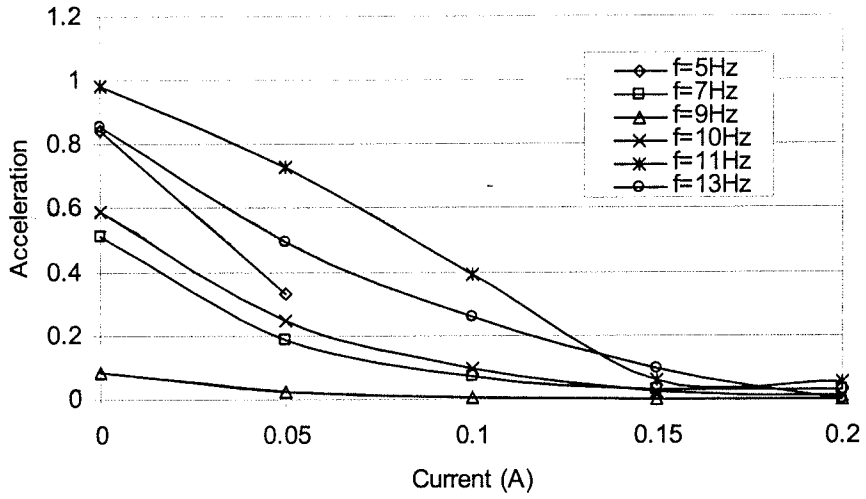

(a) Acceleration versus Current

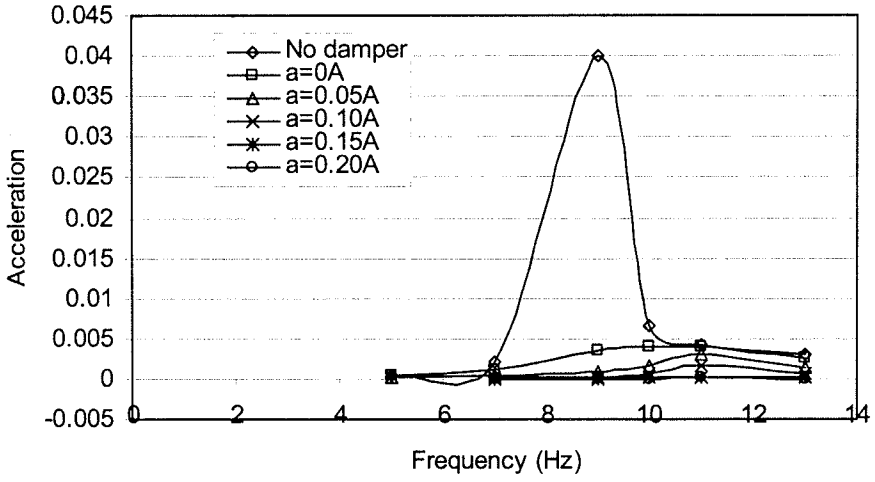

(b) Acceleration versus Frequency

Fig. 12: Peak Acceleration Response of Cable Vibration

Cable Vibration Control with TMD-MR Dampers

Concept and Principle of TMD-MR Damper

TMD dampers have been used extensively in structure vibration control. The concept of vibration control by TMD dampers can be stated as follows. The interaction between any two elastic bodies can be represented with a two-mass system shown in Fig. 13. Under the excitation of a sinusoidal force *Fsin(ωt)* acting on mass 1, the vibration amplitudes of this two-mass system are derived as

$$X_1 = \frac{Fm_2(\omega_{m_2}^2 - \omega^2)}{(k_1 + k_2 - m_1\omega^2)(k_2 - m_2\omega^2) - k_2^2},\ X_2 = \frac{Fm_2\omega_{m_2}^2}{(k_1 + k_2 - m_1\omega^2)(k_2 - m_2\omega^2) - k_2^2} \quad (5)$$

where $\omega_{m_1}^2 = k_1/m_1$ and $\omega_{m_2}^2 = k_2/m_2$. It can be seen from Eq. (5) that when $\omega_{m_2}^2 = \omega^2$, the vibration amplitude of mass 1 vanishes with $X_1 = 0$ and the amplitude of mass 2 will be $X_2 = F/k_2$.

Many pairs of components on the bridge can be visualized as this two-mass system, such as cable-deck/tower pair. If the frequencies of the cable and the deck/tower are close to excitation frequency ω, the energy of bridge vibration corresponding to that particular frequency ω will be passed to the cable. This energy could be a large amount compared to the masses of cables. Therefore, the natural frequency of cables should be designed away from the significant frequencies of the bridge to avoid resonant vibrations.

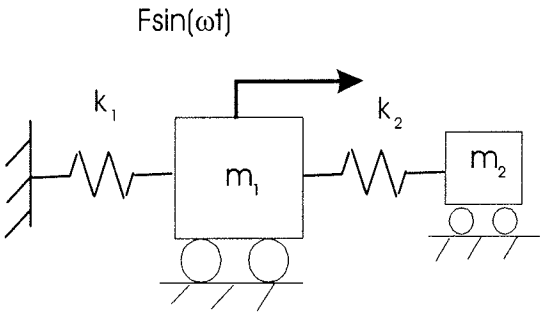

Fig. 13: A Two-mass System

The basic concept of cable vibration control by using TMD-MR damper is similar to the TMD control as shown in Fig. 14 where the cable and the TMD mass represent m_1 and m_2, respectively, as discussed above. The MR damper will provide an adjustable damping and stiffness. When MR dampers are not used in Fig. 14, then it is called TMD system, otherwise it is called TMD-MR system. The developed TMD-MR damper system will then be installed on the cable as shown in Fig. 15.

Since the cable vibration is a very complicated phenomenon and there is not only one natural frequency for the vibration mechanism, the supplemental damping of MR damper to the TMD-MR damper system can provide several advantages for the vibration control strategy. The first is the TMD function and is called TMD component hereafter. When the cable natural frequency changes, the MR damper can help adjust the natural

frequency of the TMD-MR damper system to trace the resonant excitation frequency so that the TMD-MR damper can be effective for a range of cable vibrations. The second is the MR damper function and is called MR component hereafter. When there are more than one dominating cable natural frequencies or it is hard to tune the TMD frequency to a specific value, MR component can still hope to work effectively since it can provide considerable output damping force and its damping efficiency is relatively frequency insensitive as observed earlier. More importantly, the MR damper can still work as a passive damper when the control strategy fails.

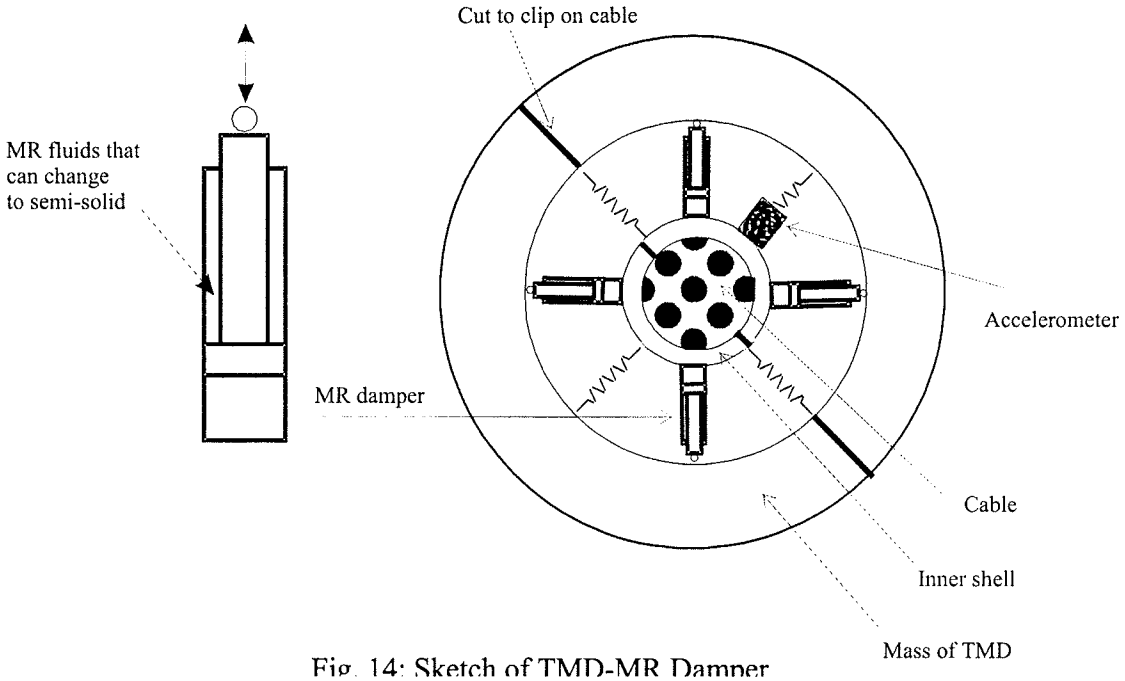

Fig. 14: Sketch of TMD-MR Damper

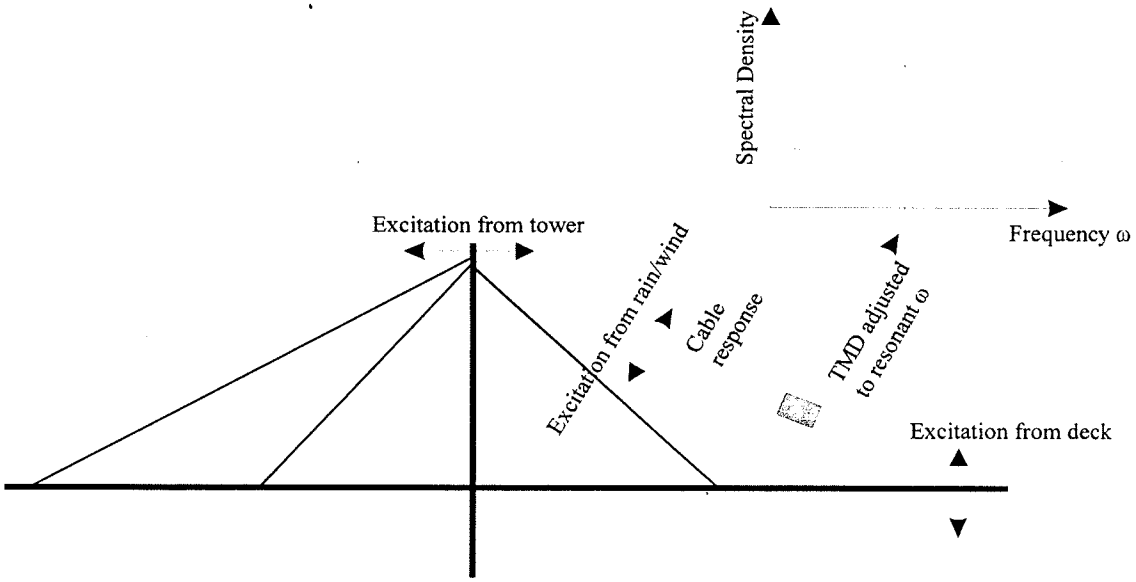

Fig. 15: Sketch of Cable Vibration Control

Adjustable TMD-MR Damper Design

None of the companies we contacted has available MR dampers with small force and size to match the model cable used in the present investigation. Therefore, we need to design and manufacture those dampers by ourselves. Two pressure driven flow modes with different sizes were designed and one of them was chosen for the TMD-MR damper system, and one type of direct shear mode was designed and discarded because of the maintenance problem, such as oil leaking. Generally, MR damper design consists of two steps: geometry design and magnetic circuit design. The main design process, which follows Lord Corporation Engineering Note (1999), is summarized in the Appendix C for reference.

Based on the information of Appendix C, more design cases are compared virtually and the following two optimal designs are chosen for comparison as listed in Table 4. All the length units in Table 4 are millimeter. The definitions of r_1 to r_4 are marked in Fig. 16.

Table 4: Design Parameter for Pressure Driven Flow Damper

Designed Data										
	r_1	r_2	r_3	r_4	t	g	L	d	τ_y (pa)	η ($pa \cdot s$)
Type 1	10	8	7.6	3	2	0.4	1	10	45000	4
Type 2	10	8	7.5	4	2	0.5	1.5	10	45000	8
Calculated Data										
	F_τ (N)		F_η (N)		λ					
Type 1	86.2		6.8		12.7					
Type 2	42.7		3.7		11.5					

Fig. 16 shows the sketch of the assembled shaft and sleeve. Fig. 17 and Fig. 18 show the details of the sleeve and the shaft of the first design case in Table 4.

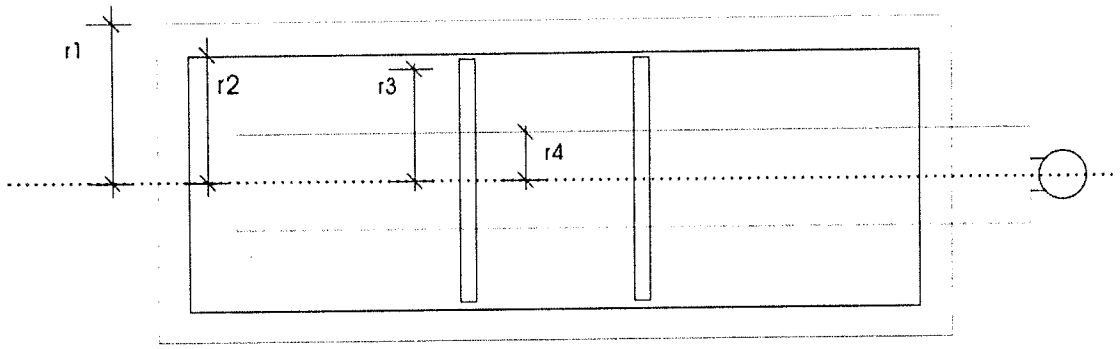

Fig. 16: Sketch for Designed MR Damper

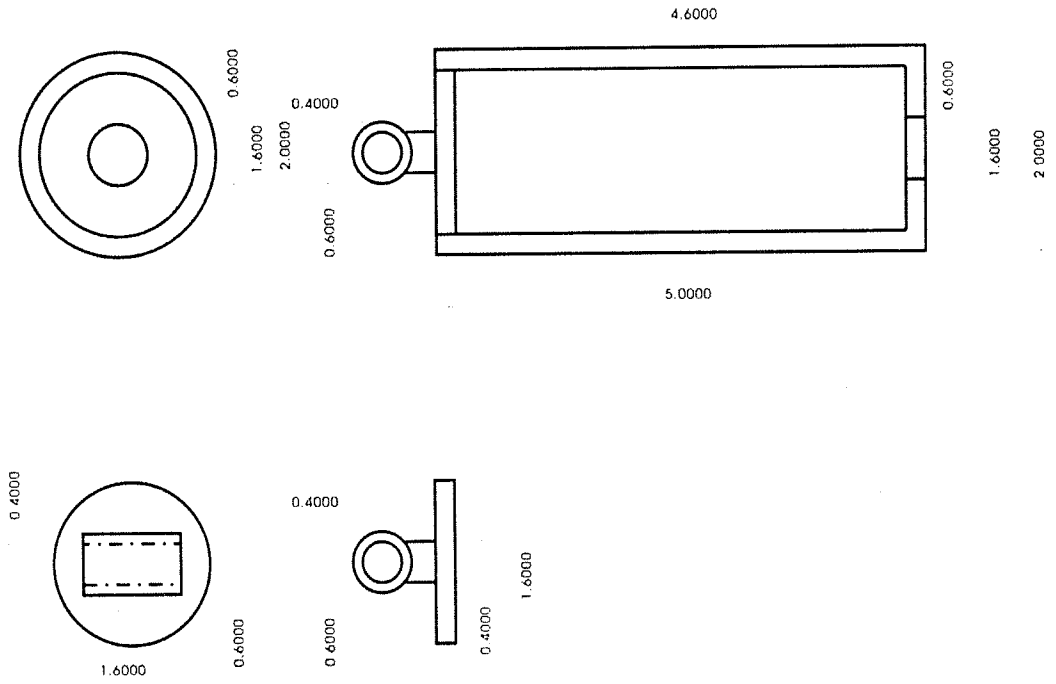

Fig. 17: Details of the Designed Sleeve

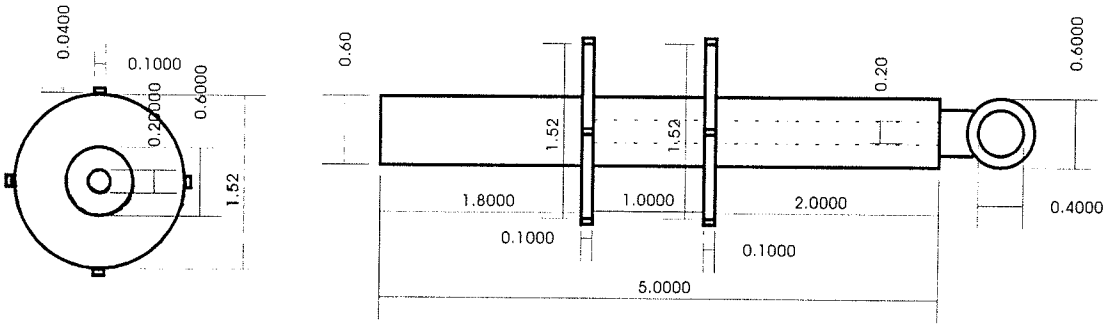

Fig. 18: Details of the Designed Shaft

Cable-TMD-MR System: Theoretical Analysis

Problem Statement

To study the cable-TMD-MR system theoretically, the effect of gravity is neglected and a horizontal cable configuration is chosen for simplicity. The problem under consideration is depicted in Fig. 19. A TMD-MR damper system is hung on the cable at an intermediate point, dividing the cable into two segments. Without losing generality, we assume $l_2 > l_1$. For the considered problem, we have the following assumptions.

1) The tension force in the cable is large compared to its self-weight, so the vertical sag is small and can be neglected.

2) The bending stiffness and internal damping of the cable is small.

3) The deflection is small so that the secondary tension force caused by cable deflection is neglected.

4) The TMD-MR damper is modeled as an equivalent system with a spring parallel with a dashpot.

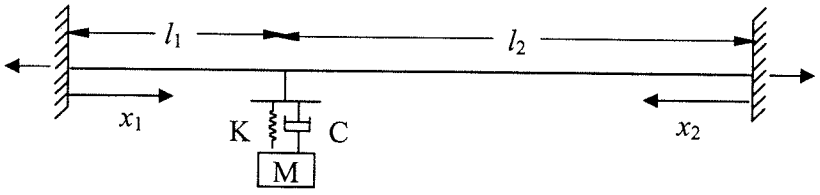

Fig. 19: Cable-TMD-MR System Model

With these conditions, the following partial differential equation is satisfied over each segment of cable:

$$T\frac{\partial^2 v_k(x_k,t)}{\partial x_k^2} = m\frac{\partial^2 v_k(x_k,t)}{\partial t^2} \tag{6}$$

where T is the axial tension force in the cable; m is the mass per unit length; x_k is the coordinate along the cable of the k th segment and v is the transverse deflection. A nondimensional time $\tau = \omega_c t$ is introduced to simplify the expression, and $\omega_c = (\pi / L)\sqrt{T/m}$ is the fundamental natural frequency of the cable. Solution for this equation is discussed in Appendix D.

Numerical Examples

According to Appendix D, when all the other parameters are specified for a particular cable, the nondimensional complex eigenvalue s in Eq. (D-12) of Appendix D can be solved by the Newton iteration method. Then the system damping ζ that is defined in Eq. (D-13) can be obtained. This information can be used to guide the TMD-MR design as shown below.

Incidences of wind-rain induced vibrations have been widely reported to be detrimental to cables of cable-stayed bridges recently (Hikami 1986, Matsumoto et al. 1992). In the following discussions, the emphasis is placed on the wind-rain vibration issues. Irwin (1997) proposed the following criterion to control the wind-rain induced cable vibration,

$$S_c = \frac{m\zeta}{\mathrm{P}D^2} \geq \alpha \tag{7}$$

where S_c is the Scruton number; P is mass density of air; D is outside diameter of cable; and α is the limiting value for Scruton number. The relationship in Eq. (7) can be rewritten as

$$\zeta \geq \frac{\alpha \mathrm{P}D^2}{m} = \frac{\alpha}{\mu} \tag{8}$$

where the mass parameter μ is defined as $\mu = m/PD^2$. Therefore, to meet the above stated criterion, the damping ratio of the cable needs to meet the requirement of Eq. (8). Based on available test results, Irwin (1997) proposed a minimum α of 10.

The modal damping of a stay-cable is composed by the intrinsic damping and the additional damping provided by damping devices. The former is typically low and cannot be reliably estimated. In this calculation, the intrinsic damping of the cable is conservatively ignored. The following example is used for demonstrating a preliminary design process.

This example was used by Tabatabai and Mehrabi (2000). Assume that a cable with the properties listed in Table 5 is in need of a TMD-MR damper to suppress wind-rain induced vibrations. To design a TMD-MR damper with its frequency tuned to the first mode, the following process can be followed.

Table 5: Properties of example cable

m ($kg \cdot m^{-1}$)	L (m)	T (N)	P (kg/m^3)	D (m)	ω_{c1} (sec^{-1})
114.09	93	$5.017*10^6$	1.29	0.225	7.08

1) Determine the demanding modal damping ratio

Since the mass parameter μ can be calculated as $\mu = m/PD^2 = 1747$, the demanding modal damping is determined from Eq. (8) as,

$$\zeta_1 \geq \beta/\mu = 10/1747 = 0.0057 = 0.57\% \tag{9}$$

2) Determine the TMD-MR parameters

Since the TMD-MR damper is tuned to the first mode, it is placed at the mid-span to achieve the best control effect. Then, following the common practice, the mass ratio of the TMD-MR damper is chosen as 2%, from which the mass of the damper is determined as

$$M = 2\% * L * m = 0.02 * 93 * 114.09 = 212.2kg \tag{10}$$

The frequency ratio between the cable frequency and damper frequency is then chosen approximately as $\rho = 1.0$ since it is a fundamental mode tuning, from which the stiffness of the TMD-MR damper can be determined as

$$K = M(\frac{\pi}{L}\sqrt{\frac{T}{m}})^2 = 212.2*(\frac{3.14159}{93}\sqrt{\frac{3.017*10^6}{114.09}})^2 = 6403.3N/m \tag{11}$$

By solving the cable equations in Appendix D, the relationship between the damper damping ratio ξ and system modal damping ratio ζ, i.e., the design aid curve, can be developed as shown in Fig. 20(a) for the first mode tuning. Shown in the figure are also the curves for a few modes with odd numbers since the damper placed at the mid-span has no effect on the vibration of modes with even numbers (these mode shapes have zero values at mid-span point). This figure is then referred to determine the equivalent damping ratio for the MR damper. If an actual first system modal damping $\zeta_1 = 1\%$ is chosen so that a safety factor of $1\%/0.57\% = 1.75$ can be achieved, the equivalent

damping ratio ξ is thus obtained from Fig. 20(a) as 2.6% by interpolation method. Once the required equivalent damping ratio ξ of the MR damper is known, a preliminary design for the MR damper (such as its MR liquid and current) can be performed (Li et al 2000), which is out of the scope of this work.

For the same cable, if the damper is located at the 1/4th point of the cable length to target the second mode vibration control, the stiffness of the damper is determined as,

$$K = 4M(\frac{\pi}{L}\sqrt{\frac{T}{m}})^2 = 4*212.2*(\frac{3.14159}{93}\sqrt{\frac{3.017*10^6}{114.09}})^2 = 25613.2N/m \qquad (12)$$

Then, similarly, Fig. 20(b) is referred to determine the equivalent damping for the MR damper. It is noted that the damper located at the 1/4th point of the cable length has no effect on the vibration of the fourth mode (this mode shape has zero value at the 1/4th point of the cable length). An actual modal damping $\zeta_2 = 1\%$ is also chosen so that equivalent damping ratio ξ is obtained from Fig. 20(b) as 2.54%.

In addition to the wind-rain induced cable vibration, other types of cable vibrations such as due to vortex excitation, galloping, etc. are also concerned. However, if a target cable damping ratio is defined for these specific types of vibrations, the design process proposed here is also applicable. For a refined optimal design, much more calculation is necessary to construct design curves that relate the damping ratio of the TMD-MR to the system modal damping of the cable-damper system under different parameters. Simultaneous multimode cable vibration control and adaptive control also deserve further studies, which will be pursued by the writers once the basic behavior of the cable-TMD-MR system is fully understood.

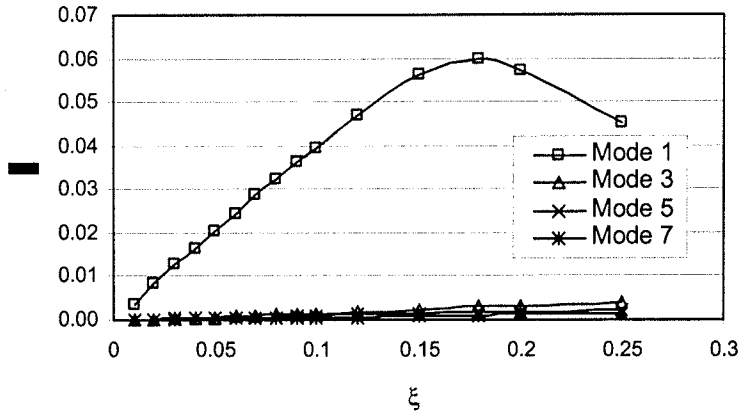

(a) Design curve of 2% mass ratio, first mode tuning

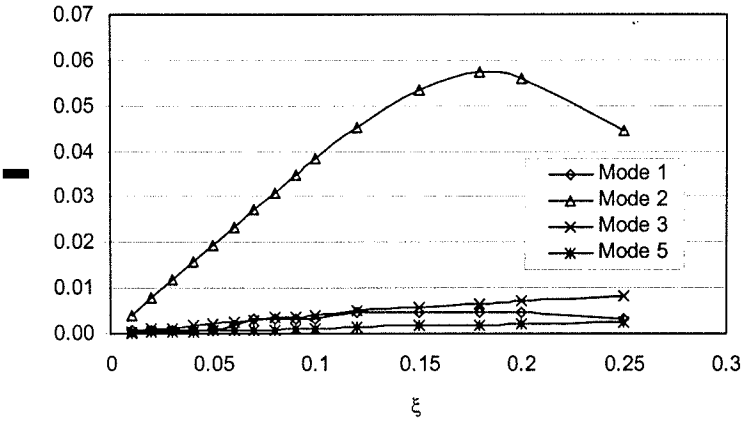

(b) Design curve of 2% mass ratio, second mode tuning

Fig. 20: System Modal Damping Ratio vs. Damper Damping Ratio

Cable-TMD-MR System: Experiments

General Discussion

After the TMD-MR damper was designed, it was installed on the cable with a tension force of 16.06 kN. The parameters of the cable-TMD-MR damper system are listed in Table 6. Since adding MR damper would affect the natural frequency of the TMD-MR damper system, the frequency of TMD damper was designed as about 7Hz, which is less than the cable natural frequency 8.93Hz, obtained from previous experiments for a tension force of 16.06 kN. One accelerometer was put on the cable and the other one was put on the outside circle of the TMD-MR damper so that the acceleration of both the cable and the TMD-MR damper can be measured as shown in Photograph 9. Since just the relative value of the cable acceleration with or without the TMD-MR damper was concerned, the unit of the measured acceleration is chosen as the unit of electronic signal volts. However, it is easy to change the electronic unit to the kinematics unit since 9.84mV equals to 1.0g according to the sensor specifications. Two baffles were installed on the cable to prevent the out of plane vibration of the TMD-MR damper.

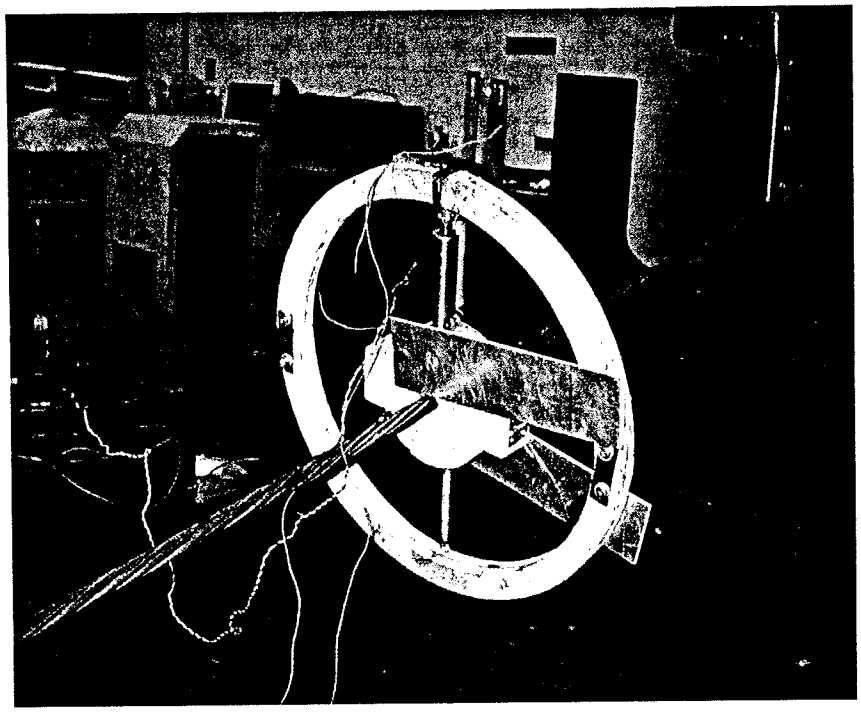

Photograph 9: TMD-MR Damper on the Cable

The following figures are results with a tension force of 16.06kN. Fig. 21 shows the acceleration time history of the cable. It is observed that when there is no damper attached on the cable, the vibration is the largest. When the TMD or TMD-MR damper is attached on the cable, the cable vibration is reduced to different extents. From Fig. 22 and

Table 7, we can find that the TMD-MR damper can reduce the cable vibration down to about 20% from the power spectral density (PSD) perspective. It is verified again that there is some saturation effect, as the reduction effects are pretty close for the 0.15A and 0.2A cases. We can observe from Fig. 23 that with the increase of current inside the MR damper, the vibration decreases for both the cable and the TMD-MR damper. This means that the existence of the MR damper also helps reduce the TMD vibration. The reduction effect of pure TMD is between that of the TMD-MR damper with 0A current and 0.05A current. From Fig. 23(b), we can also observe that the TMD damper vibrates the largest in the case of cable with TMD only, which means that the cable vibration has been transferred to the TMD vibration.

Table 6: Parameters of Cable-TMD-MR Damper Experiments

TMD-MR Damper	Mass	Upper Spring Stiffness	Lower Spring Stiffness
	0.3175 Kg	304.5 N/m	481.25 N/m
Cable-TMD-MR System	TMD-MR Location	Frequency Ratio	Mass Ratio
	Middle of the cable or point "D" in Fig. 8	1.27	0.06
Parameters Variation Range	Tension (kN)	Current in MR damper	Control Experiments
	12.85-32.13	0~0.20A	No damper, TMD only

Table 7: Cable Vibration Reduction by TMD and TMD-MR Damper
(Ratios of Controlled over uncontrolled vibration)

Case	TMD only	0A	0.05A	0.10A	0.15A	0.20A
Effect	27.1%	28.2%	21.3%	20.8%	20.2%	19.7%

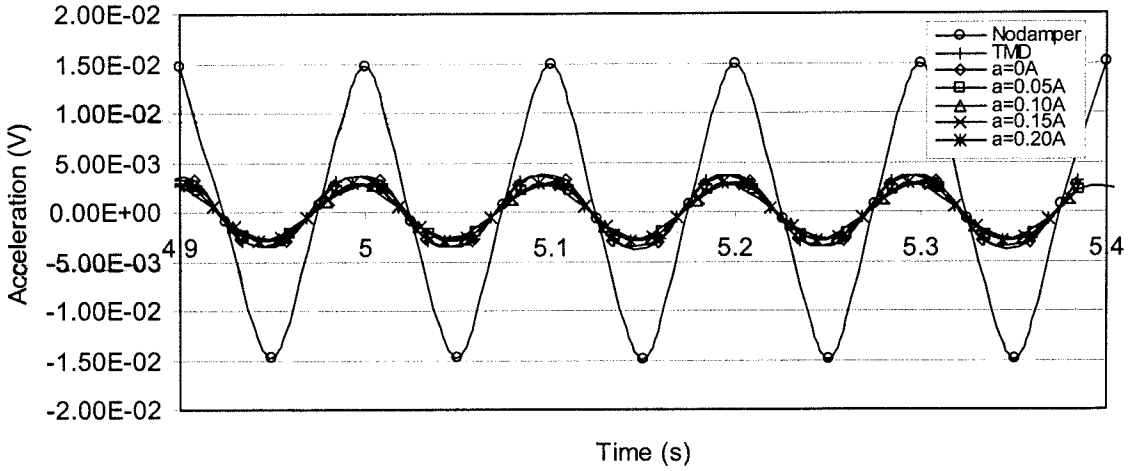

Fig. 21: Acceleration of Cable

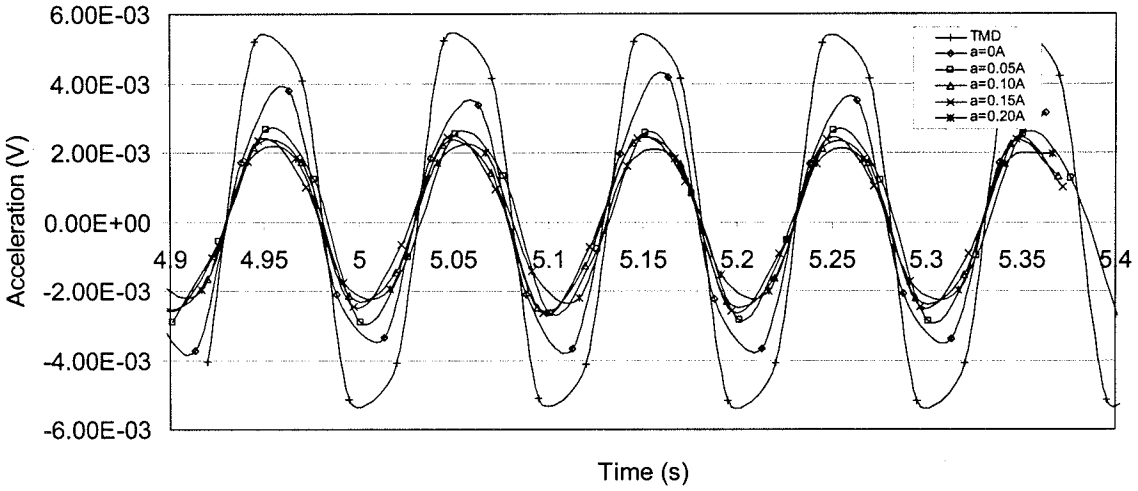

Fig. 22: Acceleration of TMD-MR Damper

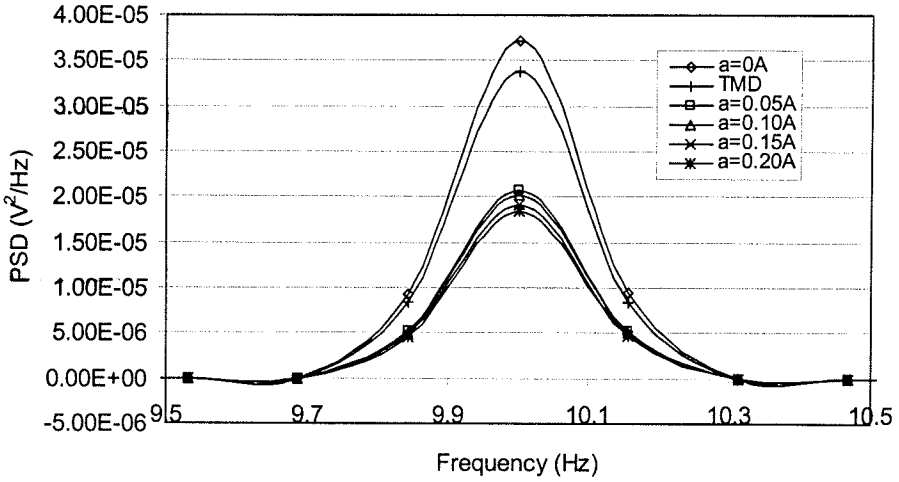

(a) Cable

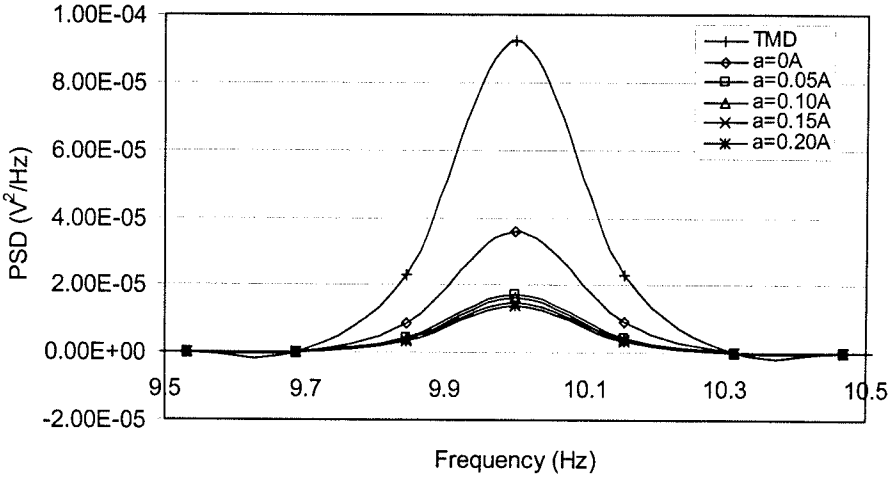

(b) TMD-MR Damper

Fig. 23: Power Spectral Density (a) Cable, (b) TMD-MR

Vibration Energy Transfer

From the perspective of energy, the goal of structure control is using control device to absorb and dissipate the structure vibration energy. In the following figure that is based on TMD only (without MR damper), we are going to discuss more about the vibration transfer with free vibration results.

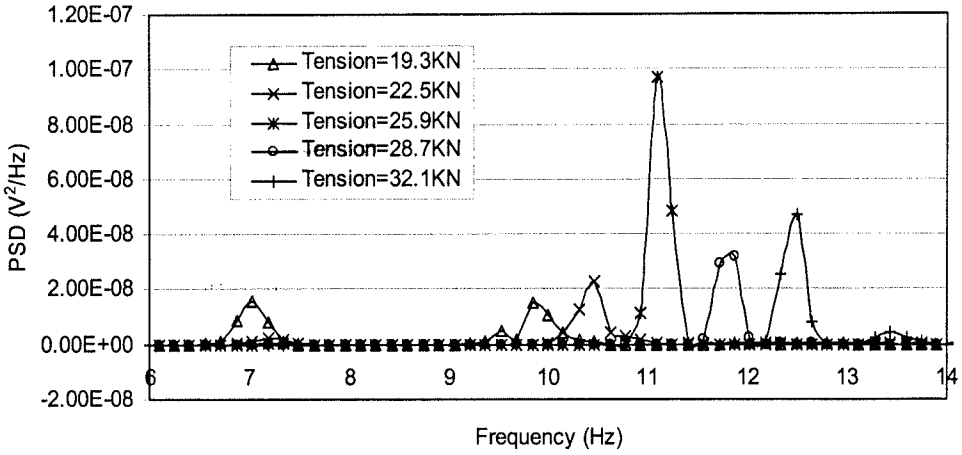

(a) Cable

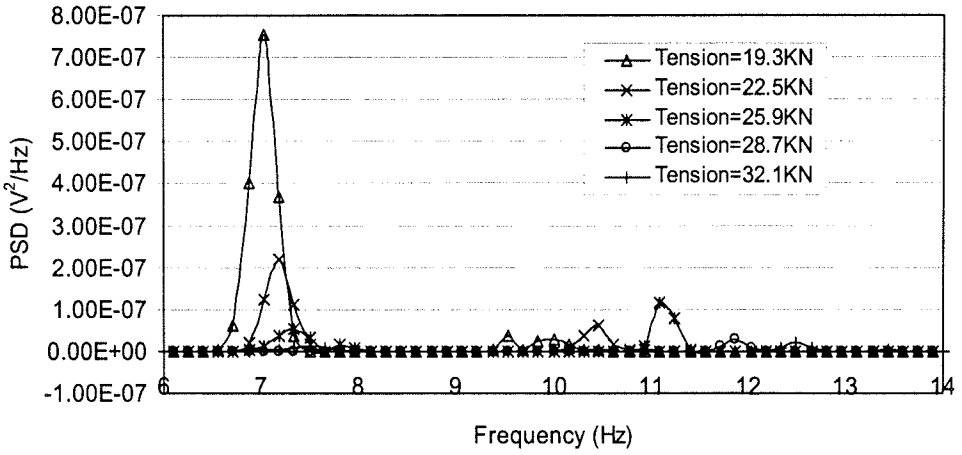

(b) TMD Damper

Fig. 24: Power Spectral Density of Cable-TMD System with Different Tension Force (a) Cable, (b) TMD

From Fig. 24, it can be observed that there are two PSD peaks for each cable tension force. One peak is related to the natural frequency of the TMD damper and the other is related to the natural frequency of the cable. With the increase of the tension force, the natural frequencies of both the cable and the TMD damper increase. This means that the measured cable frequency and TMD damper frequency are not pure cable frequency and pure TMD damper frequency any more. The frequency of cable has included the influence of TMD damper and vice verse. As shown in Fig. 24(a), the vibration energy mostly centralizes around the natural frequency of the cable (around 11.0Hz) and the energy corresponding to the TMD damper natural frequency is pretty small (around 7.0Hz). However, in Fig. 24(b), the vibration energy around the natural frequency of the TMD damper (around 7.0Hz) dominates and the energy corresponding

to the cable natural frequency (around 11.0Hz) is significantly less, which means that the energy has transferred from the cable to the TMD damper.

Frequency Shift

Adding dampers to the cable will always affect the cable natural frequency. Main and Jones (2002) made a profound discussion about the cable frequency shift due to the supplemental viscous dampers. According to the experimental results, adding TMD-MR or TMD will also affect the natural frequency of the cable. From Table 8, we can see that by adding the TMD damper, the frequency of the cable-TMD system is less than that of the pure cable, though the frequency shift is small.

Table 8: Frequency Shift of Cable-TMD System

Tension (kN)	19.3	22.5	25.9	28.7	32.1
Frequency of pure cable (Hz)	10.16	10.94	11.72	12.5	13.13
Frequency of cable-TMD (Hz)	9.84	10.47	11.09	11.88	12.5

Factors Affecting Vibration Reduction Effect

As stated earlier, adding TMD-MR damper not only improves the cable damping, but also changes the natural frequency of the cable system. The mass of the TMD-MR damper is about 6% of the entire cable weight. Fig. 25 plots the maximum acceleration of different cable experimental setups. Table 9 defines the case number that is shown as the X-axis in Fig. 25 and the corresponding experimental setup.

Table 9: Experiment Setup in Figure 25

Case Number	1	2	3	4	5	6	7
Experiment Cases	No damper	TMD only	Passive (a= 0A)	A=0.05A*	a=0.10A	a=0.15A	a=0.20A

* Meaning that the TMD-MR damper is attached to cable with a current of 0.05A.

We can make the following observations according to the different range of excitation frequencies in Fig. 25. It is noted that after the installation of the MR damper, the TMD-MR natural frequency is different from that of TMD only (7Hz). When the excitation frequency equals to 5Hz and 6Hz, which is away from the natural frequency of both the cable (about 9Hz) and the TMD-MR damper (about 8Hz), the best vibration reduction happens in the case of the passive TMD-MR damper (with 0A current, Case 3) for both the cable and the TMD-MR vibration. With the current inside the MR damper increases, the cable vibration increases from 0A case to 0.05A case and keeps almost the

same when the current changes from 0.05A to 0.20A. This observation verifies that larger current in the MR damper does not guarantee better vibration control effect for the cable. This phenomenon is due to several reasons. Firstly, when the excitation frequency is away from the cable frequency and the TMD-MR damper frequency, the cable vibration is small so that the control effect of TMD-MR damper is also small. Secondly, a larger current in the MR damper will increase the natural frequency of the TMD-MR damper so that the stiffness change effect of the TMD-MR damper, which enlarges the cable vibration in these cases, is larger than the reduction effect due to its increase in damping.

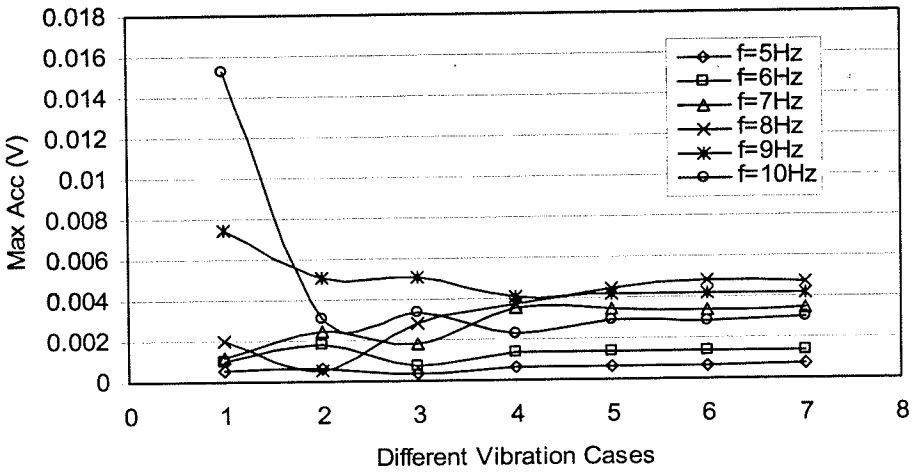

(a) Cable

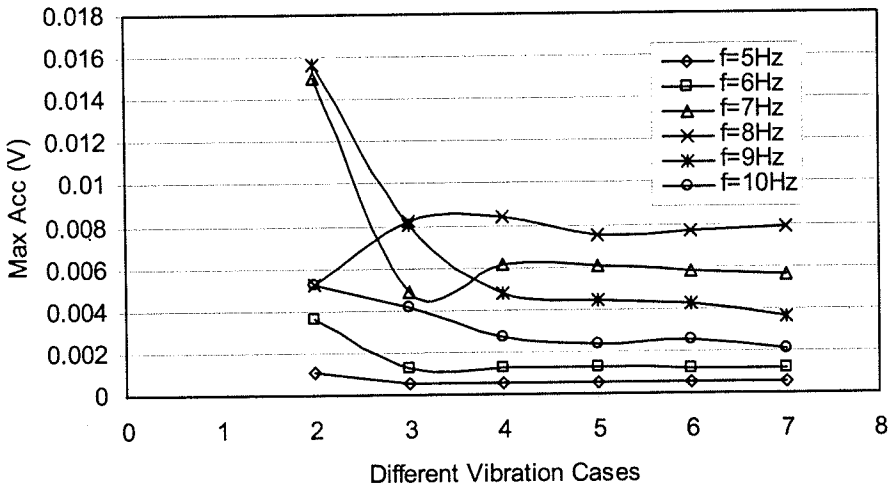

(b) TMD-MR Damper

Fig. 25: Maximum Acceleration of Cable-TMD-MR System under Different Experiment Setup (a) Cable, (b) TMD-MR

When the excitation frequency reaches 7Hz that is close to the TMD frequency, significant vibration is observed in the damper. When the excitation frequency reaches 8Hz, the most noticeable reduction of vibration is the TMD only case (Case 2). In this case, the cable vibration is reduced to 17% of that of the passive cable-TMD-MR case (Case 3). The TMD damper vibration in Case 2 is also less than that of Case 3. This is because the TMD natural frequency is very close to the excitation frequency and the TMD damper achieves its optimal vibration reduction effect. With this excitation frequency, the cable vibration increases slightly with the increase of the MR damper current until the current reaches 0.15A. The TMD-MR damper vibration reduces from 0A to 0.10A and increases a little from 0.10A to 0.20A.

In all the above cases, the excitation frequency is away from the cable natural frequency so that the cable vibration is not very large even if there is no supplemental damper. When the excitation frequency reaches 9Hz or 10Hz, the pure cable vibration is about 1 or 2-order larger than that with excitation frequency away from the cable natural frequency. The effect of the TMD-MR damper becomes obvious in these resonant vibration cases. The vibration of the cable for the passive TMD-MR damper case (Case 3) is close to that of TMD only case (Case 2) and much smaller than that of pure cable case without dampers (Case 1). Increase of the current from 0A to 0.05A leads to a smaller cable vibration, from 0.05A to 0.10A leads to a little larger cable vibration and from 0.10A to 0.20A leads to an almost constant cable vibration. Comparing these 9Hz and 10Hz cases with those of 5Hz and 6Hz, we can observe that the current in the MR damper corresponding to the best reduction effect increase from 0A to 0.05A and the current corresponding to the beginning of saturation increases from 0.05A to 0.10A. This observation shows that TMD-MR damper is more suitable for reducing large cable vibration.

From the previous discussions, some observations are summarized below.

1) Effect of excitation frequency

The relationships among the natural frequencies of the cable, the TMD-MR damper, and the excitation forces will affect the cable response significantly. When the excitation frequency is away from that of the cable and the TMD-MR damper, the cable vibration is not large, and the TMD-MR damper will reduce the cable vibration mainly depending on the MR component with two effects – providing additional damping and stiffness. When the MR component is in its passive mode, it provides damping and very small additional stiffness. However, when the current in the MR component increases, the stiffness and so the natural frequency of the TMD-MR damper changes, and so does the cable natural frequency. This change may cause the cable to vibrate more since the stiffness change effect may be larger than the increased damping effect. That may help to explain the observation that the cable vibration reduction effect gets worse with an increased current in Fig. 25. Therefore, when the vibration is small, the TMD-MR damper should be set to its passive mode.

When the excitation frequency is close to the TMD-MR damper while still away from the cable frequency, the cable vibration will be damped out mainly due to the TMD component. However, the vibration of the TMD-MR damper may still hard to tell because of the following reasons. On one hand, the vibration of TMD-MR should be larger because it absorbs the cable vibration energy, while on the other hand, the vibration of TMD-MR damper would be small because the MR damper can dissipate energy. The actual vibration of the TMD-MR damper depends on the balance of these two effects. When the excitation frequency is close to cable natural frequency, both the TMD component and the MR component of the TMD-MR damper system can work efficiently so that the vibrations of both the cable and the TMD-MR are reduced.

2) TMD component versus MR component of TMD-MR system

The observation of test results suggests that the TMD-MR natural frequency should be tuned to the natural frequency of the cable. As a result, when the excitation frequency is away from the cable natural frequency, the cable itself will not vibrate much and MR component with small current will be enough to reduce the vibration. When the excitation frequency is close to the cable natural frequency, which is also the same as the TMD-MR natural frequency, the TMD component of the TMD-MR damper will reduce the cable vibration much while the vibration will be transferred to the TMD-MR damper, which should be dissipated by MR component with a relatively larger current. This is the idea situation. However, in the practical situation, the TMD component cannot be tuned exactly the same as the natural frequency of the cable because the cable natural frequency may change due to various reasons such as deterioration. Also, when the excitation has a wide frequency range and the TMD component cannot be efficient for such a wide frequency range, the MR component should take more responsibility and help tune the TMD-MR natural frequency.

The plot of RMS (Root Mean Square) of acceleration time history leads to the same observation as that of the maximum acceleration in Fig. 25. The plots of RMS are given in Appendix E.

Future Work and Implementation

The research group believes that the proposed TMD-MR damper system should be developed further to a practical product after the experimental verification and more work needs to be done to achieve this goal. This includes a detailed design and manufacturing of a prototype TMD-MR damper, application and evaluation of the proposed damper in the field, as well as corroboration of the research results.

TMD-MR Damper Design and Fabrication Consideration

As stated earlier, the TMD-MR damper has two important components to collaborate each other. The required spring constant should be relatively small and fatigue concern should be taken into account since the cable vibration is a frequent phenomenon. MR damper needs a good balance of those parameters discussed in Appendix C. Leaking problem, which is a big problem when the investigation group manufactures the MR damper, should not be a problem for a professional manufacturer. Thus, it is more appropriate to cooperate with Lord Corporation or other manufacturer of MR dampers, to reduce the manufacturing cost.

Field Verification

It is proposed that further research work should be carried out to verify the effectiveness of the TMD-MR damper system in controlling one or more cable vibrations in the field. Several cable-stayed bridges have been monitored, measured and evaluated recently with different retrofit method in Alabama and Texas. It should be a good chance to verify the effectiveness of the TMD-MR damper system.

Corroboration of Research Findings

A large impediment to adopting new techniques is that practicing engineers are not readily exposed to the information. So the investigation group pays much attention to disseminate the research results. A presentation was made in the 17th ASCE Engineering Mechanics Conference at Delaware University, June 2004. A poster was shown in the Economic Development Assistantship demonstration hosted by Louisiana State University and the Department of Economic Development of Louisiana. Two more abstracts have been submitted to conferences and three journal papers are under review. A website at http://www.cee.lsu.edu/~cai/wwj.htm is under construction to introduce the research.

Summary and Conclusion

The concept of an adjustable TMD-MR damper system is designed to help reduce the cable vibration and the reduction effect is discussed theoretically and verified experimentally. From the investigation of individual MR dampers, cable dynamics with and without TMD-MR damper, several suggestions and conclusions can be obtained as follows.

- Based on the experimental work on individual damper, working conditions affect the output damping force of MR dampers to different extents. With the increase of current, which means the increase of the magnetic field, the output damping force increases accordingly. The maximum output damping force is almost a piecewise linear function of the provided current. Loading frequency does not affect the output damping force much, especially when the current is high. Different loading waves (excitations) affect the output damping force, and the shape of the displacement-force curves. Therefore, attention must be paid when the displacement-force curve is used, for example, in a time history analysis. Temperatures affect the output damping force in a modest way.

- Based on the analytical and experimental work on pure cables without damper, the frequencies obtained from theoretical calculation are reasonably close to the corresponding value obtained from experiments.

- Based on experimental work of cable with MR damper, MR dampers can reduce the cable vibration effectively, regardless of free vibration or forced vibration. MR damper can provide considerable damping even when it is in its passive mode. Generally speaking, the reduction effect of MR damper increases with the increase of current especially in the resonant and forced vibrations, but some saturation effect is observed. It is most effective for the resonant vibration case. When the external loading frequency is away from the resonant frequency or when the vibration is small, the reduction become less effective. With the installation of the MR damper, the frequency of the cable-MR system becomes larger than pure cable frequency.

- Many factors can affect the performance of the MR damper in the design process. Some factors even contradict each other. Balance should be made to design a good MR damper.

- Theoretically, the effect of the TMD-MR damper on the cable-TMD-MR system damping will be affected by the damper location, TMD-MR damping, frequency ratio between the TMD-MR damper and the cable. Based on the theoretical analysis, for the first mode vibration, the TMD-MR damper is most effective when it is in the mid-span of the cable; the reduction effect increases linearly with the increase of the TMD-MR damping.

- Based on the experimental work on the cable-TMD-MR damper system, to achieve the best effect of the TMD-MR damper on the cable vibration reduction, it is recommended that the natural frequency of the TMD-MR be close to that of the cable. When the excitation frequency is away from the cable natural frequency, the MR component will contribute mainly as providing an additional damping and the TMD-MR should be set in the passive mode. In those non-resonant or small vibration cases, the excitation force is too small to overcome the viscous or friction force and increasing the current of the MR damper will tend to lock the damper's movement and thus deteriorate the damping effects. When the excitation frequency is close to the cable natural frequency, the TMD component will contribute mainly by transferring the vibration energy from the cable to the damper and the MR component will work as providing an additional damping and changing natural frequency of TM-MR damper as well.

Reference

Carlson, J. D. (1994). "The Promise of Controllable Fluids." Proceedings of Actuator 94, H. Borgmann and K. Lenz, Eds., AXON Technologie Consult GmbH, 266-270.

Carlson, J. D. and Weiss, K. D. (1994). " A Growing Attraction to Magnetic Fluids." Machine Design. August, 61-64.

Carlson, J. D., Catanzarite, D. M., and St. Clair, K. A. (1995). "Commercial Magnetorheological Fluid Devices." Proceedings of 5th International Conference on ER Fluids, MR Fluidsand Associated Technolodge. University of Sheffield. UK.

Christenson, R. E., Spencer, B. F. Jr. and Johnson, E. A. (2002) "Experimental Studies on the Smart Damping of Stay Cables." Proccedings of 2002 ASCE Structures Congress, Denver, Colorado, USA

Flamand, O. (1995). "Rain-wind induced vibration of cables." Journal of Wind Engineering and Industrial Aerodynamics, 57, 353 –362

Hikami, Y. (1986). "Rain vibrations of cables in cable-stayed bridges." Journal of Wind Engineering, 27, 17-28 (in Japanese)

Irvine, H.M. and Caughey, T.K. (1974) 'The linear theory of free vibrations of a suspended cable.' Proceedings of Royal Society (London), A341, 299-315.

Irvine, H. M (1978) "Free Vibration of Inclined Cables." Journal of Structural Division, proceedings of the ASCE, Vol. 104, No. ST2, 343-347.

Irvine, H.M. (1981) 'Cable Structure.' MIT Press Series in Structural Mechanics, Cambridge, Massachusetts, and London, England, 1981

Irwin, P.A. (1997). Wind Vibrations of Cables on Cable-Stayed Bridges. Proceedings of ASCE Structures Congress. Vol. 1, April 1997, 383-387.

Johnson, E. A., Spencer, B. F., and Fujino, Y. (1999a) "Semiactive Damping of Stay Cables: A Preliminary Study" Proceedings of 17th International Modal Analysis Conference, Kissimmee, Florida.

Johnson, E. A., Baker, G. A., Spencer, B. F., and Fujino, Y. (1999b) "Mitigating Stay Cable Oscillation Using Semiactive Damping" Proceedings of SPIE, Vol. 3988, Smart Structures and Materials 2000: Smart Systems for Bridges, Structures, and Highway, S. C. Liu, Editor, 207-216

Langsoe H. E., and Larsen, O. D., (1987). "Generating mechanisms for cable stay oscillations at the FARO bridges" Proceeding, International Conference on Cable-stayed Bridges, Bangkok, November 18-20

Li, W. H., Yao, G. Z., Chen, G., Yeo, S. H. and Yap, F. F. (2000). "Testing and Steady State Modeling of a Linear MR Damper under Sinusoidal Loading." Smart Materials and Structures, Vol. 9, 95-102.

Lord Corporation (1999) "Engineering Note for Designing with MR Fluids" http://literature.lord.com/root/other/rheonetic/designing_with_MR_fluids.pdf

Lord Corporation. (2004). http://www.lord.com/Default.aspx?tabid=1127&page=1&docid=684, 04/20/2004

Lou, W. J., Ni, Y. Q., and Ko, J. M. (2000) "Dynamic Properties of a Stay Cable Incorporated with Magnetorheological Fluid Dampers." Advances in Structural Dynamics, J.M. Ko and Y.L. Xu (eds.), Elsevier Science Ltd., Oxford, UK, Vol. II, 1341-1348.

Main, J. A., and, Jones, N. P. (2001). "Evaluation of Viscous Dampers for Stay-cable vibration mitigation" Journal of Bridge Engineering, ASCE, 6(6), 385-397

Main, J. A., and, Jones, N. P. (2002a). "Free vibration of taut cable with attached damper. I: linear viscous damper." Journal of Engineering Mechanics, 128(10), 1062-1071

Main, J. A., and, Jones, N. P. (2002b). "Free vibration of taut cable with attached damper. II: Nonlinear damper." Journal of Engineering Mechanics, 128(10), 1072-1081

Matsumoto, M., Shirashi, N., Shirato, H. (1992). "Rain-wind induced vibration of cables of cable-stayed bridges." J. Wind Engineering and Industrial Aerodynamics, 44, 1992: 2011-2022

Matsumoto, M., Saitoh, T., Kitazawa, M., Shirato, H., and Nishizaki, T.(1995). "Response characteristics of rain-wind induced vibration of stay-cables of cable-stayed bridges." J. Wind Engineering and Industrial Aerodynamics, 57, 323-333

Phelan, R. S., Mehta, K. C., Sarkar, P.P. and Chen, L. (2002). "Investigation of Wind-Rain-Induced Cable-Stay Vibrations on Cable-Stayed Bridges" Final Report, Center for Multidisciplinary Research in Transportation, Texas Tech University, Lubbock, Texas.

Routh, E.J., Dynamics of a system of rigid bodies, Dover Publications, Inc., New York, NY, 1955.

Starossek, U. (1994). "Cable dynamics - A review." IABSE, Structural Engineering International, Vol. 4, No. 3, pp. 171-176.

Tabatabai, H., and Mehrabi, A. B. (1999). "Tuned dampers and cable fillers for suppression of bridge stay cable vibrations." Final report to TRB IDEA program, Construction Technology Laboratories, Inc, Skokie, Illinois

Tabatabai, H., and Mehrabi, A. B. (2000). "Design of Mechanical Viscous Dampers for Stay Cables." Journal of Bridge Engineering, 5(2), 114 – 123

Triantafyllou, M.S.(1984) "The Dynamics of Taut inclined cables." Quarterly Journal of Mechanics and Applied Mathematics, Vol. 27, NO.3, Aug., 1984, pp.421-440

Yang, G. Q. (2001) "Large-Scale Magnetorheological Fluid Damper for Vibration Mitigation: Modeling, Testing and Control." Doctoral Dissertation, University of Notro Dame, Notre Dame, IN

Appendix

Appendix A: Some Experimental Results of Individual MR Dampers

Results of MR RD-1005-3

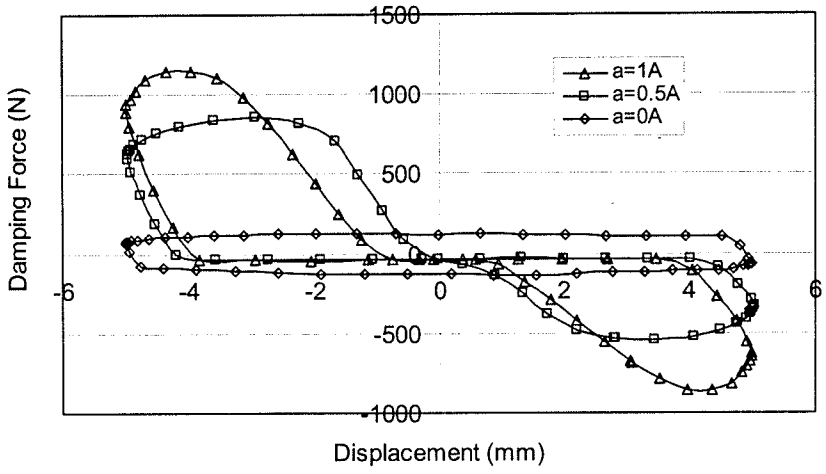

(a)

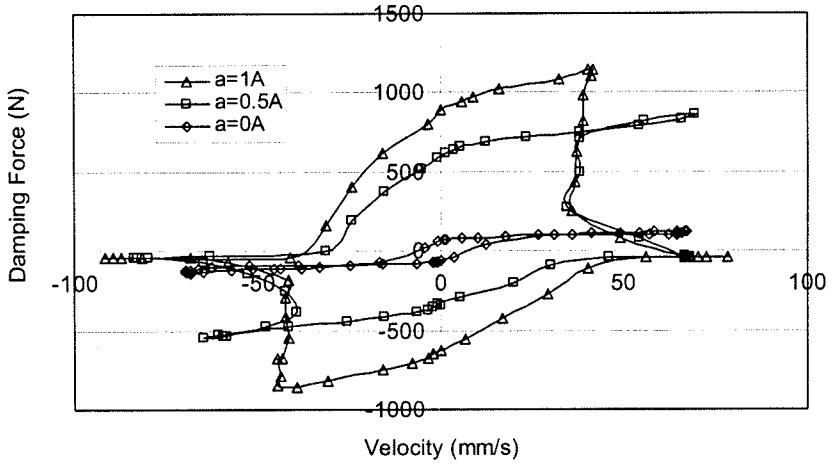

(b)

Fig. A-1: Performance Curve with Different Currents: f=0.5Hz

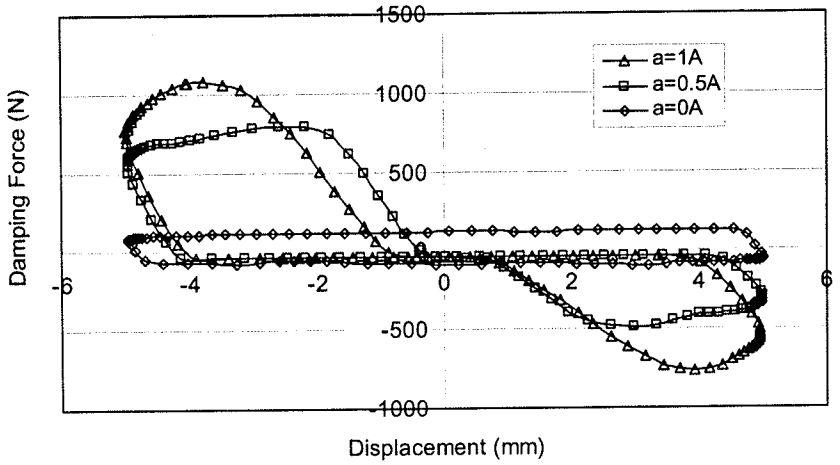

(a)

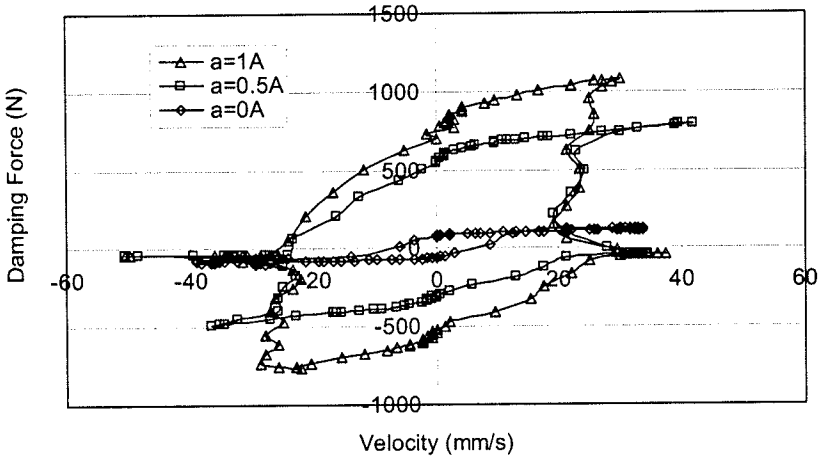

(b)

Fig. A-2: Performance Curve with Different Currents: f=1Hz

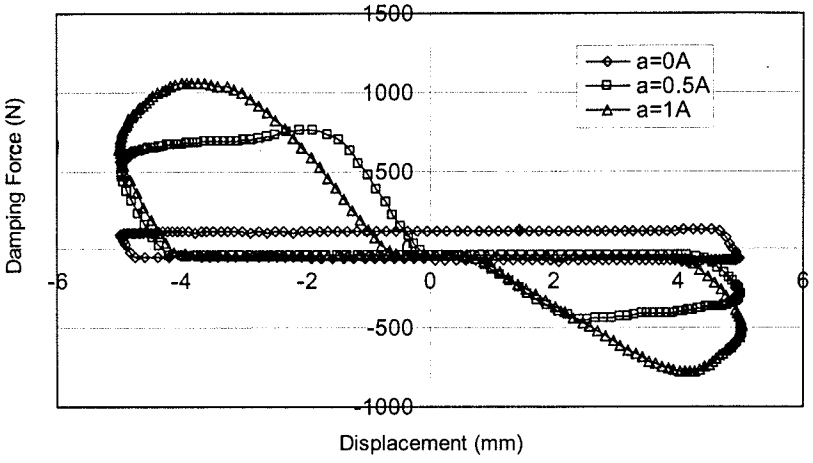

(a)

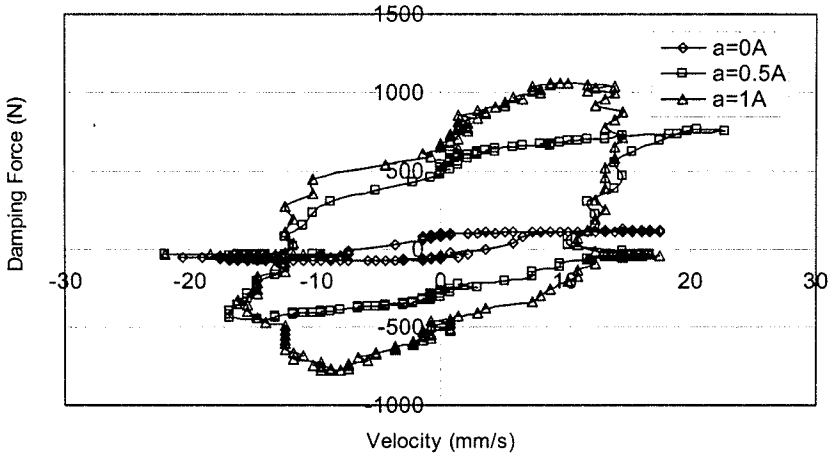

(b)

Fig. A-3: Performance Curve with Different Currents: f=2Hz

Results of MR RD-1097-01

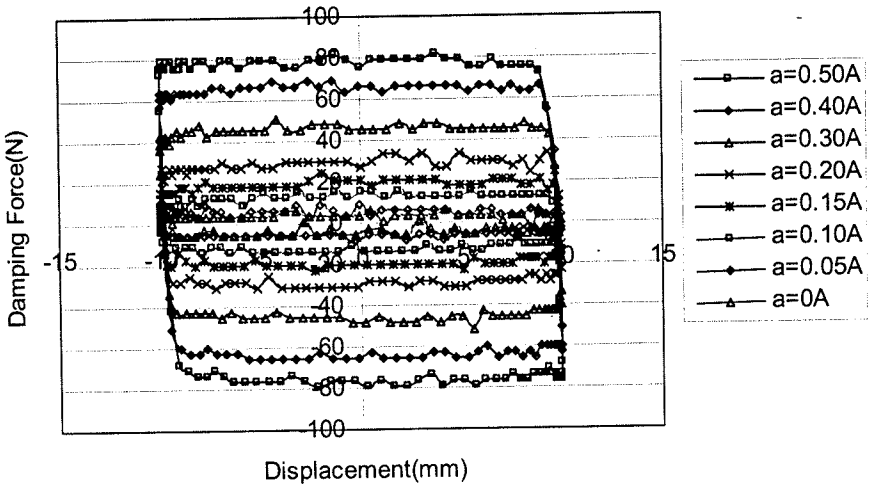

(a)

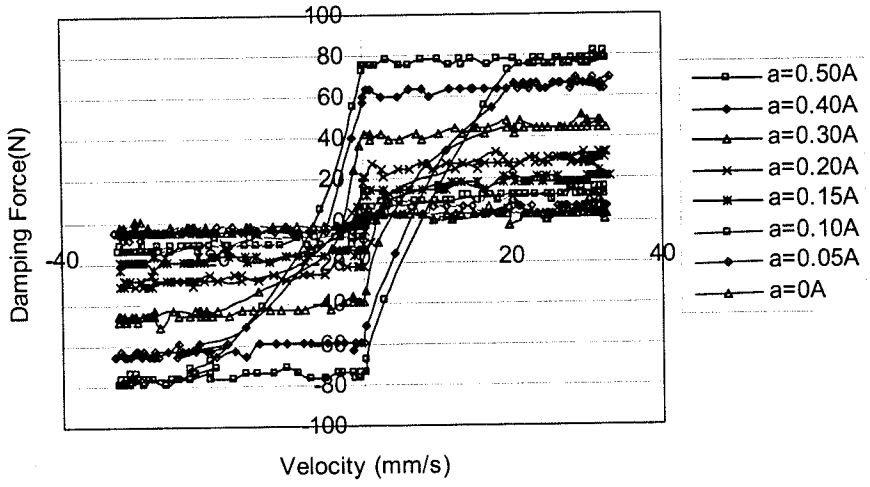

(b)

Fig. A-4: Performance Curve with Different Currents: f=0.5Hz

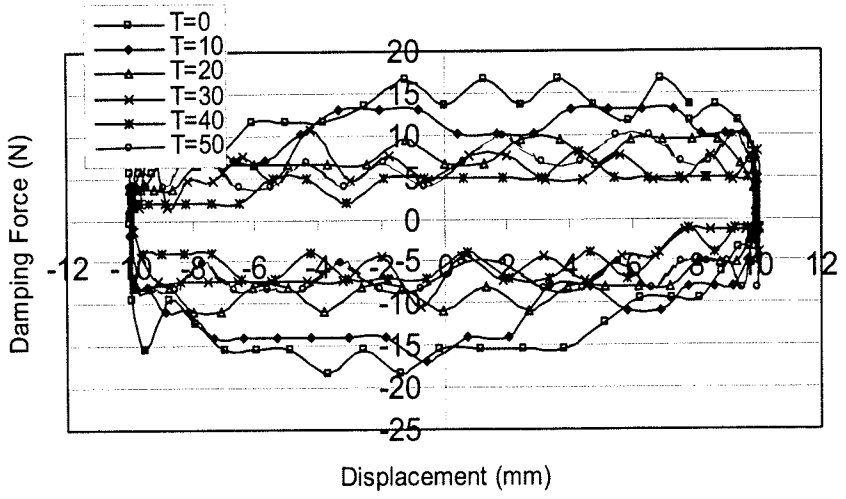

(a)

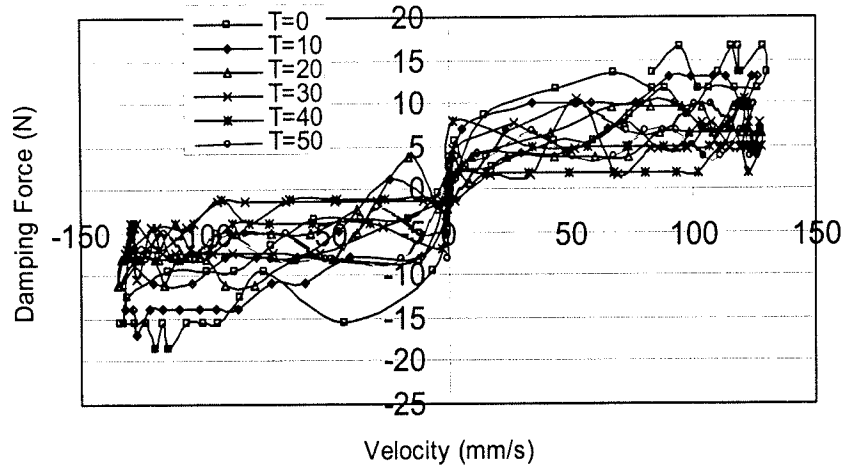

(b)

Fig. A-5: Performance Curve with Different Temperatures: f=2Hz, a=0A

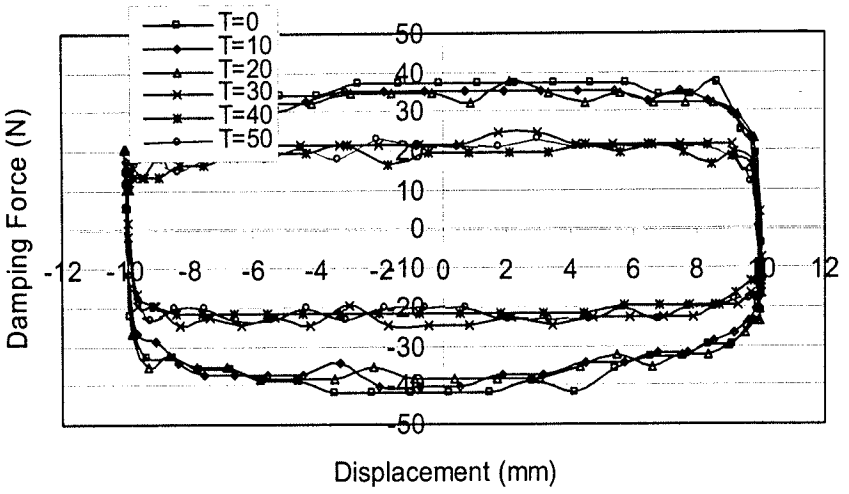

(a)

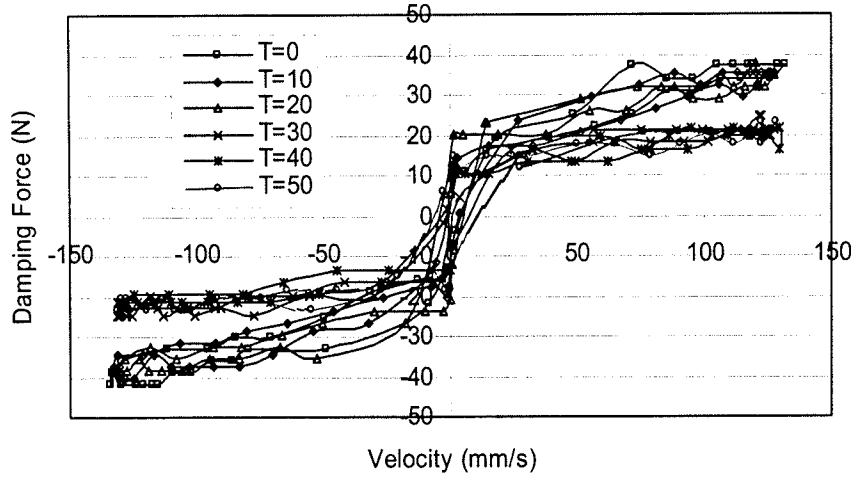

(b)

Fig. A-6: Performance Curve with Different Temperatures: f=2Hz, a=0.20A

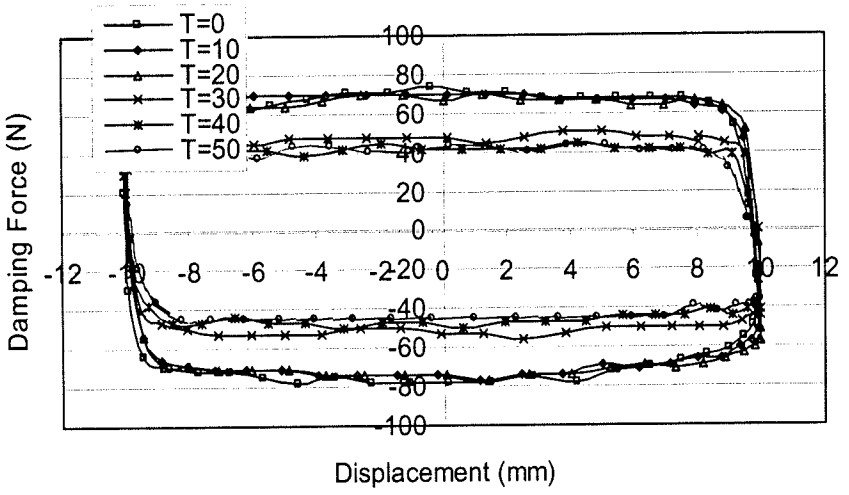

(a)

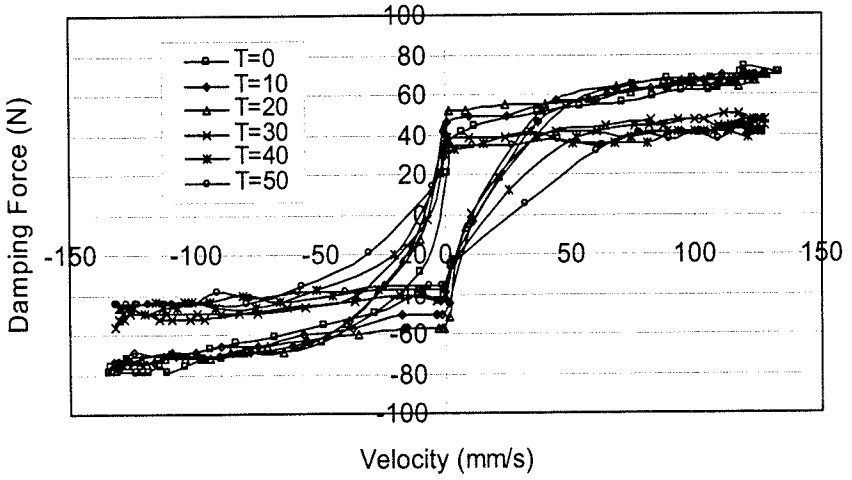

(b)

Fig. A-7: Performance Curve with Different Temperatures: f=2Hz, a=0.40A

Appendix B: Some More Experimental Results of Cable-MR System of Forced Vibration

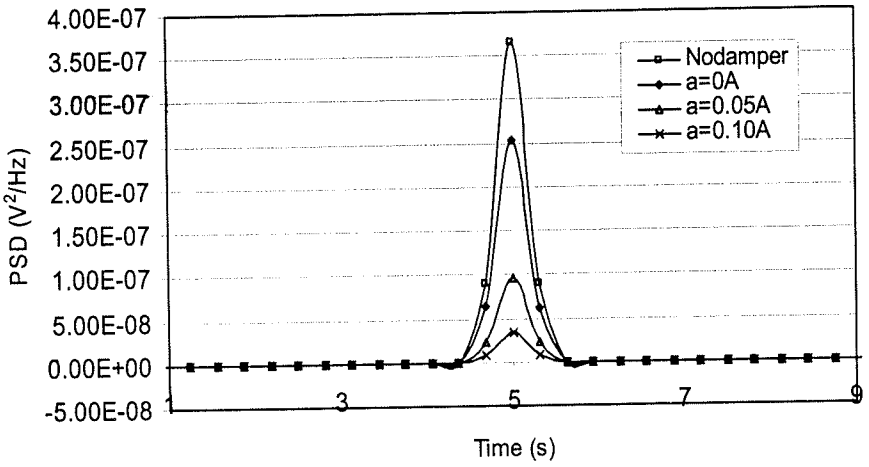

Fig. B-1: Cable Acceleration PSD with 5Hz Sine Wave

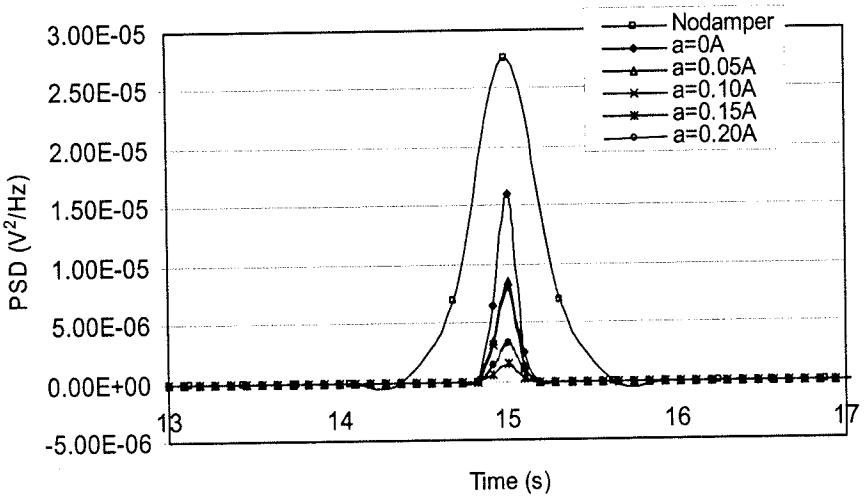

Fig. B-2: Cable Acceleration PSD with 15Hz Sine Wave

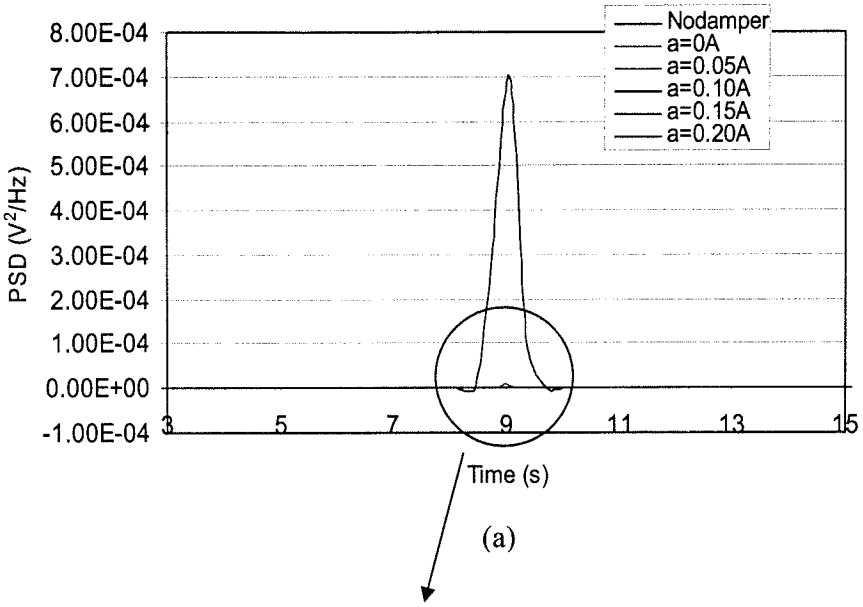

(a)

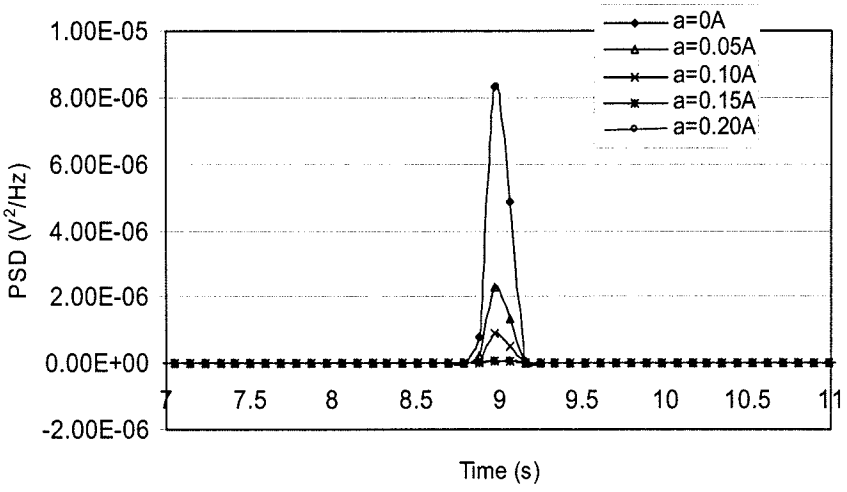

(b) Close Look of (a)

Fig. B-3: Cable Acceleration PSD with 9Hz Sine Wave

Appendix C: Details for Adjustable TMD-MR Damper Design

As stated previously, MR damper design consists of two steps: geometry design and magnetic circuit design. Lord Corporation Engineering Note (1999) provides much information about the design procedure. The main process is summarized and the detailed design and analysis done by the investigation group are provided here for reference.

Geometry Design

Most MR dampers used in civil engineering are pressure driven flow mode though some other types are applied in other areas. Fig. C-1 shows an actual pressure driven flow damper and its magnetic circuit.

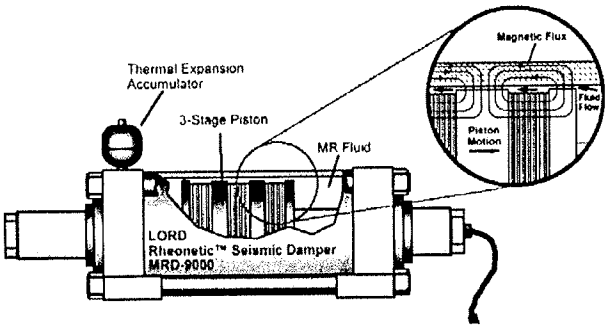

Fig. C-1: Actual Pressure Driven Flow MR Fluid Damper

According to fluid dynamics analysis (Yang 2001), the pressure drop developed in the pressure driven flow mode is assumed as the sum of a viscous component ΔP_η and a field dependent induced yield stress component ΔP_τ. Therefore, the pressure drop can be expressed as:

$$\Delta P = \Delta P_\eta + \Delta P_\tau = \frac{12\eta QL}{g^3 w} + \frac{c\tau_y L}{g} \qquad \text{(C-1)}$$

In Eq. (C-1), Q is the volumetric flow rate while c is a constant mainly determined by the ratio $\Delta P_\tau / \Delta P_\eta$. It is chosen as 2.5 in the primary TMD-MR system design in the present study.

The minimum active fluid volume V and dynamic range λ are introduced to get some insight of the parameter variation. The former is the volume of MR fluid exposed to the magnetic field and thus is responsible in providing the desired MR effect. The latter is defined as the ratio between a controllable component and an uncontrollable component. After some simplifications, the following equation can be derived:

$$V = k(\frac{\eta}{\tau_y^2})\lambda W_m \qquad \text{(C-2)}$$

In Eq. (C-2), k is a constant and $V = Lwg$ is the necessary active fluid volume in order to achieve the desired control ratio λ at a required controllable mechanical power level $W_m = Q\Delta P_\tau$. Also, the following equations can be obtained.

$$k = 12/c^2,\ \lambda = \Delta P_\tau / \Delta P_\eta,\ wg^2 = \frac{12}{c}(\frac{\eta}{\tau_y})\lambda Q \qquad \text{(C-3)}$$

Eqs. (C-2) and (C-3) provide geometric constrains for MR devices based on MR fluid properties and the desired ratio or dynamic range. If the required parameters such as the mechanical power level, the desired control ratio, the volumetric flow rate and the material properties are specified, the dimension of the MR damper can be calculated by using the corresponding equations. Maybe the existing design method can be improved by using output damping force as a required parameter directly, but the discussion of the optimal design method is out of the scope of this investigation.

MR Damper Magnetic Circuit Design

The objective of the magnetic circuit design is to determine necessary amp-turns (NI) to provide a sufficient magnetic field for MR fluid. Therefore, the magnetic circuit design is also important for MR dampers. An optimal design of the magnetic circuit requires maximizing the magnetic field energy in the fluid gap while minimize the energy lost in steel flux conduit and regions of non-working areas. Low carbon steel, which has high magnetic permeability and saturation, is used as a magnetic flux conduit to guide and focus magnetic flux into the fluid gap.

The typical design process for a magnetic circuit is:

(1) Choose a desired yield stress τ_0, and determine the corresponding magnetic induction B_f in the MR fluid from Fig. C-2(a).

(2) Determine the magnetic field intensity H_f in the MR fluid from Fig. C-2(b).

(3) According to the continuity of magnetic induction flux, we have the following equation,

$$\Phi = B_f A_f = B_s A_s \qquad \text{(C-4)}$$

where A_f is the effective pole area including the fringe of magnetic flux and A_s is the steel area. Consequently the magnetic induction B_s in the steel is given by:

$$B_s = \frac{B_f A_f}{A_s} \qquad \text{(C-5)}$$

(4) Determine the magnetic field intensity H_s in the steel, using Fig. C-2(c).

(5) By using Kirchoffs's Law of magnetic circuits, the necessary number of amp-turns (NI) is

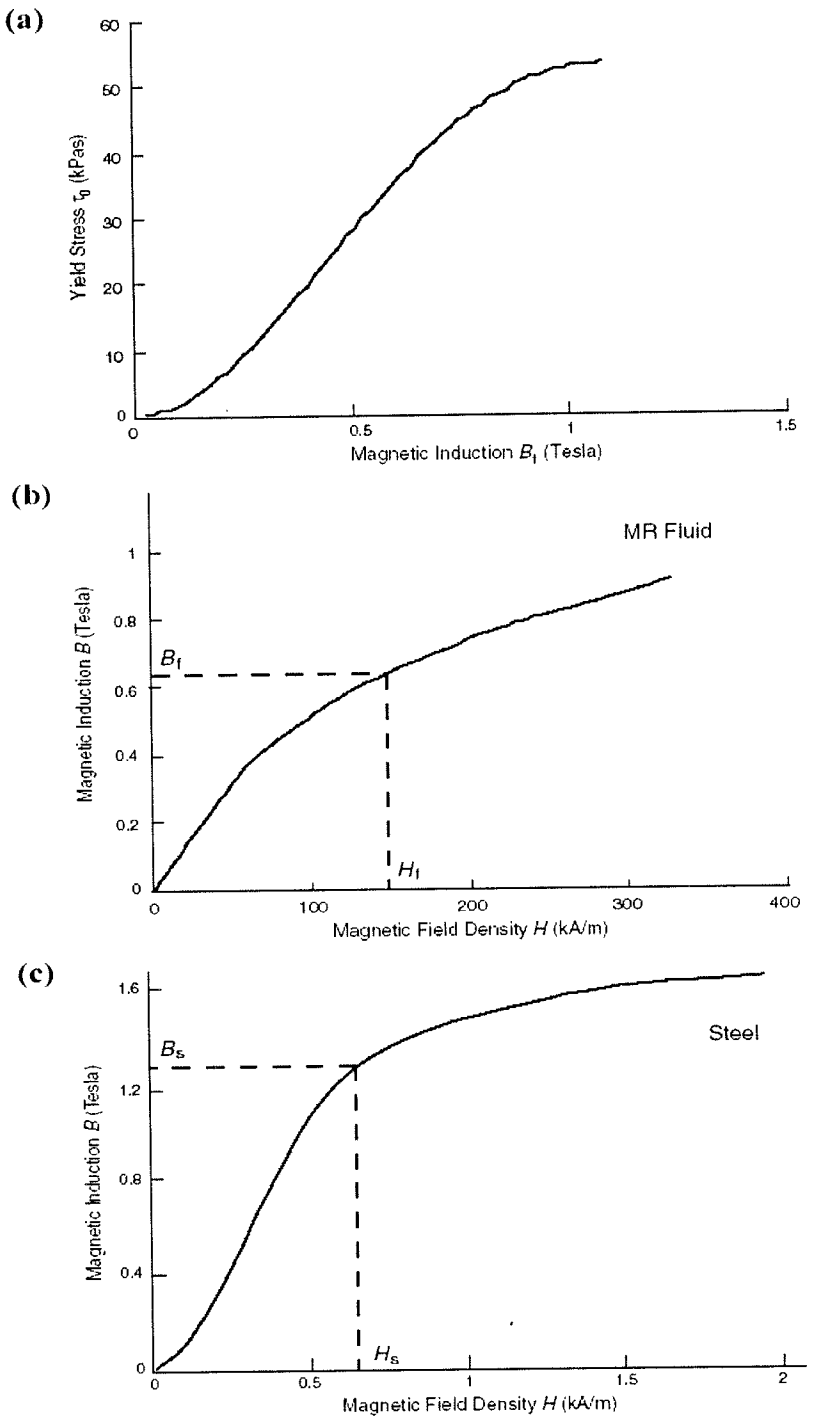

Fig. C-2: Magnetic Design Information (Courtesy of Lord Corporation)

$$NI = \sum_i H_i L_i = H_f g + H_s L \qquad \text{(C-6)}$$

Other effects should also be considered during the circuit design process, such as non-linear magnetic properties of the MR fluid and steel, possible losses at the junctions and boundaries, limits on voltage, current, and inductance, possible inclusion of permanent magnets for fail-safe operation, and eddy currents. However, those factors are out of the scope of this study.

Pressure Driven Flow Damper Design

Based on the cable experimental data obtained previously and the fluid material property of MRF-336AG provided by Lord Corporation, we assume the required parameters to match the cable as,

Table C-1: Assumed Design Parameter

Parameter	Value	Parameter	Value
Maximum force	~50 N	Minimum force	~5 N
Dynamic range	10	Outer Diameter (d_1)	20 mm
Yield Stress	45000 pa	Viscosity	4~8 $pa \cdot s$
Magnetic induction	0.75 T	Cable frequency	1~10 Hz

Assume that the active pressure drop area A_p is about 60 mm^2, then the demanded pressure drop is determined as,

$$\Delta P_\tau = 50N/60mm^2 \approx 800000pa \qquad \text{(C-7)}$$

Assume the cable frequency is about 4 Hz, and the amplitude of cable vibration is about 1 mm, then the maximum volumetric flow rate is about,

$$Q_{\max} = 2\pi faA_p = 2\times 3.14159\times 4\times 1\times 60 \approx 1500mm^3/s \qquad \text{(C-8)}$$

So, the minimum active fluid volume V can be calculated as,

$$V = k(\frac{\eta}{\tau_y^2})\lambda\Delta P_\tau Q_{\max} = \frac{12}{2.5^2}\times\left(\frac{4}{45000^2}\right)\times 10\times 800000\times 1500 = 45.5mm^3 \qquad \text{(C-9)}$$

Using Eq. (C-3), we get,

$$wg^2 = \frac{12}{c} \times \left(\frac{\eta}{\tau_y} \right) \times \lambda \times Q_{\max} = \frac{12}{2.5} \times \left(\frac{4}{45000} \right) \times 10 \times 1500 = 6.4 \qquad \text{(C-10)}$$

Followed the procedure explained earlier, we obtain,

$$g = 0.36mm\,, L = 2.5mm \qquad \text{(C-11)}$$

From Fig. C-3, the magnetic field intensity is 175 kAmp/m for the assumed value $\tau_y = 45000pa$. According to Eqs. (C-5) and (C-6), we can finally determine that the necessary number of amp-turns (NI) is about 90. Consequently, if the maximum current provided to the MR damper is 0.5 ampere, then the turn number can be determined as 180.

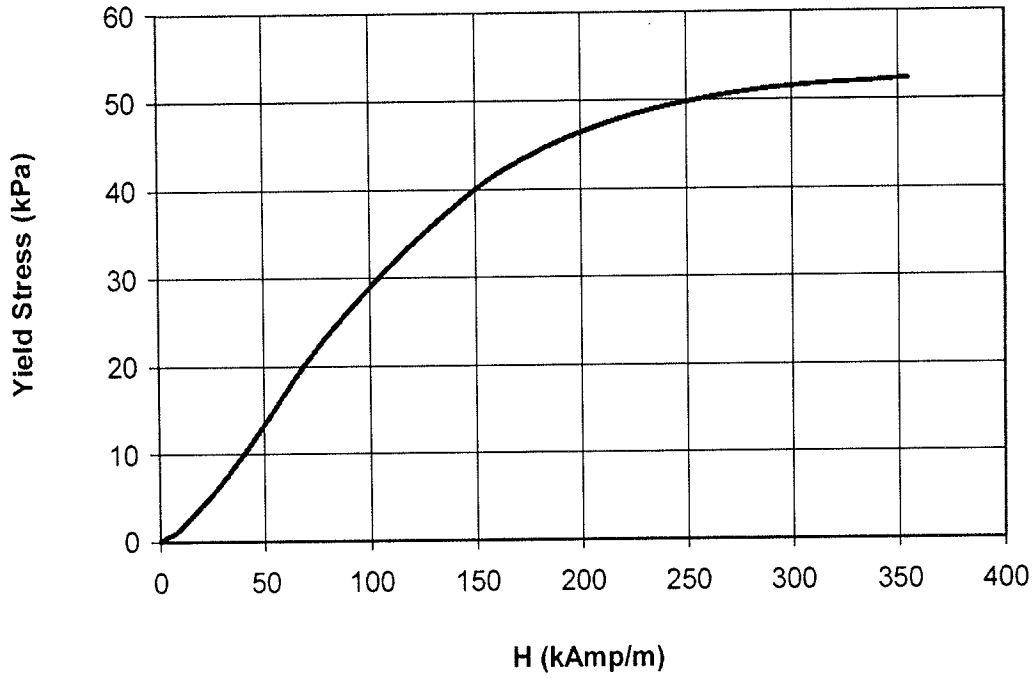

Fig. C-3: Yield Stress Versus Magnetic Field Intensity of MRF-33AG
(Courtesy of www.lord.com)

Following the procedure explained above, all the parameters for the primary geometry and magnetic circuit design can be obtained. Nevertheless, if we want to have an optimal design, we need to know the relationships between the variations of the design parameters and those assumed parameters in Table C-1. Table C-2 gives the changing rule of these parameters. In this table, f is the corresponding cable vibration frequency and d means the interval for magnetic coil winding. All the other variables are defined

before. In the table below, the symbols "↓", "↔" and "↑" mean that the corresponding value will decrease, remain unchanged, and increase, respectively.

Table C-2: Variety Rule for MR Design Parameter

	V	g	L	N	F_τ	F_η	f
$\Delta P_\tau \uparrow$	↓	↔	↓	↔	↓	↓	↔
$Q_{max} \uparrow$	↓	↓	↓	↓	↔	↔	↓
$\lambda \uparrow$	↓	↓	↓	↓	↔	↑	↔
$d_1 \uparrow$	↔	↑	↑	↑	↓	↓	↑
$\tau_y \uparrow$	↑	↑	↑	↑	↔	↔	↔
$\eta \uparrow$	↓	↓	↓	↓	↔	↔	↓
$d \uparrow$	↓	↔	↔	↓	↔	↔	↔
$t \uparrow$	↔	↓	↓	↓	↑	↑	↓
$r_4 \uparrow$	↔	↔	↔	↑	↑	↑	↓

Appendix D: Theoretical Solution of Cable-TMD-MR System

Cable Dynamics

There are a large amount of literatures discussing cable static and dynamic problems. By 1788, Lagrange and others had obtained solutions of varying degrees of completeness for the vibrations of an inextensible, massless string with hung on weights and fixed ends. These supplementary weights need a discretization model of the cable continuum. In 1820, Poison proposed a set of general partial differential equations of the motion of a cable element under the action of a general force system. However, apart from Lagrange's work on the equivalent discrete system, solutions for the sagging cable were unknown at that time (Starossek, 1994). Routh (1955) gave exact solutions for an inextensible sagging cable. Before 1970s, there was no explanation on the obvious discrepancy between the theories of an inextensible sagging cable and a taut cable. Irvine and Caughey (1974) revealed an extensive comprehension of the linear theory of free vibrations of a rigidly supported horizontal cable with a ratio of sag to span from approximately 1:8 or less. With a parameter representing the geometry and elasticity of the cable under consideration, they pointed out that if the elasticity is considered, the discrepancy could be explained. Later on, Irvine extended the theory to inclined cables by neglecting the weight component parallel to the cable chord (Irvine 1978). Triantafyllou (1984) derived a more precise asymptotic solution for small-sag, inclined, elastic cables. He demonstrated that inclined cables have different properties so that the horizontal cable results can't be simply extended. Nevertheless, validity of Irvine's theory was confirmed for a wide range of parameters.

Based on the previous extensive investigation on cable dynamics, Main and Johns (2002a, 2002b) discussed a horizontal cable with a viscous damper. In their investigation, they assume that the tension in the cable is large compared to its weight, bending stiffness and intrinsic damping of cable are negligible, and deflections are small. Following his procedure, some theoretical discussion will also be carried out in this investigation.

Theoretical Derivation

As stated previously, the equation of motion of the cable-TMD-MR system can be expressed as:

$$T\frac{\partial^2 v_k(x_k,t)}{\partial x_k^2} = m\frac{\partial^2 v_k(x_k,t)}{\partial t^2} \tag{D-1}$$

Traditionally, variable separation method is used to solve Eq. (D-1), which means the solution is assumed to have the following form:

$$v_k(x_k,\tau) = V_k(x_k)e^{s\tau} \tag{D-2}$$

where s is a dimensionless eigenvalue that is complex in general, while V_k is the mode shape of the cable vibration. Substituting Eq. (D-2) into Eq. (D-1) yields the following ordinary differential equations:

$$\frac{d^2V_k(x_k)}{dx_k^2} = (\frac{\pi s}{L})^2 V_k \tag{D-3}$$

From the boundary conditions, we have,

$$v_k(0,\tau) = 0\,,\ k = 1,2 \tag{D-4}$$

From the continuity of the cable at the conjunction point of the two segments, we have,

$$v_1(l_1,\tau) = v_2(l_2,\tau) = \gamma(\tau) \tag{D-5}$$

which means though the amplitude of the damper γ varies with time, the cable deflection is continuous for the two segments.

With these boundary and continuity conditions, the cable displacement can be expressed as,

$$v_k(x_k,\tau) = \gamma(\tau)\frac{\sinh(\pi s x_k / L)}{\sinh(\pi s l_k / L)} \tag{D-6}$$

Also, considering the vertical equilibrium condition at the hang-on point of the TMD-MR damper, we have,

$$T(-\frac{\partial v_1}{\partial x_1}\bigg|_{x_1=l_1} - \frac{\partial v_2}{\partial x_2}\bigg|_{x_2=l_2}) = K(v_1|_{x_1=l_1} - v_d) + C(\frac{dv_1}{dt}\bigg|_{x_1=l_1} - \frac{dv_d}{dt}) \tag{D-7}$$

On the other hand, from the equilibrium of the damper system itself, we have,

$$K(v_1|_{x_1=l_1} - v_d) + C(\frac{dv_1}{dt}\bigg|_{x_1=l_1} - \frac{dv_d}{dt}) - M\frac{d^2v_d}{dt^2} = 0 \tag{D-8}$$

where, v_d is the vertical displacement of the TMD-MR damper system and K, C and M are stiffness, damping coefficient and mass of the damper system, separately.

Since only the steady-state response is taken into account, it is reasonable to assume that the damper system has the same vibration pattern with the cable where it hangs on. According to this assumption, the displacement of the damper system can be expressed as,

$$v_d = \beta\gamma(\tau) \tag{D-9}$$

where constant β is the amplitude ratio between the damper and corresponding cable point.

From Eq. (D-8), and also denote $K = M\omega_d^2$ and $C = 2M\omega_d\xi$, we can express β as:

$$\beta = \frac{1+2\xi\rho s}{1+2\xi\rho s+\rho^2 s^2} \tag{D-10}$$

in which, ω_d is the natural frequency of the damper, ξ is the damping ratio, and $\rho = \frac{\omega_c}{\omega_d}$ can be viewed as a ratio between the cable frequency and the damper frequency.

Substituting β into Eq. (D-9) and then into Eq. (D-7), we have:

$$\coth(\frac{\pi s l_1}{L}) + \coth(\frac{\pi s l_2}{L}) + \frac{\pi s}{L}\frac{M}{m}\frac{1+2\xi\rho s}{1+2\xi\rho s+\rho^2 s^2} = 0 \tag{D-11}$$

From this transcendental equation, s can be obtained if the cable and damper parameters are specified.

Usually, the complex value s can be expressed as the sum of its real part and its imaginary part as:

$$s_i = \sigma_i + j\varphi_i \tag{D-12}$$

where the subscript i corresponding to the ith mode. σ_i and φ_i are both real values, and $j = \sqrt{-1}$. The system damping is defined as,

$$\zeta_i = (\frac{\varphi_i^2}{\sigma_i^2}+1)^{-1/2} \tag{D-13}$$

Treating the real and imaginary parts of Eq. (D-11) separately, we can obtain:

$$\begin{aligned}&\frac{\sinh(2\pi\sigma_i l_1/L)}{\cosh(2\pi\sigma_i l_1/L)-\cos(2\pi\varphi_i l_1/L)} + \frac{\sinh(2\pi\sigma_i l_2/L)}{\cosh(2\pi\sigma_i l_2/L)-\cos(2\pi\varphi_i l_2/L)} + \\ &\frac{\pi M}{Lm}\Big(\frac{\sigma_i+\sigma_i^2(4\xi\rho)+\sigma_i^3(\rho^2+4\xi^2\rho^2)+\varphi_i^2\sigma_i(\rho^2+4\xi^2\rho^2)}{(1+2\xi\rho\sigma_i+\rho^2\sigma_i^2-\rho^2\varphi_i^2)^2+(2\xi\rho\varphi_i+2\rho^2\varphi_i\sigma_i)^2} \\ &+\frac{\sigma_i^4(2\xi\rho^3)+\varphi_i^2\sigma_i^2(4\xi\rho^3)+\varphi_i^4(2\xi\rho^3)}{(1+2\xi\rho\sigma_i+\rho^2\sigma_i^2-\rho^2\varphi_i^2)^2+(2\xi\rho\varphi_i+2\rho^2\varphi_i\sigma_i)^2}\Big) = 0\end{aligned} \tag{D-14}$$

$$\frac{-2\sin(2\pi\varphi_i l_1/L)\cosh(2\pi\sigma_i l_1/L)-2\sin(2\pi\varphi_i l_2/L)\cosh(2\pi\sigma_i l_2/L)+2\sin(2\pi\varphi_i)}{(\cosh(2\pi\sigma_i l_1/L)-\cos(2\pi\varphi_i l_1/L))(\cosh(2\pi\sigma_i l_2/L)-\cos(2\pi\varphi_i l_2/L))}+$$

$$\frac{\pi M}{Lm}\frac{\varphi_i+\varphi_i\sigma_i(4\xi\rho)+\varphi_i\sigma_i^{\,3}(4\xi\rho-4\xi\rho^3)+\varphi_i^{\,2}\sigma_i^{\,2}(4\xi^2\rho^2-\rho^2)+\varphi_i^{\,3}(4\xi^2\rho^2-\rho^2)}{(1+2\xi\rho\sigma_i+\rho^2\sigma_i^{\,2}-\rho^2\varphi_i^{\,2})^2+(2\xi\rho\varphi_i+2\rho^2\varphi_i\sigma_i)^2}=0 \qquad \text{(D-15)}$$

These equations are solved numerically and some of the results have been discussed earlier in the text.

Appendix E: Some More Experimental Results of Cable-TMD-MR System

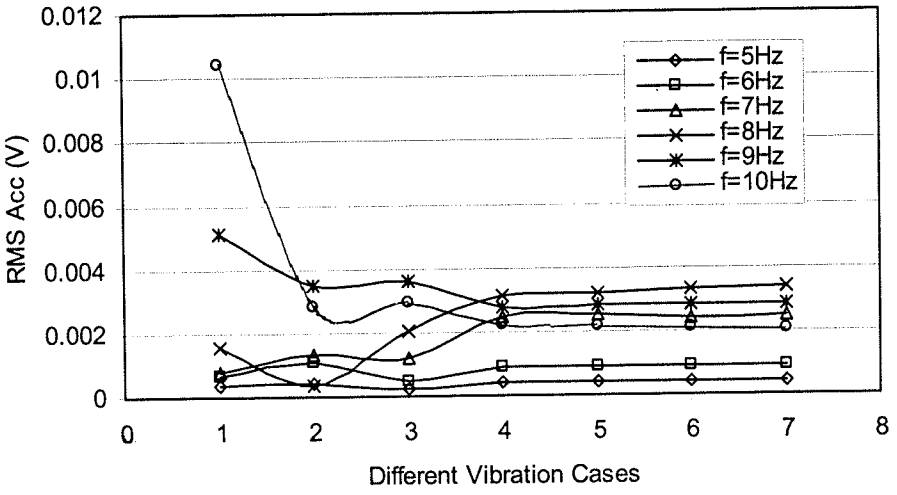

(a)

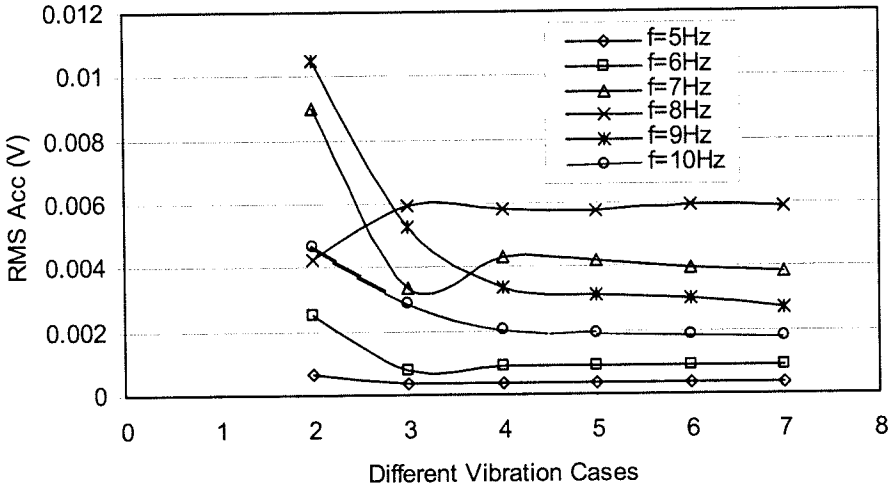

(b)

Fig. E-1: RMS Acceleration of Cable-TMD-MR System under Different Experiment Setup (a) Cable, (b) TMD-MR